CREATING A MULTIVALENT SUBUNIT VACCINE USING TYPE III SECRETION SYSTEM TIP PROTEINS AS ANTIGENS

BY

Aaron Paul Markham

Submitted to the graduate degree program in Pharmaceutical Chemistry and the Graduate Faculty of the University of Kansas in partial fulfillment of the requirements for the degree of Doctor of Philosophy.

_____
Chairperson*

_____

_____

_____

_____

Date Defended June 29, 2009

The Dissertation Committee for Aaron P. Markham certifies that this is the approved version of the following dissertation:

CREATING A MULTIVALENT SUBUNIT VACCINE USING TYPE III SECRETION SYSTEM TIP PROTEINS AS ANTIGENS

Committee:

_____
Chairperson*

_____

_____

_____

_____

Date Approved June 29, 2009

ABSTRACT

Many gram-negative bacterial pathogens employ type III secretion systems (TTSS) to transport effector proteins into eukaryotic host cell membranes and cytoplasms to subvert normal cellular functions. TTSSs contain a basal body which spans the inner and outer bacterial membranes and a needle which extends the into extracellular space. With the increasing prevalence of drug resistant bacterial strains, vaccines represent one of the most promising strategies to combat these diseases. Proteins located at the extracellular needle tip of TTSSs appear to be excellent candidates for a sub-unit vaccine approach. These so called tip proteins are surface exposed and regulate the secretion of other effector proteins. This work presents pre-formulation, formulation and animal studies focused on creating a single multivalent sub-unit vaccine for five gram-negative pathogenic systems. In addition, a putative tip protein from Chlamydiae is compared to the other tip proteins using biophysical methods.

DEDICATION

This work is dedicated to my wife Mariah Markham

and my parents Paul and Debra Markham.

ACKNOWLEDGEMENTS

First, I would like to express my sincere gratitude to my research advisor Russ Middaugh. Your passion for science and dedication has been an inspirational, motivating force during my time in the lab. I have never left your office without having an increased desire to understand and solve the really important problems. I personally believe that is the greatest trait an advisor can have. Next, I must thank Sangeeta who has always given excellent advice and ensured that everything in lab runs smoothly. Thanks you for your kindness and friendship.

I would also like to thank the members of my PhD committee for their time and help. Your input on this project has been invaluable.

Thanks to all of the members of the Middaugh lab past and present for their help and friendship. There are simply too many to name everyone individually but I have enjoyed working with everyone from the day I joined the lab until now. I would especially like to acknowledge the other members of my year in the lab. To Brooke Barrett, Reza Esfandiary and Julian Kissmann: you are awesome. It's been a fantastic four years.

Finally, but most importantly I would like to thank my family. Thank you to my parents for your love. Without you I never would have made it this far. To, Mariah, I love you so much. Thanks for being patient during the long hours of my absence. This has required your sacrifice as much as mine.

TABLE OF CONTENTS

Chapter 1

Introduction

1.1 Overview

Since Edward Jenner's work *Variolae Vaccinae* in 1798, vaccines have held the promise of eradicating many serious diseases from the world. Naturally occurring infections from smallpox, the focus of Jenner's initial experiment, have been relegated to history and polio is on the verge of being so.[1] Despite such success, progress in vaccination has historically been viewed with skepticism and fear in some segments of society. Shortly after Jenner's publication, British satirist James Gillray distributed cartoons of vaccinated subjects growing bovine heads on their appendages. More recently, assertions that MMR (measles, mumps, and rubella) and thimerosal containing vaccines caused autism in children set off a firestorm of anti-vaccination campaigns despite a lack of evidence.[2] Regardless of its detractors, vaccination has had a greater impact on mortality reduction than any other factor except for water sanitation and treatment in the last 200 years.[3] Diseases such as smallpox, diphtheria, tetanus, yellow fever, poliomyelitis, measles, mumps and rubella have been completely eradicated from many parts of the world.

While there has been much success, many serious infectious diseases remain without effective vaccines. Pathogenic gram-negative bacteria have been responsible for some of the most serious epidemics in the history of mankind including the bubonic plague. Salmonella outbreaks still occur in the United States with regularity.[4,5] Until the discovery of penicillin by Alexander Fleming and the subsequent proliferation of antibiotics, little could be done to effectively treat

patients. Almost immediately, however, after the introduction of antibiotics, drug resistant bacterial strains emerged.[6-8] The need for protective vaccines has therefore become paramount.

Many of these pathogens employ type III secretion systems (TTSS) to facilitate interactions with host organisms.[9-11] These systems possess proteins which are ideal candidates for sub-unit vaccines based on their location and function. Detailed in the following pages are pre-formulation and formulation experiments for five of these TTSS proteins. Additional experiments for a putative sixth candidate receive attention in the fifth chapter. Despite extensive research on two of these proteins (LcrV and PcrV), this work represents the first publication describing formulation of these antigens. In addition, results here establish the antigenicity of proteins IpaD and SipD when adsorbed to an aluminum salt adjuvant. The overall goal of this work is explore the possibility of creating one protective, multivalent sub-unit vaccine against several gram-negative pathogens with sufficient stability for distribution in the developing world.

1.2 Pathogens

Six proteins are analyzed in this work, each of which belongs to a different gram-negative bacterial system. The first pathogen that will be discussed is *Shigella flexneri* which is responsible for an estimated one million deaths a year.[12] *S. flexneri* is a rod shaped bacteria which causes bacillary dysentery (commonly referred to as

Shigellosis) by invading the colonic epithelium. Transmission occurs via the fecal-oral route typically through contaminated food or water. The agent requires as few as 100 bacteria to initiate infection.[13,14] Unlike many of the pathogens listed here, only other primates exhibit a disease state upon *S. flexneri* exposure.[15]

The genus *Yersinia* spp. contains rod shaped species responsible for a diverse list of diseases. The infamous bubonic plague is attributed to *Yersinia pestis*. *Y. pestis* primarily infects rodents and the pathogen is transmitted to humans through flea vectors.[16] The pathogen has a tropism for lymph tissue where it evades the immune system through a number of methods including inducing apoptosis of macrophages.[17,18] Draining lymph nodes swell during infection, becoming hemorrhagic causing the black buboes associated with the disease. As the disease progresses in human hosts, it induces bacterial pneumonia creating a second route of infection.[16] Aerosol droplets from patients in this late stage are highly contagious and without treatment individuals infected by this route have a nearly 100% mortality rate.

Y. enterocolitia induces the other significant infection caused by this genus in humans. Like *Y. pestis*, humans are not the natural host but are typically infected by ingesting dairy products or water contaminated with carrier animal feces.[19-21] *Y. enterocolitia* invades the Peyer's patch causing necrosis which leads to diarrhea, splenic and hepatic abscesses and lymphadenopathy.[19,22] Loci for infection are northern Europe and Japan.

The *Salmonella* genus encompasses an amazingly diverse set of organisms with a complicated and perpetually evolving taxonomy. In general, the genus is characterized by flagellated, rod shaped, aerobic organisms which are nearly all pathogenic. *S. enterica* alone includes up to 2000 recognized serovars including Typhi, Paratyphi and Typhimurium. Typhoidal serovars are responsible for an estimated 20 million cases yearly (mostly in the developing world) with patient relapses common.[23,24] Diagnosis is at times difficult since infection causes a broad range of symptoms. Severe cases, however, generally present with high fever, myalgia, abdominal pain and malaise.[25] Transmission typically occurs through contaminated water although a human carrier state also plays a role in endemic areas.[26]

The *S. enterica* serovar Typhimurium is also typically spread through unclean water or food and induces gastroenteritis. Recently, there have been several outbreaks of this pathogen in the U.S. and it continues to be a health threat throughout the world.[4,5] Like serovar Typhi, Typhimurium invade the intestinal mucosa, although, the pathogenesis of the serovar diverge after that initial stage. Typhi incubates in the reticuloendothelial system eventually precipitating systemic infection while Typhimurium remains near the intestinal mucosa causing acute inflammation ultimately leading to diarrhea.[27-29]

Burkholderia pseudomallei, the causative agent of melioidosis, is a disease endemic to Southeast Asia. This gram-negative, aerobic, rod shaped bacillus is found in the soil throughout that region with northern Thailand considered a major

focus.[30,31] *B. pseudomallei* typically infects humans through inhalation or cutaneous inoculation with cases occurring most often in the rainy season.[31] The pathogen is capable of invading many cell types including epithelial cells and spreads between cells through a number of routes including inducing cell fusion.[32] Compared to other bacteria discussed here, less in known about the virulence factors and life cycle of *Burkholderia* pathogens.

Pseudomonas aeruginosa causes many of the nosocomial infections encountered in hospitals today.[33] *P. aeruginosa* survives in most moist environments encountered in daily life. Populations considered most at risk include cystic fibrosis, AIDS and other severely immunocompromised patients.[34,35] Like the bacteria above, this pathogen is aerobic and rod shaped. As an opportunistic pathogen, *P. aeruginosa* infects both animals and some plants with infection in humans leading to sepsis in severe cases. Hospital acquired cases are sometimes antibiotic-resistant making some infections chronic.[34,36]

The Chlamydiae phylum contains obligate intracellular pathogens which cause numerous sexually transmitted diseases and ocular trachoma. *Chlamydia trachomatis* has received more study than other related species due to its prevalence (~92 million cases yearly).[37] Many of the pathogenic details discussed here for *C. trachomatis* apply to other species as well. The pathogen invades epithelial host cells as a metabolically inactive elementary body (EB) which forms an inclusion in the eukaryotic cytosol.[38-40] Within the inclusion, EB's transform into metabolically active reticulate bodies capable of binary fusion.[38] After proliferation within the

inclusion, the EBs differentiate back to RBs and are ultimately exocytosed to infect neighboring eukaryotic cells.[41]

1.3 Vaccines and other therapeutic approaches

While antibiotics have been invaluable in combating the infections of many of these pathogens, drug resistance (more alarmingly multi-drug resistance) has increased dramatically in the last 25 years.[7] In the case of *Shigella* and *Salmonella,* multiple drug resistance appears increasingly commonplace in the developing world and is beginning to emerge in more developed nations.[42-47] Antibiotic resistance appears less advanced in *Yersinia* spp. with only sporadic cases reported.[48,49] Both *B. pseudomallei* and *P. aeruginosa* exhibit some intrinsic multi-drug resistance due to an homologous drug efflux pump.[50-52] Interestingly, while the two bacterial systems have similar efflux machinery, the drugs selected for export are different. As noted above, in addition to the inherent resistance, hospitals are reporting strains of *P. aeruginosa* seemingly unaffected even by later generation antibiotics.[34,36] The first clinical report of multi-drug resistance to *C. trachomatis* did not appear until 2000,[53] however, given the high percentage of asymptomatic cases, the number of patients presenting with resistant strains is expected to explode in the coming years.[53-55]

Given the prevalence of drug resistant organisms, vaccines represent an attractive, prophylactic alternative. Vaccine strategies for most of these pathogens have focused on attenuated or killed whole cells with less consideration given to sub-

unit strategies. Phase I or even more advanced trials have been conducted on attenuated constructs for *Shigella flexneri*, *Salmonella enterica* serovar Typhi, *Burkholderia pseudomallei, Yesinia pestis* and *Pseudomonas aeruginosa*.[15,16,31,33,56-64] The trials show promise for this approach, but safety concerns along with scale-up challenges have so far prevented their commercialization.[15,65-67] Interestingly, *Salmonella enterica* serovar Typhimurium and *Yersinia enterocolitica* attenuated strains have been employed primarily as vehicles for other vaccine candidates including cancer prophylaxis.[68-72]

Initial attempts at creating vaccines for most of these pathogens involved killed whole cells. These approaches were less successful than hoped. Near the end of the second world war for instance, a vaccine for *Yersinia pestis* was created and manufactured by treating a strain with formaldehyde.[73] Unfortunately, the vaccine requires multiple subcutaneous injections over the course of the first year and annual boosts thereafter.[74] Common side-effects of the vaccine include malaise, headaches and elevated temperatures.[75,76] For similar reasons, many killed vaccines to these gram-negative bacteria have been abandoned.[77,78]

Many of the initial sub-unit vaccines relied on lipopolysaccharides as the primary antigen with varying degrees of success.[15,33,79-81] One of the most promising studies with this approach was conducted in the late 1990's in Israel using an O-specific polysaccharide conjugate.[82,83] The results indicated that in 74 % of the volunteers protection was conferred (or at least significant mediation of symptoms) and titers to the conjugate were still detectable two years after the administration

cycle. This sub-unit vaccine also exhibited an excellent safety record with no serious side effects indicated. Despite these encouraging signs, the high production cost of the candidate is considered the major challenge to further scale up.[84] Other sub-unit antigens currently being explored include pili, flagella, bacterial nucleic acids and a number of bacterial extracellular and outer membrane proteins.[15,16,31,33,61,62,64,85,86]

1.4 The Type III Secretion System

One relatively new source of potential antigens for sub-unit vaccines is the type III secretion system (TTSS). Over 25 bacterial species employ TTSS machinery to facilitate interactions with other organisms either as symbionts or pathogens.[9] These systems function as injectisomes, translocating effector proteins from the bacterial cytosol to the eukaryotic host cell membrane or into its cytoplasm. The genetic information for TTSSs is typically located on separate virulence plasmids or in clusters near one locus known as pathogenicity islands.[11] Furthermore, pathogenic bacterial strains are often only distinguishable from closely related species by these genetic islands while distantly related pathogens often contain closely related virulence genes.[11] These two observations suggest that the horizontal transfers, in which many of these organisms acquired virulence factors, occurred after evolutionary branching. Chlamydiae represent an unusual case since virulence genes for these pathogens are located at multiple loci throughout the genome.[87]

While the TTSSs are related genetically, the effectors translocated by respective organisms possess a wide array of diverse functions. It appears that subsequent to horizontal gene transfer that the gram-negative pathogens adapted a secretion apparatus to meet their needs. Based on genetic and phylogenic studies, TTSSs are divided into seven sub-families.[9,88] The Clamydia phylum has its own sub-family as does the Rhizobiales order. The two groupings which receive most of the focus in the work presented here are the Ysc and SPI-1 sub-families whose archetypes are the *Yersinia* spp. and *Shigella flexneri* injectisomes respectively. Some pathogens, such as *Salmonella* spp., encode two separate injectisomes, each having a different role. These differences in TTSS groups are important to remember for the following chapters. The proteins explored here are shown to divide into analogous sub-famlies based on response to pH and temperature.

TTSSs are composed of more than 20 distinct proteins which form a basal body which extends from the bacterial cytosol through both the inner and outer membrane. A needle, comprised of monomers which polymerize, extends from this structure into the extracellular space. It is through a pore in the needle which effector proteins must ultimately pass. One of the most highly conserved injectisome proteins is an ATPase associated with the inner membrane. In *Pseudomonas syringae* this proteins forms a hexamer which in turn becomes a dodecamer.[89] Upon oligomerization this complex becomes active. The purpose of this complex is two-fold. First, the ATPase energizes transport of effector proteins into the needle and second, the complex is believed to detach the effector substrates from their

chaperones.[90] The stoichiometry and location of many of the other basal components has not yet been been elucidated and will not be discussed here.

Using single particle analysis cryo-electron microscopy, Blocker, et al. were able to determine the structure of the needle complex of *Shigella flexneri* at high resolution.[91] This work revealed the dimensions of the inner channel which extends from the cytosol to the extracellular needle tip. The diameter of this channel was shown to be 2-3 nm indicating that effector proteins must unfold (at least their tertiary structural elements) to pass through. Notably, an additional role for the ATPase complex may be to unfold the effector proteins before passing them into the needle complex.

The needle is a straight tube approximately 60 nm in length composed of 100-150 identical molecules.[92-94] Needle monomers polymerize in a helical pattern forming part of the channel discussed above with ~5.6 monomers per turn.[94] One of the major areas of current investigation is how needle length is determined. At least three theories have been proposed to account for the change in substrate passage (from needle monomer to other effectors) which would determine needle length.[9,10] The cup model asserts that subunits accumulate in a cavity just below the apparatus and the volume of monomers in that cavity determines the length. Flagellar system are proposed to function by a similar mechanism and genetic and phylogenic information suggest that TTSSs and flagella have a common ancestor.[88,95] Indeed, the physical polymerization mechanism of TTSS needle monomers is analogous to

extracellular flagellum growth.[94,96] While these similarities make this an attractive model, no requisite C ring (the "cup" in this model) has been discovered.

The second theory proposes that a "molecular ruler" controls the length of the needle. In this case, an extended polypeptide (YscP in *Yersinia* spp.) is anchored to the tip of the growing needle and the base of the needle complex.[97] Once this protein is fully extended it would, through some unknown mechanism, signal a switch in substrate specificity in the secretion apparatus. One major challenge of this model is the location of the "ruler". If this protein were located inside the channel as seems most likely, it would block the channel for the passage of needle monomer. Finally, the third model proposes that completion of the inner rod switches the substrate specificity.[98] The inner rod creates the channel within the basal body and connects to the needle. This model proposes that the two different channel components are assembled simultaneously and that once the rod is completed, the needle stops growing as well. Recent experiments suggest however, that this model (developed in *Salmonella* spp.) may not work in *Yersinia* spp. where rod formation is not concurrent to needle polymerization.[9]

After the needle has been assembled, a protein passes through the channel and localizes on the needle tip.[99,100] The so called tip proteins possess a central coiled coil flanked by N and C-terminal domains.[101-103] The N-terminal domain of these proteins appears to serve as a molecular chaperone, preventing premature oligomerization.[101] Many of the tip proteins that have been studied are between 33 and 38 kDa in size

and have pI's between 4.8 and 5.5. These tip proteins regulate the secretion of other effectors passing through the needle complex.

Studies of Invasion plasmid antigen D (IpaD), the tip protein in *Shigella flexneri*, were the first to elucidate much of what is currently understood about the function of these proteins. Transmission electron micrograph (TEM) assays, with immunogold-labeled IpaD, demonstrated that IpaD is localized at the needle tip.[99] A close homolog, BipD of *Burkholderia pseudomallei*, also localizes to the needle tip in the *Shigella* system. *In silico* modeling of other tip proteins suggest that both the N-terminal domain and the C-terminal end of the coiled coil are required for docking to the needle although this has not yet been demonstrated *in vitro*.[104] It has been shown, however, that IpaD controls the secretion of the ensuing proteins and that IpaD may form a pentamer (or possibly heteropentamer) on the needle tip.[99,101,105,106] The protein which may be involved in the oligomer besides IpaD is IpaB. IpaB and IpaC form the translocon pore in the eukaryotic host cell permitting entry of further substrates to subvert normal cell function. In aqueous conditions only IpaD is detectable on the needle tip. When bile salts such as deoxycholate (DOC) are added, however, IpaB translocates to the needle tip.[107] Since *Shigella flexneri* invades the intestinal mucosa, the presence of bile salts is potentially physiologically relevant. Additional work has demonstrated that IpaD binds DOC.[108] These results suggest that bile salts trigger the needle complex to prepare IpaB for insertion into the eukaryotic membrane. Thus, IpaD has a possible role in facilitating the insertion of IpaB into the membrane.

While interactions with small molecules have not been demonstrated for other tip proteins, characteristics such as pentamer formation have been shown. Employing molecular modeling, Deane et al. first predicted that the *Yersinia* spp. tip protein, Low Calcium Reponse protein V (LcrV), would form such a structure at the needle tip.[104] Recently, the oligomerization behavior of LcrV has been confirmed *in vitro*, although, the exact size of the higher order species was not determined.[109] This oligomerization tendency will be important in chapter 5 when we study a newly discovered putative tip protein for Clamydiae.

1.5 TTSS Tip Proteins as Potential Vaccine Antigens

Due to their location at the tip of the needle where they are solvent exposed, tip proteins make promising candidates for sub-unit vaccine antigens. Furthermore, studies with IpaD, LcrV and PcrV (of *Pseudomonas aeruginosa*) have shown that, *in vitro*, antibodies against them block host cell invasion.[99,110,111] This makes sense since antibodies might prevent interactions with small molecules or with other external stimuli. The antibodies may also physically impede the passage of other effector proteins and roles that tip proteins may play in inserting pore forming effectors into the host cell membrane.

While many of the tip proteins discussed here have received attention as possible antigens for sub-unit vaccines, the most interest has been in LcrV and PcrV. These antigens were considered promising even before their function was known.

Antibodies to LcrV (then known as the V-antigen) were purified in small quantities in 1963 and shown to passively protect against plague in mice.[112] Immunization studies with attenuated *Yersinia* vaccines in 1983 suggested that LcrV had a significant role in protection in humans and was cross protective within the genus.[113] Though not discovered as early, anti-PcrV production has been shown to correlate with higher survival rates in humans.[114] In addition, passive immunization with polyclonal antibodies to PcrV was protective in murine models as well.[115,116] These results prompted researchers to begin vaccine tests with recombinant LcrV when it became available.

In the mid-1990's, immunization with recombinant LcrV was shown to protect against the plague.[117] Initial efforts for LcrV focused on a combination vaccine that included capsular antigen F1. A single dose of F1 purified from cell culture supernatant with recombinant LcrV adsorbed to aluminum salt adjuvant protected mice from a lethal dose of the plague organism.[111] Fusion proteins of LcrV and F1 have also been created and tested with some success.[118] Strains of acapsular *Yersinia* spp., however, are not uncommon. Therefore, LcrV is the key antigen in any such combination. Other vaccine strategies with LcrV include microsphere encapsulation with poly-L-lactide (PLLA) which was then homogenized by sonication with polyvinyl alcohol to form a double emulsion.[119] Included in the polymeric sphere was another capsular protein known as Caf1. This microsphere only required a single dose delivered intra-nasally to produce protection. Both helper T cell 1 and 2 (Th1 and Th2) cytokines were detected in response to immunization

indicating that both cellular and humoral immune responses were activated. Finally, DNA based vaccines which encode LcrV have been tested. The most successful of these nucleic acid based approaches include additional sequences known to elicit strong immune response.[120] PcrV has also been successfully administered as a sub-unit vaccine in BALB/c mice with challenge studies indicating protection.[115] Many of the same approaches which have shown promise with LcrV also work for PcrV.[33,121]

While LcrV is considered a promising antigen, the protein has been reported to suppress gamma interferon (IFN-γ) and tumor necrosis factor alpha (TNF-α). These cytokines function as important proinflammatory signals in the immune response.[122] It is currently thought that this is accomplished by induction of interleukin 10 (IL-10) which is achieved by signaling from a TLR2/TLR6/CD14 complex.[123,124] Since the full length LcrV sub-unit vaccines discussed above protect against lethal challenges given days after inoculation, it is not clear what implications this has for immunization purposes. The primary concern raised by some researchers is that immediately following vaccination a patient might be immunosuppressed and more susceptible to other infections. This has not, however, been established. In light of this concern, two regions of LcrV primarily responsible for protection have been identified. These regions are from amino acids 2 to 235 and from 235 to 275 in the primary sequences.[125,126] In addition, deletion of residues from 271 to 300 was reported to mitigate anti-inflammatory activity while preserving protective effects.[127] This deletion removes an α-helical portion of the protein involved in the coiled coil.

While the mutant retained solubility characteristics similar to the wild type, it is not clear what effect this deletion had on overall protein secondary and tertiary structure and their stability.

IpaD has received less attention as a sub-unit vaccine but shows promise. In most monkeys in one study, anti-IpaD IgG and IgA immune responses increase dramatically after *Shigella* infection.[128] A few of the monkeys in that experiment were infected and fully recovered without producing detectable concentrations of IpaD antibodies indicating that while immune response to IpaD may be protective, it is not the only antigen which provides protection. In a study of humans in an area of Peru where *Shigella* inefections are endemic, it was shown that Ipa (IpaB and C included) antibodies in the mucosa limited the severity and spread of shigellosis.[79] Epitope mapping of IpaD revealed that most of the surface exposed epitopes were located in the N-terminal domain between residues 14 and 77.[129] In contrast, residues in the carboxyl-terminal region were primarily buried and would therefore be inaccessible to antibodies. It is likely that these epitopes are exposed during processing in antigen-presenting cells and are subsequently presented to the adaptive immune system. Interestingly, most of the sequence homology occurs between IpaD, BipD and SipD (*Salmonella* spp.) in the C-terminal region. Epitopes recognized by antibodies are probably therefore heterogeneous while sequences presented by antigen presenting cells may have high sequence homology. It is not yet clear if such a pattern would result in immunological cross-reactivity.

BipD is the last of the tip proteins discussed here to have undergone significant sub-unit vaccine testing. Immunization using BipD with Freund's complete adjuvant (FCA) or *Brucella abortus* O-polysaccharide as an adjuvant failed to prolong survival of mice given a lethal dose of *Burkholderia pseudomallei.*[130] FCA is an oil in water emulsion which contains inactivated mycobacteria. Both of the adjuvants boosted the cellular immune response while FCA also elicited a robust humoral response in this study. *B. pseudomallei* functions primarily as an intracellular pathogen so antibody production might not be expected to protect. Why protection was not affected by the Th1 immune pathway is unknown. The authors noted that BipD was not detected during infection suggesting that BipD expression may be significantly lower upon infection compared to other pathogens' TTSS tip proteins. Additionally, human antibody responses to BipD upon *B. pseudomallei* infection are higher than that detected in murine models which could be due to differences in the nature of the host immune response.

1.6 Creating Sub-unit vaccines

While several of the antigens in this study have been shown to be highly immunogenic and protective, little has been done to systematically formulate these antigens as vaccine products. Vaccines for *Shigella flexneri*, *Salmonella* spp., *Burholderia pseudomallei* and *Yersinia pestis* are particularly important in the developing world where these diseases are endemic.[12,23,30,50,64] As antibiotic

resistance increases, treatment requiring second line antibiotics may become too expensive for regions most in need. Additionally, effective vaccines would eliminate the danger of bacteria resistant to all antibiotics. Creating viable vaccines for the developing world requires highly stable formulations. In developed countries, a labile product might prove commercially viable by employing freezing or refrigeration. The lack of a reliable cold chain, however, in parts of the developing world requires formulations with sufficient stability for distribution and administration in harsher conditions.[131] As such, a systematic, scientifically sound approach must be undertaken to ensure that a vaccine is as stable and viable as possible. One of the goals of the formulation process discussed in this work is to formulate a vaccine containing IpaD, BipD, SipD, LcrV and PcrV in various combinations for specific locations. This plan for a multivalent vaccine presents further challenges since a successful formulation must increase stability for all five proteins.

To achieve formulations with maximal stability, we employ various spectroscopic techniques to measure the conformational stability of the tip proteins with respect to pH and temperature. Far-UV circular dichroism, fourier transform infrared spectroscopy, UV absorbance spectroscopy, ANS extrinsic fluorescence, turbidity and right angle static light scattering are all employed to monitor secondary, tertiary and quaternary structure as well as aggregation behavior. This biophysical characterization lays the groundwork for selecting formulation conditions, excipient screening and optimization parameters and long term stability studies. Data produced

later in the formulation process can usually be understood in the context of the initial characterization. Thus, biophysical characterization provides a wealth of background information concerning protein conformational stability which enables us to logically arrive at an optimized formulation and interpret subsequent findings.

In addition to its utility in formulation, biophysical characterization and the empirical phase diagrams (EPD) produced as a result afford insights into the biological structure/function of proteins as well. EPDs provide an intuitive way analyze data combined from disparate techniques. The theory and mathematics underlying EPDs are covered in detail by Kueltzo et al. elsewhere.[132] Briefly, however, at each pH and temperature, data are combined from multiple techniques and used to create multi-dimensional vectors. Vectors for each pH\temperature conditions are assembled to produce a density matrix. Eigenvectors and eigenvalues are calculated from this matrix. The three largest eigenvalues are selected to create eigenvectors which expand a truncated form of the data set to three dimensions. These newly constructed vectors are finally plotted as a combination of three colors (red, green and blue). Differences in color between pH/temperature blocks in an EPD represent changes in the protein structural and association state. Such alterations in conformation and aggregation represent apparent "phases" of protein stability. These phases are not, however, thermodynamic in nature since no equilibria are implied between the "states". Proteins with little primary sequence homology but similar structure/function relationships generally produce EPD's which have comparable phases.[133] In the following chapters, the EPD's ability to indicate structure/function

relationships is used to reveal tip protein sub-families and to indicate the potential function of a newly discovered protein from the Chlamydiae TTSS.

Stabilizing proteins in solution is often accomplished by adding various chemical agents, termed excipients. These excipients stabilize through a number of mechanisms including preferential hydration, minimization of protein-protein interactions, exclusion of proteins from destabilizing interfaces and inhibition of chemical degradation.[134] To achieve significant shelf life, particularly in harsher temperature environments, excipients are usually necessary. Preferential hydration occurs when the excipients are excluded from the protein's immediate environment which favors a smaller surface area and increases the free energy of unfolding.[135-137] This mechanism of protein stabilization proved to be the most important in the work described here. Stabilizers which preclude protein-protein interactions and surfactants which exclude proteins from the air-water interface would be expected to be less important in this case because the proteins will generally be adsorbed to an aluminum salt adjuvant (see below). A GRAS (generally regarded as safe) list of stabilizers was compiled for screening the proteins discussed here and included amino acids, antioxidants, cyclodextrans, carbohydrates, surfactants, polyols and proteins.

As has been alluded to previously, most sub-unit vaccines require an adjuvant to boost the immune response. Adjuvants boost the immune system response through a number of mechanisms including binding Toll-like receptors on antigen presenting cells, creating a depot from which antigen is released over time and inducing inflammation.[138] Some antigens are capable of eliciting both humoral and cellular

immune responses while others only actively stimulate one branch. It is no yet clear for the proteins investigated here what kind of immune response will afford the most protection. LcrV and PcrV belong to bacteria which cause systemic, extracellular infection. For these, a strong antibody response may be the most important factor in protection. Studies in which humoral immunopotentiators were included in LcrV and PcrV trials support this assumption. Studies of long term protection, however, using attenuated whole cell vaccines suggested that the cellular immune response was important in generating memory cells and thus long term protection.[113] *Shigella flexneri* invades the intestinal mucosa and is primarily an intracellular pathogen. It has been shown that IgA production limits the severity and spread of *S. flexneri* infections presumably by preventing bacterial entry at the apical membrane of the intestinal cells.[79] With a subunit vaccine containing O polysaccharides as the antigen, protection was conferred with serum IgG levels correlating with protection (or at least mediation).[82,83] While it is possible that the IgG itself was protecting, it seems more likely that IgG mirrored IgA concentration which actually afforded the critical protection.

The adjuvant chosen for the studies presented in chapters 3 and 4 is the aluminum salt adjuvant, Alhydrogel®. This adjuvant elicits a strong humoral response.[138] The exact mechanism of its immune system stimulation is not known but it is possibly the result of a depot effect.[139] This adjuvant was chosen because it is one of only a handful approved by the FDA and has a good safety record. LcrV and PcrV, adsorbed to aluminum salt adjuvants, successfully protected mice in challenge

studies. IpaD and SipD have not been administered in conjunction with this adjuvant class until now. In fact, little is know about SipD's antigenicity compared with the other proteins discussed above. BipD may still prove to be an effective antigen despite the results of the studies discussed previously. Future work will be needed to ascertain if an aluminum adjuvant is successful in producing a protective immune response or whether the use of alternative adjuvants needs to be explored.

1.7 Chapter overviews

Chapter 2 presents a biophysical characterization of the five tip proteins IpaD, BipD, SipD, LcrV and PcrV. The temperature and pH response of these proteins are compared using EPDs and based on these results the tip proteins are classified into two sub-families. The first sub-family contains IpaD, BipD and SipD whle the second is comprised of LcrV and PcrV. This characterization comprises the pre-formulation aspect of the potential vaccine(s).

The immunogenicity of IpaD and SipD adsorbed to Alhydrogel® as measured by IgG antibody titers is described in Chapter 3. Immune response to monomer needle proteins is also explored. These antigens are tested in 1, 10 and 50 μg doses and when co-administered with their TTSS counterparts. The tip proteins elicited a strong humoral immune response even in low quantities. The presence of needle protein showed no effect.

Chapter 4 discusses the formulation of the five tip proteins from Chapter 1. Excipient screening and optimization are detailed. In addition, aluminum salt adjuvant binding studies are discussed as well as adjuvant effects on stability. Long term stability studies monitoring physical and chemical degradation are presented and evaluated. From these tests, the formulation is shown to inhibit chemical degradation.

Chapter 5 presents biophysical studies of a newly discovered putative TTSS tip protein from Chlamydiae (CT584). EPDs and individual spectroscopic data are compared to known tip proteins. In addition, analytical ultracentrifugation in both sedimentation and equilibrium modes reveals that CT584 oligomerizes in solution.

Finally, Chapter 6 summarizes the conclusions from the previous chapters. Future work and implications of the data from TTSS proteins presented here are discussed.

1.8 References

1. WHO GCftCoSE. 1979. The Achievement of the Global Eradication of Smallpox., ed., Geneva: World Health Organization.
2. Offit PA. 2008. Autism's False Prophets: Bad Science, Risky Medicine and the Search for a Cure. ed., New York: Columbia University Press. p 328.
3. Plotkin SL, Plotkin SA. 2004. A Short History of Vaccination. In Plotkin SA, Orenstein WA, editors. Vaccines, 4th ed.: Saunders. p 1-15.

4. FDA. 2008. *Salmonella Saintpaul* Outbreak. ed.
5. FDA. 2008. Peanut Product Recalls: *Salmonella Typhimurium*. ed.
6. Barber M, Rozwadowska-Dowzenko M 1948. Infection by penicillin-resistant *Staphylococci*. Lancet 2(6530):641-644.
7. Levy SB, Marshall B 2004. Antibacterial resistance worldwide: causes, challenges and responses. Nat Med 10(12 Suppl):S122-129.
8. Crofton J, Mitchison DA 1948. Streptomycin resistance in pulmonary tuberculosis. Br Med J 2(4588):1009-1015.
9. Cornelis GR 2006. The type III secretion injectisome. Nat Rev Microbiol 4(11):811-825.
10. Galan JE, Wolf-Watz H 2006. Protein delivery into eukaryotic cells by type III secretion machines. Nature 444(7119):567-573.
11. Hueck CJ 1998. Type III protein secretion systems in bacterial pathogens of animals and plants. Microbiol Mol Biol Rev 62(2):379-433.
12. WHO. 2009. *Shigella*. ed.
13. Levine MM, DuPont HL, Formal SB, Hornick RB, Takeuchi A, Gangarosa EJ, Snyder MJ, Libonati JP 1973. Pathogenesis of *Shigella dysenteriae* 1 (Shiga) dysentery. J Infect Dis 127(3):261-270.
14. DuPont HL, Hornick RB, Dawkins AT, Snyder MJ, Formal SB 1969. The response of man to virulent *Shigella flexneri* 2a. J Infect Dis 119(3):296-299.
15. Levine MM, Kotloff KL, Barry EM, Pasetti MF, Sztein MB 2007. Clinical trials of *Shigella* vaccines: two steps forward and one step back on a long, hard road. Nat Rev Microbiol 5(7):540-553.
16. Cornelius C, Quenee L, Anderson D, Schneewind O 2007. Protective immunity against plague. Adv Exp Med Biol 603:415-424.
17. Chen Y, Zychlinsky A 1994. Apoptosis induced by bacterial pathogens. Microb Pathog 17(4):203-212.
18. Monack DM, Mecsas J, Bouley D, Falkow S 1998. *Yersinia*-induced apoptosis in vivo aids in the establishment of a systemic infection of mice. J Exp Med 188(11):2127-2137.
19. Bottone EJ 1999. *Yersinia enterocolitica*: overview and epidemiologic correlates. Microbes Infect 1(4):323-333.
20. Fantasia M, Grazia Mingrone M, Crotti D, Boscato C 1985. Isolation of *Yersinia enterocolitica* biotype 4 serotype O3 from canine sources in Italy. J Clin Microbiol 22(2):314-315.
21. Fredriksson-Ahomaa M, Korte T, Korkeala H 2001. Transmission of *Yersinia enterocolitica* 4/O:3 to pets via contaminated pork. Lett Appl Microbiol 32(6):375-378.
22. Grutzkau A, Hanski C, Hahn H, Riecken EO 1990. Involvement of M cells in the bacterial invasion of Peyer's patches: a common mechanism shared by *Yersinia enterocolitica* and other enteroinvasive bacteria. Gut 31(9):1011-1015.
23. Crump JA, Luby SP, Mintz ED 2004. The global burden of typhoid fever. Bull World Health Organ 82(5):346-353.
24. Parry CM 2004. Typhoid Fever. Curr Infect Dis Rep 6(1):27-33.

25. Hoffman TA, Ruiz CJ, Counts GW, Sachs JM, Nitzkin JL 1975. Waterborne typhoid fever in Dade County, Florida. Clinical and therapeutic evaluation of 105 bacteremic patients. Am J Med 59(4):481-487.
26. Ames WR, Robins M 1943. Age and Sex as Factors in the Development of the Typhoid Carrier State, and a Method for Estimating Carrier Prevalence. Am J Public Health Nations Health 33(3):221-230.
27. Takeuchi A 1967. Electron microscope studies of experimental *Salmonella* infection. I. Penetration into the intestinal epithelium by *Salmonella typhimurium*. Am J Pathol 50(1):109-136.
28. Kohbata S, Yokoyama H, Yabuuchi E 1986. Cytopathogenic effect of *Salmonella typhi* GIFU 10007 on M cells of murine ileal Peyer's patches in ligated ileal loops: an ultrastructural study. Microbiol Immunol 30(12):1225-1237.
29. Kops SK, Lowe DK, Bement WM, West AB 1996. Migration of *Salmonella typhi* through intestinal epithelial monolayers: an in vitro study. Microbiol Immunol 40(11):799-811.
30. Dance DA 1991. Melioidosis: the tip of the iceberg? Clin Microbiol Rev 4(1):52-60.
31. Wiersinga WJ, van der Poll T, White NJ, Day NP, Peacock SJ 2006. Melioidosis: insights into the pathogenicity of *Burkholderia pseudomallei*. Nat Rev Microbiol 4(4):272-282.
32. Kespichayawattana W, Rattanachetkul S, Wanun T, Utaisincharoen P, Sirisinha S 2000. *Burkholderia pseudomallei* induces cell fusion and actin-associated membrane protrusion: a possible mechanism for cell-to-cell spreading. Infect Immun 68(9):5377-5384.
33. Doring G, Pier GB 2008. Vaccines and immunotherapy against *Pseudomonas aeruginosa*. Vaccine 26(8):1011-1024.
34. Agnihotri N, Gupta V, Joshi RM 2004. Aerobic bacterial isolates from burn wound infections and their antibiograms--a five-year study. Burns 30(3):241-243.
35. Driscoll JA, Brody SL, Kollef MH 2007. The epidemiology, pathogenesis and treatment of *Pseudomonas aeruginosa* infections. Drugs 67(3):351-368.
36. Erol S, Altoparlak U, Akcay MN, Celebi F, Parlak M 2004. Changes of microbial flora and wound colonization in burned patients. Burns 30(4):357-361.
37. WHO. 2001. Global Prevalence and Incidence of Selected Curable Sexually Transmitted Infections: Overview and Estimates. ed.: World Health Organization.
38. Bedson SP, Bland JOW 1932. A morphological study of psittacosis virus with the description of a developmental cycle. Brit J Exptl Pathol 13:461-466.
39. Byrne GI, Moulder JW 1978. Parasite-specified phagocytosis of *Chlamydia psittaci* and *Chlamydia trachomatis* by L and HeLa cells. Infect Immun 19(2):598-606.
40. Scidmore MA, Rockey DD, Fischer ER, Heinzen RA, Hackstadt T 1996. Vesicular interactions of the *Chlamydia trachomatis* inclusion are determined by chlamydial early protein synthesis rather than route of entry. Infect Immun 64(12):5366-5372.

41. Brunham RC, Rey-Ladino J 2005. Immunology of *Chlamydia* infection: implications for a *Chlamydia trachomatis* vaccine. Nat Rev Immunol 5(2):149-161.
42. Cohen ML, Tauxe RV 1986. Drug-resistant *Salmonella* in the United States: an epidemiologic perspective. Science 234(4779):964-969.
43. Brooks JT, Shapiro RL, Kumar L, Wells JG, Phillips-Howard PA, Shi Y-P, Vulule JM, Hoekstra RM, Mintz E, Slutsker L 2003. Epidemiology of Sporadic Bloody Diarrhea in Rural Western Kenya. Am J Trop Med Hyg 68(6):671-677.
44. Fulla N, Prado V, Duran C, Lagos R, Levine M 2005. Surveillance for Antimicrobial Resistance Profiles Among *Shigella* Species Isolated from a Semirural Community in the Northern Administrative Area of Santiago, Chile. Am J Trop Med Hyg 72(6):851-854.
45. Glynn MK, Bopp C, Dewitt W, Dabney P, Mokhtar M, Angulo FJ 1998. Emergence of Multidrug-Resistant *Salmonella enterica* SerotypeTyphimurium DT104 Infections in the United States. N Engl J Med 338(19):1333-1339.
46. Kariaki S, Gilks C, Corkill J, Kimari J, Benea A, Waiyaki P, Hart CA 1996. Multi-drug resistant non-typhi salmonellae in Kenya. J Antimicrob Chemother 38(3):425-434.
47. Frost JA, Willshaw GA, Barclay EA, Rowe B, Lemmens P, Vandepitte J 1985. Plasmid characterization of drug-resistant *Shigella dysenteriae* 1 from an epidemic in Central Africa. J Hyg (Lond) 94(2):163-172.
48. Galimand M, Guiyoule A, Gerbaud G, Rasoamanana B, Chanteau S, Carniel E, Courvalin P 1997. Multidrug resistance in *Yersinia pestis* mediated by a transferable plasmid. N Engl J Med 337(10):677-680.
49. Kanazawa Y, Ikemura K 1979. Isolation of *Yersinia enterocolitica* and *Yersinia pseudotuberculosis* from human specimens and their drug-resistance in the Niigata District of Japan. Contrib Microbiol Immunol 5:106-114.
50. Howe C, Sampath A, Spotnitz M 1971. The pseudomallei group: a review. J Infect Dis 124(6):598-606.
51. Moore RA, DeShazer D, Reckseidler S, Weissman A, Woods DE 1999. Efflux-mediated aminoglycoside and macrolide resistance in *Burkholderia pseudomallei*. Antimicrob Agents Chemother 43(3):465-470.
52. Kohler T, Michea-Hamzehpour M, Henze U, Gotoh N, Curty LK, Pechere JC 1997. Characterization of MexE-MexF-OprN, a positively regulated multidrug efflux system of *Pseudomonas aeruginosa*. Mol Microbiol 23(2):345-354.
53. Somani J, Bhullar VB, Workowski KA, Farshy CE, Black CM 2000. Multiple drug-resistant *Chlamydia trachomatis* associated with clinical treatment failure. J Infect Dis 181(4):1421-1427.
54. Rice RJ, Bhullar V, Mitchell SH, Bullard J, Knapp JS 1995. Susceptibilities of *Chlamydia trachomatis* isolates causing uncomplicated female genital tract infections and pelvic inflammatory disease. Antimicrob Agents Chemother 39(3):760-762.
55. Jones RB, Van der Pol B, Martin DH, Shepard MK 1990. Partial characterization of *Chlamydia trachomatis* isolates resistant to multiple antibiotics. J Infect Dis 162(6):1309-1315.

56. Girard MP, Steele D, Chaignat CL, Kieny MP 2006. A review of vaccine research and development: human enteric infections. Vaccine 24(15):2732-2750.
57. Katz DE, Coster TS, Wolf MK, Trespalacios FC, Cohen D, Robins G, Hartman AB, Venkatesan MM, Taylor DN, Hale TL 2004. Two studies evaluating the safety and immunogenicity of a live, attenuated *Shigella flexneri* 2a vaccine (SC602) and excretion of vaccine organisms in North American volunteers. Infect Immun 72(2):923-930.
58. Kotloff KL, Nataro JP, Losonsky GA, Wasserman SS, Hale TL, Taylor DN, Sadoff JC, Levine MM 1995. A modified Shigella volunteer challenge model in which the inoculum is administered with bicarbonate buffer: clinical experience and implications for *Shigella* infectivity. Vaccine 13(16):1488-1494.
59. Boyle EC, Bishop JL, Grassl GA, Finlay BB 2007. *Salmonella*: from pathogenesis to therapeutics. J Bacteriol 189(5):1489-1495.
60. Garmory HS, Brown KA, Titball RW 2002. *Salmonella* vaccines for use in humans: present and future perspectives. FEMS Microbiol Rev 26(4):339-353.
61. Guzman CA, Borsutzky S, Griot-Wenk M, Metcalfe IC, Pearman J, Collioud A, Favre D, Dietrich G 2006. Vaccines against typhoid fever. Vaccine 24(18):3804-3811.
62. Bondi SK, Goldberg JB 2008. Strategies toward vaccines against *Burkholderia mallei* and *Burkholderia pseudomallei*. Expert Rev Vaccines 7(9):1357-1365.
63. Priebe GP, Brinig MM, Hatano K, Grout M, Coleman FT, Pier GB, Goldberg JB 2002. Construction and characterization of a live, attenuated aroA deletion mutant of *Pseudomonas aeruginosa* as a candidate intranasal vaccine. Infect Immun 70(3):1507-1517.
64. Titball RW, Williamson ED 2004. *Yersinia pestis* (plague) vaccines. Expert Opin Biol Ther 4(6):965-973.
65. Damjanovic V 1972. Freeze-drying of live oral streptomycin-dependent mutant *Shigella* vaccines: survival of streptomycin-dependent *Shigella flexneri* 2a after freeze-drying. Cryobiology 9(6):565-568.
66. Stocker BA 1988. Auxotrophic *Salmonella* typhi as live vaccine. Vaccine 6(2):141-145.
67. Medina E, Guzman CA 2001. Use of live bacterial vaccine vectors for antigen delivery: potential and limitations. Vaccine 19(13-14):1573-1580.
68. Hopkins SA, Niedergang F, Corthesy-Theulaz IE, Kraehenbuhl JP 2000. A recombinant *Salmonella typhimurium* vaccine strain is taken up and survives within murine Peyer's patch dendritic cells. Cell Microbiol 2(1):59-68.
69. Tsunetsugu-Yokota Y, Ishige M, Murakami M 2007. Oral attenuated *Salmonella enterica* serovar Typhimurium vaccine expressing codon-optimized HIV type 1 Gag enhanced intestinal immunity in mice. AIDS Res Hum Retroviruses 23(2):278-286.
70. Konjufca V, Jenkins M, Wang S, Juarez-Rodriguez MD, Curtiss R, 3rd 2008. Immunogenicity of recombinant attenuated *Salmonella enterica* serovar

Typhimurium vaccine strains carrying a gene that encodes *Eimeria tenella* antigen SO7. Infect Immun 76(12):5745-5753.
71. Sadoff JC, Ballou WR, Baron LS, Majarian WR, Brey RN, Hockmeyer WT, Young JF, Cryz SJ, Ou J, Lowell GH, et al. 1988. Oral *Salmonella typhimurium* vaccine expressing circumsporozoite protein protects against malaria. Science 240(4850):336-338.
72. Al-Mariri A, Tibor A, Lestrate P, Mertens P, De Bolle X, Letesson JJ 2002. *Yersinia enterocolitica* as a vehicle for a naked DNA vaccine encoding *Brucella abortus* bacterioferritin or P39 antigen. Infect Immun 70(4):1915-1923.
73. Meyer KF, Cavanaugh DC, Bartelloni PJ, Marshall JD, Jr. 1974. Plague immunization. I. Past and present trends. J Infect Dis 129:Suppl:S13-18.
74. Williams JE, Altieri PL, Berman S, Lowenthal JP, Cavanaugh DC 1980. Potency of killed plague vaccines prepared from avirulent *Yersinia pestis*. Bull World Health Organ 58(5):753-756.
75. Marshall JD, Jr., Bartelloni PJ, Cavanaugh DC, Kadull PJ, Meyer KF 1974. Plague immunization. II. Relation of adverse clinical reactions to multiple immunizations with killed vaccine. J Infect Dis 129:Suppl:S19-25.
76. Reisman RE 1970. Allergic reactions due to plague vaccine. J Allergy 46(1):49-55.
77. Amemiya K, Meyers JL, Trevino SR, Chanh TC, Norris SL, Waag DM 2006. Interleukin-12 induces a Th1-like response to *Burkholderia mallei* and limited protection in BALB/c mice. Vaccine 24(9):1413-1420.
78. Cripps AW, Peek K, Dunkley M, Vento K, Marjason JK, McIntyre ME, Sizer P, Croft D, Sedlak-Weinstein L 2006. Safety and immunogenicity of an oral inactivated whole-cell *pseudomonas aeruginosa* vaccine administered to healthy human subjects. Infect Immun 74(2):968-974.
79. Oberhelman RA, Kopecko DJ, Salazar-Lindo E, Gotuzzo E, Buysse JM, Venkatesan MM, Yi A, Fernandez-Prada C, Guzman M, Leon-Barua R, et al. 1991. Prospective study of systemic and mucosal immune responses in dysenteric patients to specific *Shigella* invasion plasmid antigens and lipopolysaccharides. Infect Immun 59(7):2341-2350.
80. Nelson M, Prior JL, Lever MS, Jones HE, Atkins TP, Titball RW 2004. Evaluation of lipopolysaccharide and capsular polysaccharide as subunit vaccines against experimental melioidosis. J Med Microbiol 53(Pt 12):1177-1182.
81. Sarkar-Tyson M, Thwaite JE, Harding SV, Smither SJ, Oyston PC, Atkins TP, Titball RW 2007. Polysaccharides and virulence of *Burkholderia pseudomallei*. J Med Microbiol 56(Pt 8):1005-1010.
82. Cohen D, Ashkenazi S, Green M, Lerman Y, Slepon R, Robin G, Orr N, Taylor DN, Sadoff JC, Chu C, Shiloach J, Schneerson R, Robbins JB 1996. Safety and immunogenicity of investigational *Shigella conjugate* vaccines in Israeli volunteers. Infect Immun 64(10):4074-4077.
83. Cohen D, Ashkenazi S, Green MS, Gdalevich M, Robin G, Slepon R, Yavzori M, Orr N, Block C, Ashkenazi I, Shemer J, Taylor DN, Hale TL, Sadoff JC, Pavliakova D, Schneerson R, Robbins JB 1997. Double-blind vaccine-controlled

randomised efficacy trial of an investigational *Shigella sonnei* conjugate vaccine in young adults. Lancet 349(9046):155-159.
84. Phalipon A, Costachel C, Grandjean C, Thuizat A, Guerreiro C, Tanguy M, Nato F, Vulliez-Le Normand B, Belot F, Wright K, Marcel-Peyre V, Sansonetti PJ, Mulard LA 2006. Characterization of functional oligosaccharide mimics of the *Shigella flexneri* serotype 2a O-antigen: implications for the development of a chemically defined glycoconjugate vaccine. J Immunol 176(3):1686-1694.
85. Harland DN, Chu K, Haque A, Nelson M, Walker NJ, Sarkar-Tyson M, Atkins TP, Moore B, Brown KA, Bancroft G, Titball RW, Atkins HS 2007. Identification of a LolC homologue in *Burkholderia pseudomallei*, a novel protective antigen for melioidosis. Infect Immun 75(8):4173-4180.
86. Ohama M, Hiramatsu K, Miyajima Y, Kishi K, Nasu M, Kadota J 2006. Intratracheal immunization with pili protein protects against mortality associated with *Pseudomonas aeruginosa* pneumonia in mice. FEMS Immunol Med Microbiol 47(1):107-115.
87. Hefty PS, Stephens RS 2007. Chlamydial type III secretion system is encoded on ten operons preceded by sigma 70-like promoter elements. J Bacteriol 189(1):198-206.
88. Gophna U, Ron EZ, Graur D 2003. Bacterial type III secretion systems are ancient and evolved by multiple horizontal-transfer events. Gene 312:151-163.
89. Pozidis C, Chalkiadaki A, Gomez-Serrano A, Stahlberg H, Brown I, Tampakaki AP, Lustig A, Sianidis G, Politou AS, Engel A, Panopoulos NJ, Mansfield J, Pugsley AP, Karamanou S, Economou A 2003. Type III protein translocase: HrcN is a peripheral ATPase that is activated by oligomerization. J Biol Chem 278(28):25816-25824.
90. Akeda Y, Galan JE 2005. Chaperone release and unfolding of substrates in type III secretion. Nature 437(7060):911-915.
91. Blocker A, Jouihri N, Larquet E, Gounon P, Ebel F, Parsot C, Sansonetti P, Allaoui A 2001. Structure and composition of the *Shigella flexneri* "needle complex", a part of its type III secreton. Mol Microbiol 39(3):652-663.
92. Kubori T, Sukhan A, Aizawa SI, Galan JE 2000. Molecular characterization and assembly of the needle complex of the *Salmonella typhimurium* type III protein secretion system. Proc Natl Acad Sci U S A 97(18):10225-10230.
93. Hoiczyk E, Blobel G 2001. Polymerization of a single protein of the pathogen *Yersinia enterocolitica* into needles punctures eukaryotic cells. Proc Natl Acad Sci U S A 98(8):4669-4674.
94. Cordes FS, Komoriya K, Larquet E, Yang S, Egelman EH, Blocker A, Lea SM 2003. Helical structure of the needle of the type III secretion system of *Shigella flexneri*. J Biol Chem 278(19):17103-17107.
95. Kubori T, Matsushima Y, Nakamura D, Uralil J, Lara-Tejero M, Sukhan A, Gal, aacute, n JE, Aizawa S-I 1998. Supramolecular Structure of the *Salmonella typhimurium* Type III Protein Secretion System. Science 280(5363):602-605.

96. Cordes FS, Daniell S, Kenjale R, Saurya S, Picking WL, Picking WD, Booy F, Lea SM, Blocker A 2005. Helical packing of needles from functionally altered *Shigella* type III secretion systems. J Mol Biol 354(2):206-211.
97. Journet L, Agrain C, Broz P, Cornelis GR 2003. The needle length of bacterial injectisomes is determined by a molecular ruler. Science 302(5651):1757-1760.
98. Marlovits TC, Kubori T, Lara-Tejero M, Thomas D, Unger VM, Galan JE 2006. Assembly of the inner rod determines needle length in the type III secretion injectisome. Nature 441(7093):637-640.
99. Espina M, Olive AJ, Kenjale R, Moore DS, Ausar SF, Kaminski RW, Oaks EV, Middaugh CR, Picking WD, Picking WL 2006. IpaD Localizes to the Tip of the Type III Secretion System Needle of *Shigella flexneri*. Infect Immun 74(8):4391-4400.
100. Mueller CA, Broz P, Mueller SA, Ringler P, Erne-Brand F, Sorg I, Kuhn M, Engel A, Cornelis GR 2005. The V-Antigen of *Yersinia* Forms a Distinct Structure at the Tip of Injectisome Needles. Science (Washington, DC, United States) 310(5748):674-676.
101. Johnson S, Roversi P, Espina M, Olive A, Deane JE, Birket S, Field T, Picking WD, Blocker AJ, Galyov EE, Picking WL, Lea SM 2006. Self-chaperoning of the type III secretion system needle tip proteins IpaD and BipD. J Biol Chem:M607945200.
102. Derewenda U, Mateja A, Devedjiev Y, Routzahn KM, Evdokimov AG, Derewenda ZS, Waugh DS 2004. The structure of *Yersinia pestis* V-antigen, an essential virulence factor and mediator of immunity against plague. Structure (Cambridge, MA, United States) 12(2):301-306.
103. Erskine PT, Knight MJ, Ruaux A, Mikolajek H, Sang NW, Withers J, Gill R, Wood SP, Wood M, Fox GC, Cooper JB 2006. High Resolution Structure of BipD: An Invasion Protein Associated with the Type III Secretion System of *Burkholderia Pseudomallei*. J Mol Biol 363(1):125-136.
104. Deane JE, Roversi P, Cordes FS, Johnson S, Kenjale R, Daniell S, Booy F, Picking WD, Picking WL, Blocker AJ, Lea SM 2006. Molecular model of a type III secretion system needle: Implications for host-cell sensing. Proc Natl Acad Sci USA 103(33):12529-12533.
105. Picking WL, Nishioka H, Hearn PD, Baxter MA, Harrington AT, Blocker A, Picking WD 2005. IpaD of *Shigella flexneri* is independently required for regulation of Ipa protein secretion and efficient insertion of IpaB and IpaC into host membranes. Infect Immun 73(3):1432-1440.
106. Blocker AJ, Deane JE, Veenendaal AK, Roversi P, Hodgkinson JL, Johnson S, Lea SM 2008. What's the point of the type III secretion system needle? Proc Natl Acad Sci U S A 105(18):6507-6513.
107. Olive AJ, Kenjale R, Espina M, Moore DS, Picking WL, Picking WD 2007. Bile salts stimulate recruitment of IpaB to the *Shigella flexneri* surface, where it colocalizes with IpaD at the tip of the type III secretion needle. Infect Immun 75(5):2626-2629.

108. Stensrud KF, Adam PR, La Mar CD, Olive AJ, Lushington GH, Sudharsan R, Shelton NL, Givens RS, Picking WL, Picking WD 2008. Deoxycholate interacts with IpaD of *Shigella flexneri* in inducing the recruitment of IpaB to the type III secretion apparatus needle tip. J Biol Chem 283(27):18646-18654.
109. Caroline G, Eric F, Bohn YS, Sylvie E, Attree I 2008. Oligomerization of PcrV and LcrV, protective antigens of *Pseudomonas aeruginosa* and *Yersinia pestis*. J Biol Chem 283(35):23940-23949.
110. Frank DW, Vallis A, Wiener-Kronish JP, Roy-Burman A, Spack EG, Mullaney BP, Megdoud M, Marks JD, Fritz R, Sawa T 2002. Generation and characterization of a protective monoclonal antibody to *Pseudomonas aeruginosa* PcrV. J Infect Dis 186(1):64-73.
111. Williamson ED, Eley SM, Stagg AJ, Green M, Russell P, Titball RW 2000. A single dose sub-unit vaccine protects against pneumonic plague. Vaccine 19(4-5):566-571.
112. Lawton WD, Erdman RL, Surgalla MJ 1963. Biosynthesis and Purification of V and W Antigen in *Pasteurella Pestis*. J Immunol 91:179-184.
113. Wake A, Maruyama T, Akiyama Y, Yamamoto M 1983. The role of virulence antigen (VW) in the protection of mice against *Yersinia pestis* infection. Curr Microbiol 8:73-77.
114. Roy-Burman A, Savel RH, Racine S, Swanson BL, Revadigar NS, Fujimoto J, Sawa T, Frank DW, Wiener-Kronish JP 2001. Type III protein secretion is associated with death in lower respiratory and systemic Pseudomonas aeruginosa infections. J Infect Dis 183(12):1767-1774.
115. Sawa T, Yahr TL, Ohara M, Kurahashi K, Gropper MA, Wiener-Kronish JP, Frank DW 1999. Active and passive immunization with the *Pseudomonas* V antigen protects against type III intoxication and lung injury. Nat Med 5(4):392-398.
116. Neely AN, Holder IA, Wiener-Kronish JP, Sawa T 2005. Passive anti-PcrV treatment protects burned mice against *Pseudomonas aeruginosa* challenge. Burns 31(2):153-158.
117. Leary SE, Williamson ED, Griffin KF, Russell P, Eley SM, Titball RW 1995. Active immunization with recombinant V antigen from *Yersinia pestis* protects mice against plague. Infect Immun 63(8):2854-2858.
118. Powell BS, Andrews GP, Enama JT, Jendrek S, Bolt C, Worsham P, Pullen JK, Ribot W, Hines H, Smith L, Heath DG, Adamovicz JJ 2005. Design and testing for a nontagged F1-V fusion protein as vaccine antigen against bubonic and pneumonic plague. Biotechnol Prog 21(5):1490-1510.
119. Elvin SJ, Eyles JE, Howard KA, Ravichandran E, Somavarappu S, Alpar HO, Williamson ED 2006. Protection against bubonic and pneumonic plague with a single dose microencapsulated sub-unit vaccine. Vaccine 24(20):4433-4439.
120. Wang S, Heilman D, Liu F, Giehl T, Joshi S, Huang X, Chou TH, Goguen J, Lu S 2004. A DNA vaccine producing LcrV antigen in oligomers is effective in protecting mice from lethal mucosal challenge of plague. Vaccine 22(25-26):3348-3357.

121. Saha S, Takeshita F, Sasaki S, Matsuda T, Tanaka T, Tozuka M, Takase K, Matsumoto T, Okuda K, Ishii N, Yamaguchi K, Klinman DM, Xin KQ, Okuda K 2006. Multivalent DNA vaccine protects mice against pulmonary infection caused by *Pseudomonas aeruginosa*. Vaccine 24(37-39):6240-6249.
122. Nakajima R, Motin VL, Brubaker RR 1995. Suppression of cytokines in mice by protein A-V antigen fusion peptide and restoration of synthesis by active immunization. Infect Immun 63(8):3021-3029.
123. Nedialkov YA, Motin VL, Brubaker RR 1997. Resistance to lipopolysaccharide mediated by the *Yersinia pestis* V antigen-polyhistidine fusion peptide: amplification of interleukin-10. Infect Immun 65(4):1196-1203.
124. Depaolo RW, Tang F, Kim I, Han M, Levin N, Ciletti N, Lin A, Anderson D, Schneewind O, Jabri B 2008. Toll-like receptor 6 drives differentiation of tolerogenic dendritic cells and contributes to LcrV-mediated plague pathogenesis. Cell Host Microbe 4(4):350-361.
125. Hill J, Leary SE, Griffin KF, Williamson ED, Titball RW 1997. Regions of *Yersinia pestis* V antigen that contribute to protection against plague identified by passive and active immunization. Infect Immun 65(11):4476-4482.
126. Vernazza C, Lingard B, Flick-Smith HC, Baillie LW, Hill J, Atkins HS 2009. Small protective fragments of the *Yersinia pestis* V antigen. Vaccine 27(21):2775-2780.
127. Overheim KA, Depaolo RW, Debord KL, Morrin EM, Anderson DM, Green NM, Brubaker RR, Jabri B, Schneewind O 2005. LcrV plague vaccine with altered immunomodulatory properties. Infect Immun 73(8):5152-5159.
128. Oaks EV, Picking WD, Picking WL 1996. Antibody response of monkeys to invasion plasmid antigen D after infection with *Shigella* spp. Clin Diagn Lab Immunol 3(2):242-245.
129. Turbyfill KR, Mertz JA, Mallett CP, Oaks EV 1998. Identification of epitope and surface-exposed domains of *Shigella flexneri* invasion plasmid antigen D (IpaD). Infect Immun 66(5):1999-2006.
130. Druar C, Yu F, Barnes JL, Okinaka RT, Chantratita N, Beg S, Stratilo CW, Olive AJ, Soltes G, Russell ML, Limmathurotsakul D, Norton RE, Ni SX, Picking WD, Jackson PJ, Stewart DI, Tsvetnitsky V, Picking WL, Cherwonogrodzky JW, Ketheesan N, Peacock SJ, Wiersma EJ 2008. Evaluating *Burkholderia pseudomallei* Bip proteins as vaccines and Bip antibodies as detection agents. FEMS Immunol Med Microbiol 52(1):78-87.
131. Brandau DT, . JLS, C.M. W, C. R, Middaugh CR 2003. Thermal stability of vaccines. Journal of Pharmaceutical Sciences 92(2):218-231.
132. Kueltzo LA, Ersoy B, Ralston JP, Middaugh CR 2003. Derivative absorbance spectroscopy and protein phase diagrams as tools for comprehensive protein characterization: A bGCSF case study. J Pharm Sci 92(9):1805-1820.
133. Fan H, Kashi RS, Middaugh CR 2006. Conformational lability of two molecular chaperones Hsc70 and gp96: effects of pH and temperature. Arch Biochem Biophys 447(1):34-45.

134. Frokjaer S, Otzen DE 2005. Protein drug stability: a formulation challenge. Nat Rev Drug Discov 4(4):298-306.
135. Kendrick BS, Chang BS, Arakawa T, Peterson B, Randolph TW, Manning MC, Carpenter JF 1997. Preferential exclusion of sucrose from recombinant interleukin-1 receptor antagonist: role in restricted conformational mobility and compaction of native state. Proc Natl Acad Sci U S A 94(22):11917-11922.
136. Lee JC, Timasheff SN 1981. The stabilization of proteins by sucrose. J Biol Chem 256(14):7193-7201.
137. Timasheff SN 1993. The control of protein stability and association by weak interactions with water: how do solvents affect these processes? Annu Rev Biophys Biomol Struct 22:67-97.
138. Vogel FR, Hem SL. 2004. Immunologic Adjuvant. In Plotkin SA, Orenstein WA, editors. Vaccines, 4th ed., Philadelphia, PA: Elsevier, Inc. p 69-79.
139. Cox JC, Coulter AR 1997. Adjuvants--a classification and review of their modes of action. Vaccine 15(3):248-256.

Chapter 2

pH Sensitivity of Type III Secretion System Tip Proteins

IpaD, BipD, SipD, LcrV and PcrV

2.1 Introduction

Gram-negative bacteria are responsible for some of the most serious epidemics in history and continue to cause serious outbreaks in modern times. These bacteria cause conditions such as gastroenteritis (*Salmonella typhimurium, Yersinia enterocolitica*), septicemia (*Salmonella typhi, Pseudomonas aeruginosa* and *Yersinia Pestis*), lesions (*P. aeruginosa*), bacillary dysentery (*Shigella flexneri*) and melioidosis (*Burkholderia pseudomallei*). Common among these bacterial pathogens is the use of a type III secretion system (TTSS),[1] which ultimately transports proteins from the bacterium to the membrane and cytoplasm of targeted eukaryotic host cells to initiate bacterial infection.[1,2] The TTSS operates through a molecular needle comprised of repeating units of a protein connected to a basal body which spans the inner and outer bacterial membranes.[1-3] The external needle and basal body are referred to as the type III secretion apparatus (TTSA). Through this nanomachine, the translocator proteins are inserted into the host cell membrane to form a pore through which effectors subsequently pass into the host cell cytoplasm to subvert normal cellular processes.[1,2]

Recently, it was shown that invasion plasmid antigen D (IpaD) of *S. flexneri* localizes to the tip of the TTSA to control IpaB and IpaC secretion.[4] IpaB and IpaC form a translocon pore in the host cell membrane permitting the passage of effector proteins into the host cell cytoplasm.[5] IpaB and IpaC also induce cytoskeletal rearrangements in epithelial cells and apoptosis of macrophages.[5-7] LcrV in *Y.*

enterocolitica also localizes to the tip of the TTSA, therefore it may function analogously.[8] Antibodies to either LcrV or IpaD inhibit pore formation.[4,9] BipD from *B. pseudomallei* will localize to the *Shigella* TTSA[10] while PcrV from *P. aeruginosa* does the same in *Yersinia* TTSA.[8] The similarity of the response of SipD from *S. typhimurium* to temperature and pH, compared to IpaD and BipD, described below suggest that it also may localize to the tip of the TTSA.

Based on sequence homology and the conformational responses to pH and temperature reported here, the tip protein family can be divided into two sub-families. The IpaD sub-family consists of IpaD, BipD and SipD which have >25% sequence similarity overall and >90% similarity at the C-termini.[11-13] The crystal structures of BipD and IpaD have been solved. They are dumbbell shaped, possessing a coiled-coil that separates the N and C-terminal domains.[13] Studies of SipD also suggest the existence of two domains separated by a coiled-coil segment.[14] LcrV and PcrV belong to a second sub-family of tip proteins.[15] The LcrV crystal structure also displays a dumbbell shape[16] and it is likely that PcrV has a structure and function similar to LcrV.[8,15] All five of these proteins possess high helical content based on far-UV CD consistent with high resolution structural data.[14,17]

The purpose of this chapter is to systematically examine these five proteins with the goal of seeking common structural features that might be related to their regulatory functions. Some limited stability data exists for these tip proteins at pH 7.4.[14,17] It is probable, however, as discussed below, that these proteins encounter other pH conditions either in the gastrointestinal tract (in the case of *S. flexneri*, *S.*

typhimurium and *Y. enterocolitica*) or in pH microenvironments near cell membrane surfaces.[18,19] Thus, elucidating the conformation and stability of these proteins in different pH environments may reveal significant aspects of their functional relationships to each other. The results from the various analyses are summarized using empirical phase diagrams (EPDs).[20] The EPDs presented below display structural differences in proteins as a function of environmental variables of pH and temperature using color to provide an intuitive picture of molecular behavior. It has been demonstrated that such diagrams can reveal structural similarity related to function, even in the absence of sequence homology.[21]

2.2 Materials and Methods

2.2.1. Materials

Details of plasmid preparation and affinity purification of recombinant proteins are described previously.[14,15,17,22] The proteins were dialyzed in 20 mM citrate/20 mM phosphate buffer at pH 7 and then stored at -80 °C.

2.2.2 Sample Preparation

The samples were diluted to 0.14 mg/mL for UV absorption, CD and ANS fluorescence assays. The same concentration was used for intrinsic fluorescence studies except when collecting light scattering data where the concentrations were reduced to 0.07 mg/ml. The concentration of each sample was confirmed using UV absorption spectroscopy.[23] The samples were diluted in buffers at the desired pH

value. The dilution factor for all samples was at least 1:10 (in most cases 1:40). The final pH for each sample was then confirmed.

2.2.3 Ultraviolet Absorption Spectroscopy

An Agilent 8453 diode-array spectrophotometer in conjunction with a peltier temperature controller was used to obtain ultraviolet (UV) absorption spectra. Spectra for each protein were examined from 200-400 nm. The experimental resolution of each spectrum was 1 nm. The spectra were recorded over a temperature range of 10-90 °C at intervals of 2.5 °C. The optical density at 350 nm (OD_{350nm}) was similarly monitored over the same temperature range. The sample was incubated for 5 min at each temperature to ensure equilibrium (i.e. no further spectral change). The resulting spectra were analyzed using Agilent UV-visible ChemStation™ software using a fifth degree Savitzky-Golay polynomial after a 9 point filter to calculate the second derivative spectra.[20] The derivative spectra were then fit to a cubic function with 99 interpolated points. This provides an effective 0.01 nm resolution.

2.2.4 Far-UV circular dichroism

A Jasco J-720 spectrometer equipped with a peltier temperature controller (Tokyo, Japan) was used for far-UV circular dichroism (CD) analysis. CD spectra were obtained for each sample at 20 °C with a resolution of 0.1 nm at 20 nm/min. CD signals at 222 nm were monitored from 10 to 85 °C at a rate of 15 °C/hr to

measure changes in α-helical content with respect to temperature. CD signals were then converted to molar ellipticity using Microsoft® Excel 2002.

2.2.5 Trp fluorescence

Fluorescence spectra for both intrinsic and extrinsic fluorescence were collected using a PTI QM-1 spectrofluorimeter with a four cell position holder (Brunswick, NJ). The temperature of the cuvettes was controlled using a circulating water bath. The cuvettes used were quartz and had a 1 cm pathlength. For Trp fluorescence studies, the samples were excited at 295 nm (>95% Trp emission). Emission spectra were collected from 290-400 nm with resolution of 1 nm using 1 s of signal integration per point. Light scattering was measured by monitoring the intensity of the light at 295 nm at 180° from the fluorescence photomultiplier tube. Analysis was performed from 10 to 87.5 °C at 2.5 °C increments. A spectrum of citrate-phosphate buffer alone was subtracted from the sample spectra. Peak positions were calculated in Origin® by fitting the data to a 2° polynomial curve followed by a first derivative calculation.

2.2.6 ANS fluorescence

ANS was added from a 2 mg/ml ethanol solution to the sample to reach a 10:1 ANS/protein ratio. Samples were excited at 372 nm with emission spectra collected between 400 and 600 nm. Each spectrum was subtracted with a spectrum of buffer

and ANS alone at the corresponding temperature. Peak positions were obtained as in the Trp fluorescence analyses.

2.2.7 Empirical Phase Diagrams

The theory and mathematics underlying EPDs are covered in detail elsewhere.[20] At a given pH and temperature, data were combined from multiple techniques to create multi-dimensional vectors (each technique representing one dimension). Vectors were formed for all pH\temperature values and assembled to produce a density matrix. Eigenvectors and eigenvalues were calculated from the matrix. The three largest eigenvalues were used to create eigenvectors which would expand a truncated form of the data set to only three dimensions. These newly constructed vectors can be plotted as a combination of three colors (red, green and blue). Data from CD molar ellipticity at 222nm, the Trp fluorescence emission peak wavelength and intensity, light scattering, ANS emission peak wavelength and intensity, second derivative UV absorption negative peaks at 253, 259, 279, 284 and 291 and optical density at 350 nm as a function of temperature and pH were included to construct the EPDs.

2.3 Results

2.3.1 IpaD

All spectra displayed double minima at 208 nm and 222 nm at 20 °C (not illustrated), indicating substantial α-helical content.[24] This is consistent with a

previous study which estimated the percentage of α-helical structure to be 50% at pH 7.4.[17] Peak minima are most intense at pH 3 and smallest at pH 5 suggesting loss of secondary structure. The differences in peak intensity at 20 °C for 222 nm are seen in Figure 2.1A. The molar ellipticity of IpaD was measured from 10 to 85 °C in 2.5 °C increments at 222 nm to monitor changes in secondary structure (Figure 2.1A). Upon exposure to increasing temperature, two distinct thermal transitions are observed at pH 3. The onset temperature for the first transition is near 20 °C while the second begins at about 60 °C. At pH 4 and 5 only one broad transition occurs. Two transitions appear at pH 6-8 with the transitions occurring near 47 °C and 72 °C indicating greater stability under these pH conditions.

Intrinsic Trp fluorescence was recorded over the same pH range as that for CD to follow changes in tertiary structure of IpaD which possesses four Trp residues.[25] The initial peak positions at all pH values except 3 are very similar (ca. 329 nm) indicating the Trp residues are in comparable environments, which on average are relatively apolar (Figure 2.1B). At pH 3 the peak position at 10 °C is 333 nm which suggests the Trp residues are more solvent exposed. Biphasic thermal transitions are evident for pH 3 with the red shift of both transitions indicative of protein unfolding. At pH 4, a single red shifted transition is seen followed by a slight blue shift. Transitions at pH 5 and 6 are to shorter wavelengths and occur near 35 °C. These blue shifts precede considerable variability in individual peak values and greater uncertainty. This variability is probably due to aggregation. This conclusion is supported for pH 6 by both light scattering results obtained by measuring signal at

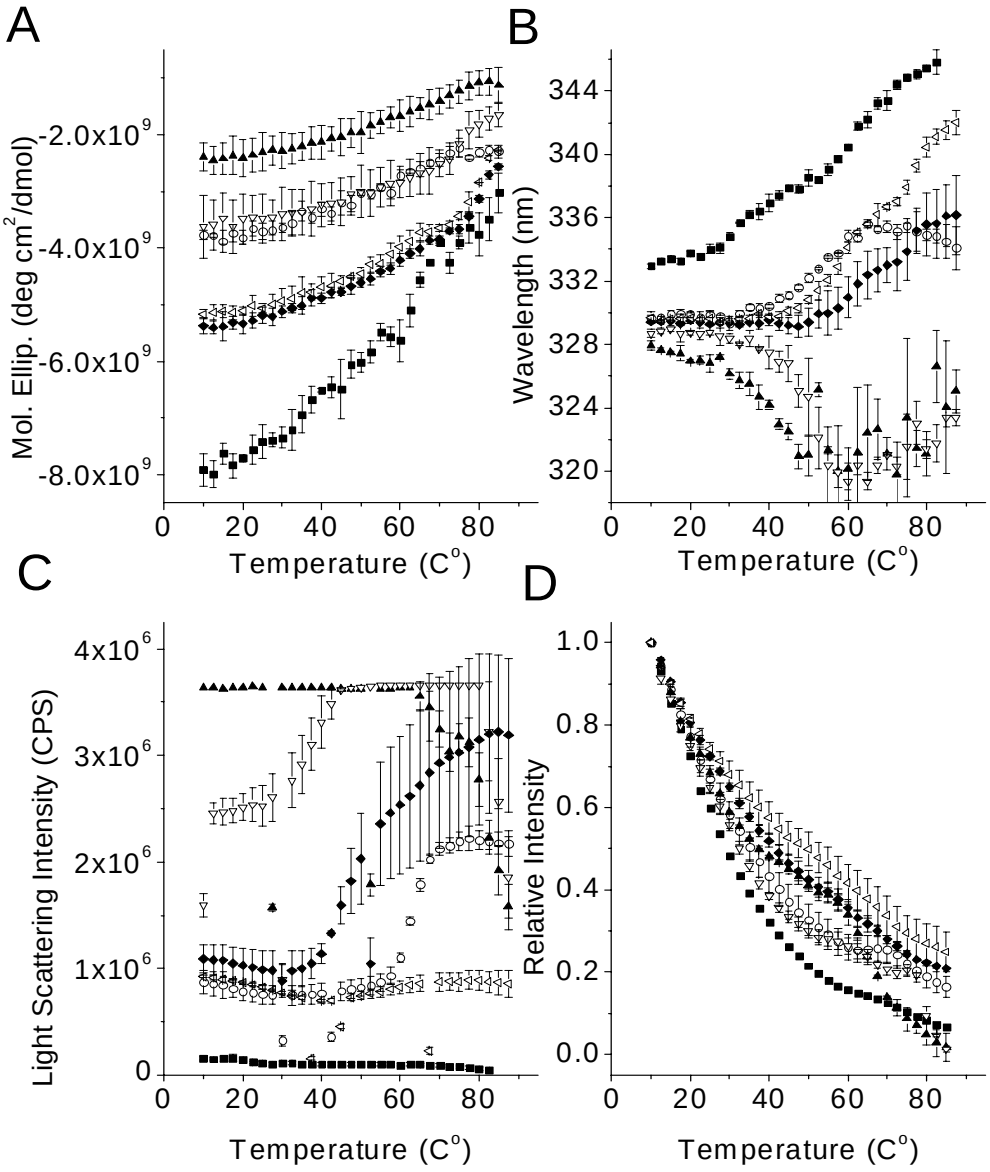

Figure 2.1. IpaD spectroscopic data. Far-UV CD molar ellipticity at 222 nm was monitored from 10 to 85 °C (A). Intrinsic Trp fluorescence emission peak position wavelength (B) and light scattering intensity at 295 nm (C) were measured from 10 to 87.5 °C. The excitation wavelength for Trp fluorescence is 295 nm. ANS fluorescence emission peak intensity (D) was measured from 10 to 87.5 °C. The excitation wavelength was 372 nm. ANS fluorescence peak intensity data were normalized to the intensity at 10 °C. Error bars are the standard deviation from at least three trials. ■, pH 3; ○, pH 4; ▲, pH 5; ▽, pH 6; ◆, pH 7; ◁, pH 8.

the excitation wavelength (295 nm) and turbidity data recorded at 350 nm during UV absorbance measurements (Figures 2.1C, 2.2C). The light scattering signal is saturated at pH 5; however, turbidity data are in agreement. Aggregation at pH 5 and 6 is not surprising given an isoelectric point (pI) of 5.55 for IpaD. For pH 7 and 8, biphasic transitions are evident similar to those at pH 3 (Figure 2.1B). Intrinsic Trp fluorescence peak intensity was also recorded for all five tip proteins but generally did not display any transitions not seen in the other techniques presented here.

The structure of IpaD was also probed using an extrinsic ANS probe. ANS molecules typically bind to apolar regions of molecules and increasingly fluoresce in response to such binding events.[26] Because of the negative charge on the dye, there may also be some electrostatic interactions with oppositely charged regions of proteins,[27] especially at low pH. Fluorescence wavelength positions were recorded with ANS dyes; however, the results exhibited little temperature dependence for any of the tip proteins being presented. The intensity data provided clearer trends despite the small scale of the transitions (Figure 2.1D). It is commonly postulated that when proteins unfold, ANS is able to bind to more apolar sites resulting in an increase in fluorescence. At pH 3, a spike in intensity occurs near the same temperature as the second transition seen in both the Trp fluorescence and CD studies. Transitions at pH 4-6 appear to reflect aggregation events since the onset temperatures of aggregation seen in static light scattering measurements are nearly identical to those observed in ANS fluorescence. Unlike pH 3, at pH 7 and 8 the transitions correspond to the first of the two thermal events observed in intrinsic fluorescence.

In addition to intrinsic Trp fluorescence, the IpaD tertiary structure was monitored using second derivative UV absorption spectroscopy. All three aromatic side chains in a protein can be monitored using this technique to provide a more global picture of tertiary structural changes.[28-30] IpaD has six Phe residues and ten Tyr residues in addition to the four Trp residues.[25] Shifts to shorter wavelengths in second derivative UV absorption spectroscopy indicate movement to a more polar environment. For the five recombinant proteins studied here, it is possible to resolve 6-8 major negative peaks using second derivative UV absorption spectroscopy. In this case, two peaks were selected for presentation which were consistently identifiable at all temperature and pH conditions. These peaks were a Tyr signal at 284 nm and a Trp minimum at 291 nm. Two Phe peaks are also present at 253 and 259 nm but these peaks were often independent of temperature and provided little new information. Simultaneous with measuring peak position, the optical density at 350 nm ($OD_{350\ nm}$) was recorded to detect possible temperature-induced aggregation.

In the case of the Tyr peak at 284 nm, the blue shifts for pH 3 and 4 have onset temperatures of 55 °C and 57 °C respectively (Figure 2.2A). The trend at pH 4, however, shows some attenuation of the blue shift and large uncertainty probably due to moderate aggregation. Red shifts accompanied by increased uncertainty in peak positions at pH 5 and 6 suggest aggregation as well. At pH 7 and 8, shifts to shorter wavelength at 65 °C agree with trends seen in both Trp fluorescence peak position and ANS fluorescence intensity. Almost identical trends occur for the peaks at 291 nm with blue shifts at all pH values with the exception of pH 4-6 which displays a red

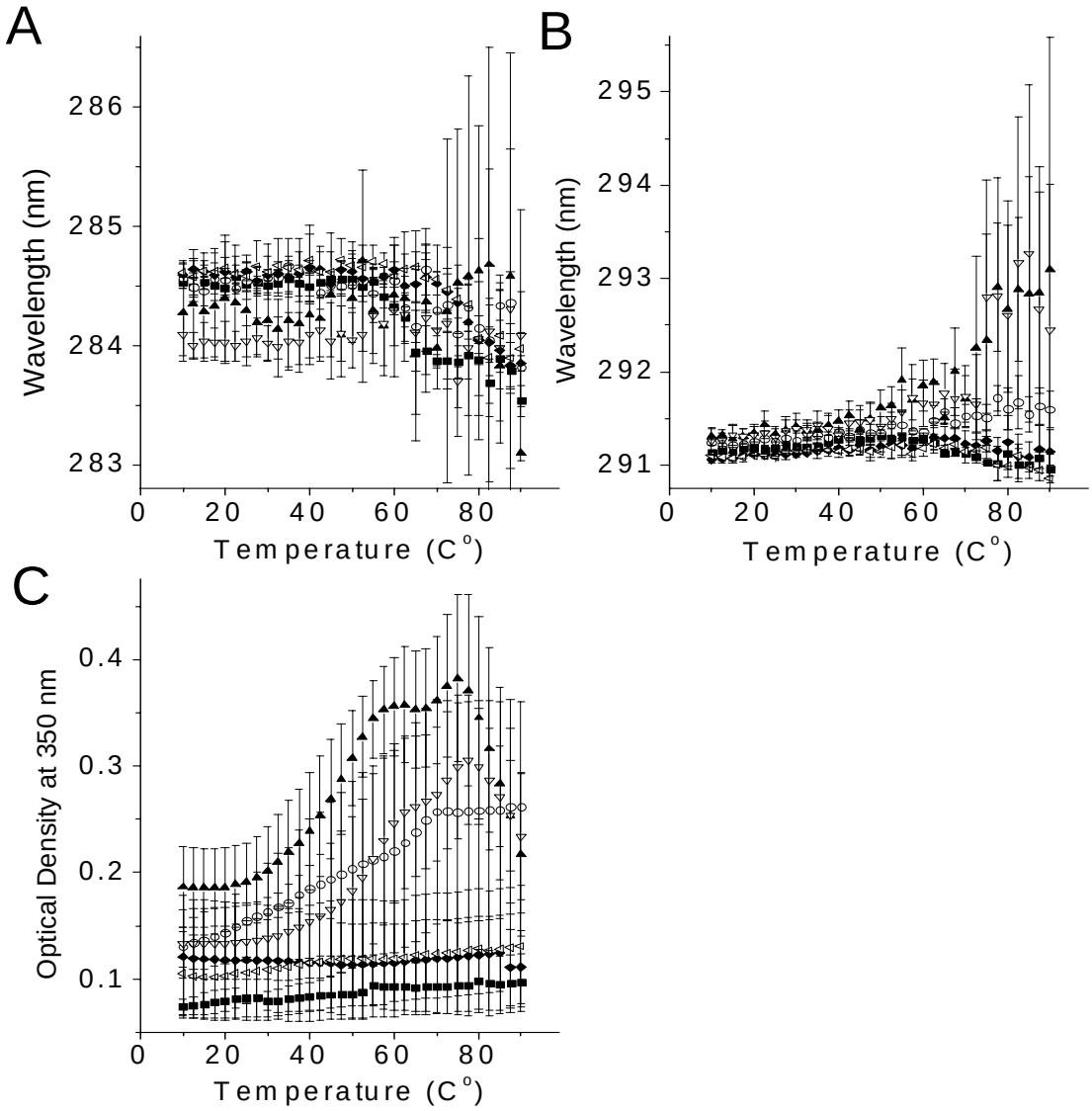

Figure 2.2. IpaD second derivative UV absorption spectroscopy. Absorption peak position minima centered around 285 nm (Tyr, A) and 291 nm (Trp, B) are recorded as a function of temperature from 10 to 90 °C. Optical densities at 350 nm (C) are recorded over the same temperature range. Error bars are the standard deviation from at least three trials. ■, pH 3; ○, pH 4; ▲, pH 5; ▽, pH 6; ◆, pH 7; ◁, pH 8.

shift at pH 4 immediately preceded by a small transition to shorter wavelengths (Figure 2.2B). Unlike CD and intrinsic fluorescence measurements which display multiple transitions, only one transition is clearly defined for transitions seen in most second derivative UV absorption spectroscopy melting curves. The turbidity data as measured by optical density at 350 nm agrees with the previously described light scattering data in that the major transitions indicative of aggregation occur at pH 5-6. The $OD_{350\ nm}$ data do not show any transition at pH 4 in contrast to right-angle light scattering reflecting the greater sensitivity of the latter.

2.3.2 BipD

The same conditions which were applied to IpaD were used for measurements taken of BipD and the three remaining proteins. Far-UV CD spectra of BipD from 190-260 nm display the characteristic double minima at 208 and 222 nm of α-helices (not illustrated). This is expected based on the high resolution X-ray structure of BipD which shows 59% α-helical content.[13] There is little variation in intensity of the two peaks with respect to pH at low temperature. Monitoring the CD spectra intensity at 222 nm shows a single thermal transition for BipD occurring at each pH which transpires at significantly higher temperatures than those seen for IpaD or other tip protein studied here (Figure 2.3A). The transition at pH 3 begins at 32 °C and is fairly broad. At pH 4, the transition begins at 65°C and is sharper than at pH 3 and ends at about 80 °C. Transitions at pH 5-8 do not begin until at least 75°C and are more abrupt.

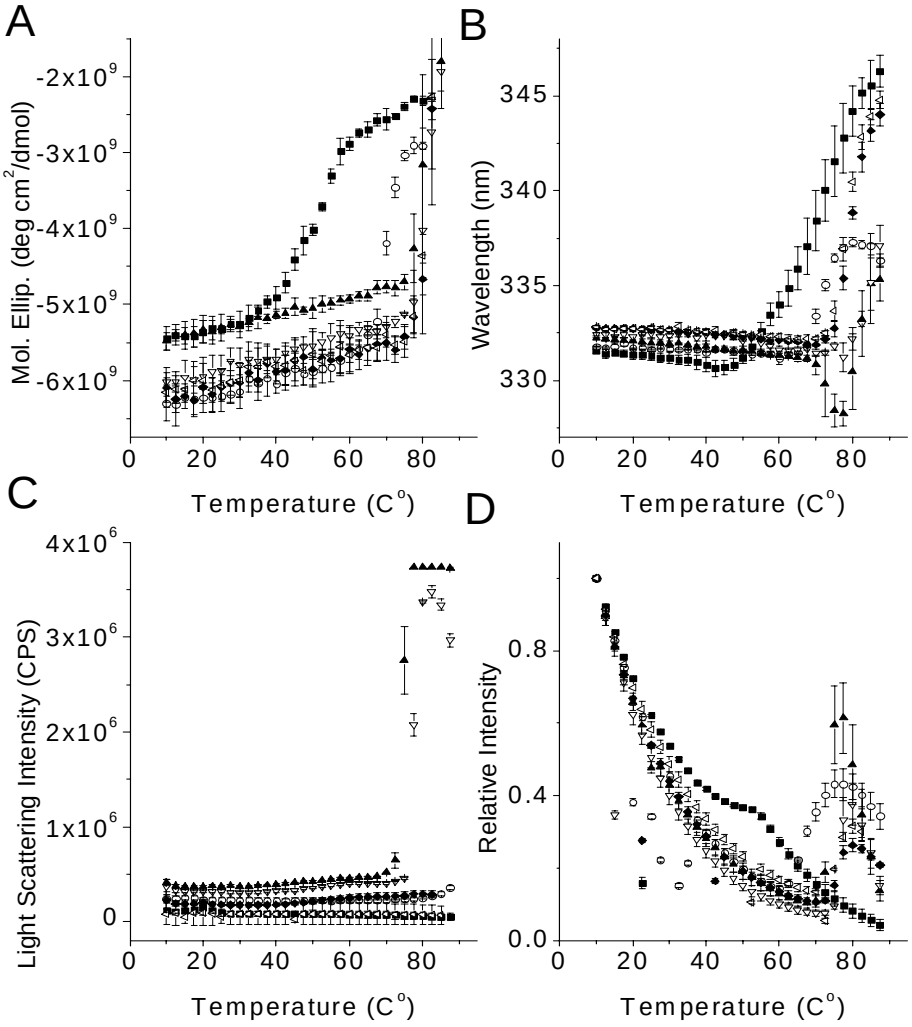

Figure 2.3. BipD spectroscopic data. Far-UV CD molar ellipticity at 222 nm was monitored from 10 to 85 °C (A). Intrinsic Trp fluorescence emission peak position wavelength (B) and light scattering intensity at 295 nm (C) were measured from 10 to 87.5 °C. The excitation wavelength for Trp fluorescence is 295 nm. ANS fluorescence emission peak intensity (D) was measured from 10 to 87.5 °C. The excitation wavelength was 372 nm. ANS fluorescence peak intensity data were normalized to the intensity at 10 °C. Error bars are the standard deviation from at least three trials. ■, pH 3; ○, pH 4; ▲, pH 5; ▽, pH 6; ◆, pH 7; ◁, pH 8.

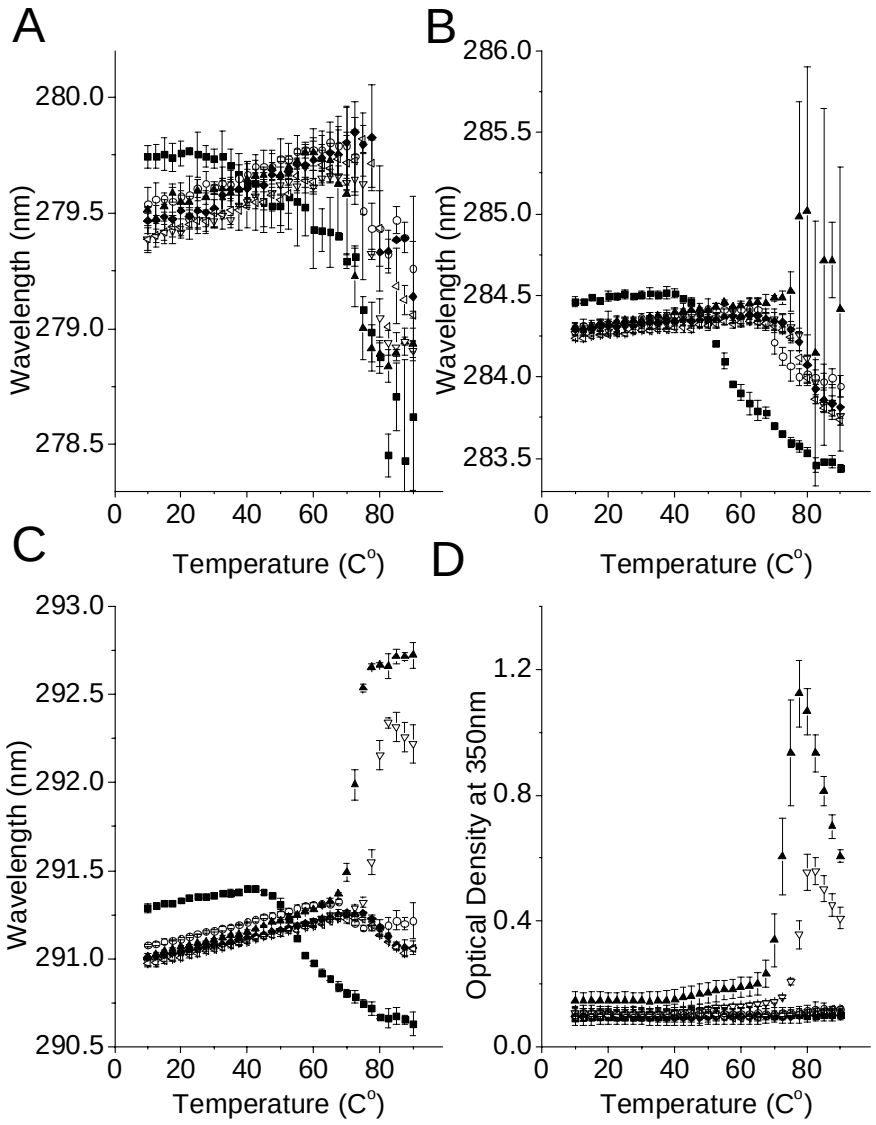

Figure 2.4. BipD second derivative UV absorption spectroscopy. Absorption peak position minima centered around 279 nm (Tyr/Trp, A), 285 nm (Tyr, B) and 291 nm (Trp, C) are recorded as a function of temperature from 10 to 90 °C. Optical densities at 350 nm (D) are recorded over the same temperature range. Error bars are the standard deviation from at least three trials. ■, pH 3; ○, pH 4; ▲, pH 5; ▽, pH 6; ◆, pH 7; ◁, pH 8.

Similar to CD measurements, transitions seen in intrinsic Trp fluorescence begin primarily after 70 °C for peak position data (Figure 2.3B). Also, like IpaD, the peak positions shift to longer wavelengths at high temperatures indicating the four Trp residues[31] are entering a more polar environment except at pH 5 and 6. At pH 5, an initial blue shift occurs at approximately 67 °C followed by a larger red shift beginning at 77 °C. While the transition at pH 4 is primarily a shift to longer wavelengths, it appears attenuated by possible aggregation as suggested by the large increase in error values.[32] This is confirmed by both light scattering and turbidity data (Figures 2.3C and 2.4D). Light scattering and $OD_{350\ nm}$ measurements for BipD reveal that significant aggregation occurs, primarily at pH 5 and 6. BipD has a pI of 5.04, which is consistent with the aggregation and precipitation observed under these conditions.

Transitions in ANS fluorescence peak intensity data also occur primarily after 70 °C (Figure 2.3D). The earliest transition is at pH 3 with an onset temperature of 37 °C. These results agree with those observed in either the temperature dependent CD or intrinsic fluorescence experiments. What is apparent from results produced by all of these techniques is the high stability of BipD compared to the other tip proteins except at low pH.

In addition to the two negative second derivative peaks shown above for IpaD, a Tyr/Trp peak at 279 nm was also resolved with BipD and the other tip proteins. BipD contains four Trp, six Phe (peaks not illustrated) and six Tyr residues.[31] The negative Tyr/Trp (279 nm) peak displays shifts to shorter wavelengths at all pH

conditions (Figure 2.4A). The negative Tyr peak at 284 nm shows transitions to shorter wavelengths for all pH environments except pH 5 (Figure 2.4B). The same is true for the Trp peak around 291 nm (Figure 2.4C) with it moving to longer wavelengths at both pH 5 and 6. The reason for the differences in trends at pH 6 between Figures 2.4B and 2.4C is not clear. Nevertheless, red shifts at pH 5 and 6 are consistent with data from the other techniques. The blue shifts present in Figure 2.4A suggest that some of the buried Tyr and Trp residues in BipD may be moving into more aqueous environments despite aggregation which might be expected to bury the aromatic side chains.

2.3.3 SipD

This protein also displays helix rich CD spectra (not illustrated) with the 208 and 222 nm peaks most intense at pH 4 and smallest at pH 6. A previous study estimated the percentage of α-helical structure to be 55%.[14] The differences in peak intensities observed across the spectra can be seen at 10 °C in Figure 2.5A. Molar ellipticity of SipD measured at 222 nm from 10 to 85 °C shows biphasic transitions for all pH conditions with the lowest onset temperatures at pH 3 (Figure 2.5A).

Intrinsic Trp fluorescence shows thermally induced conformational changes and aggregation (Figure 2.5B-C). Changes in peak position manifest low and high temperature transitions for all pH values, with the second transitions at pH 4-6

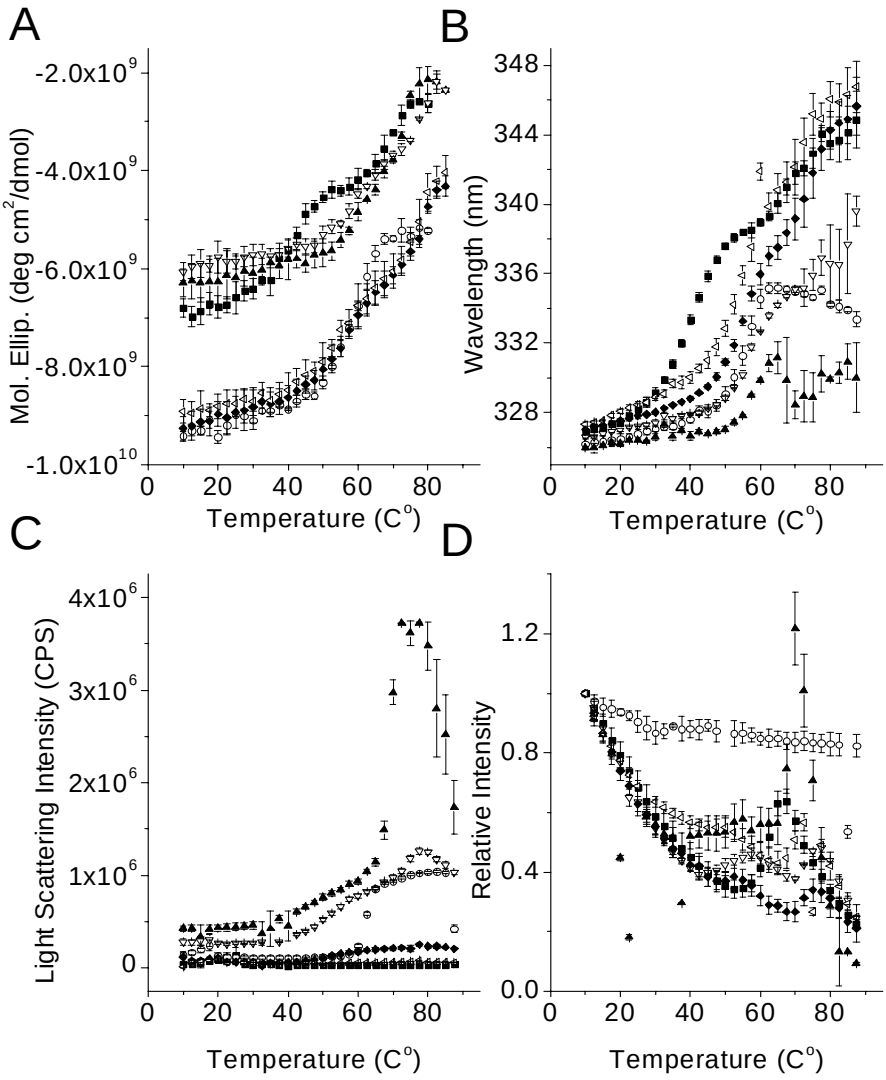

Figure 2.5. SipD spectroscopic data. Far-UV CD molar ellipticity at 222 nm was monitored from 10 to 85 °C (A). Intrinsic Trp fluorescence emission peak position wavelength (B) and light scattering intensity at 295 nm (C) were measured from 10 to 87.5 °C. The excitation wavelength for Trp fluorescence is 295 nm. ANS fluorescence emission peak intensity (D) was measured from 10 to 87.5 °C. The excitation wavelength was 372 nm. ANS fluorescence peak intensity data were normalized to the intensity at 10 °C. Error bars are the standard deviation from at least three trials. ■, pH 3; ○, pH 4; ▲, pH 5; ▽, pH 6; ◆, pH 7; ◁, pH 8.

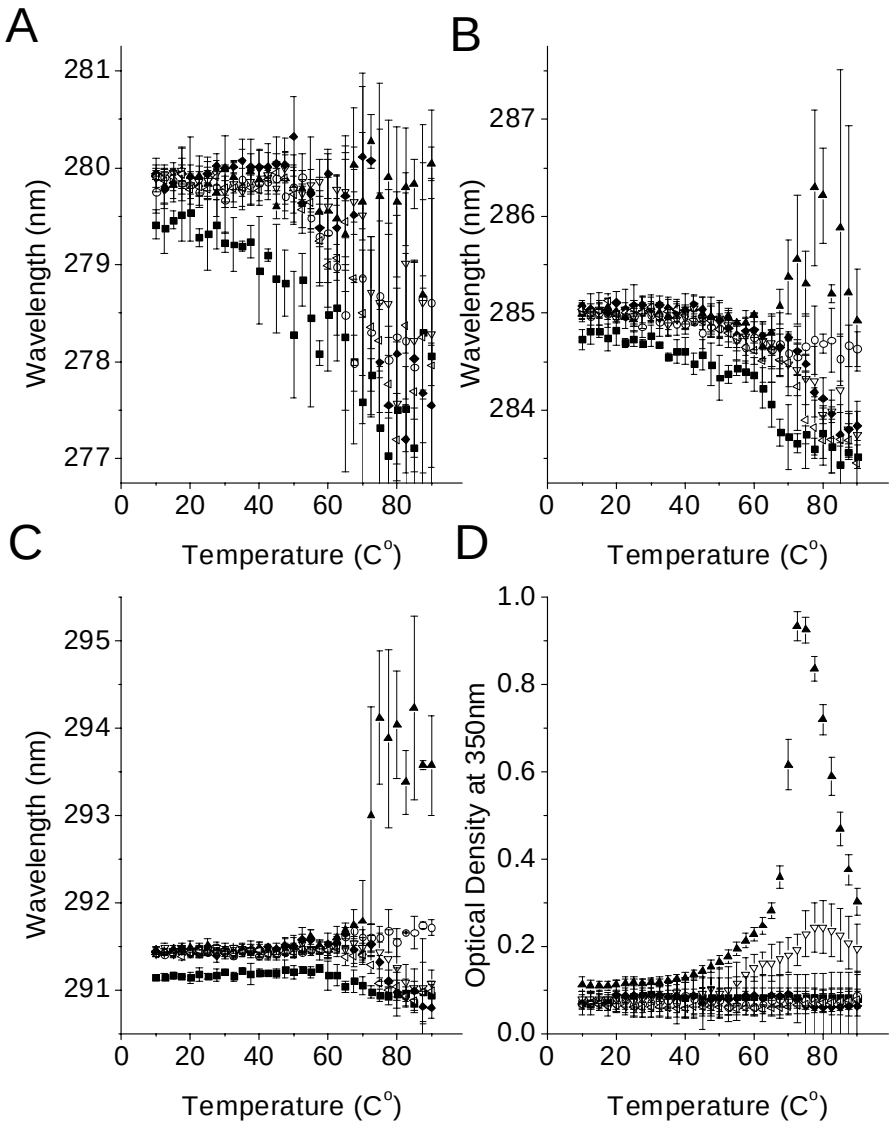

Figure 2.6. SipD second derivative UV absorption spectroscopy. Absorption peak position minima centered around 279 nm (Tyr/Trp, A), 285 nm (Tyr, B) and 291 nm (Trp, C) are recorded as a function of temperature from 10 to 90 °C. Optical densities at 350 nm (D) are recorded over the same temperature range. Error bars are the standard deviation from at least three trials. ■, pH 3; ○, pH 4; ▲, pH 5; ▽, pH 6; ◆, pH 7; ◁, pH 8.

indicating aggregation. At pH 4-6, the initial red shifts are followed by transitions that appear either as blue shifts or as attenuated shifts to longer wavelength with increased uncertainty in peak position values. Increases in both light scattering and turbidity indicate these trends are caused by aggregation (Figures 2.5C, 2.6D). As seen with BipD, the pI of SipD is near 5 suggesting that pH 5 and 6 is where insoluble aggregation would be expected. Extrinsic fluorescence employing ANS shows a transition in intensity at pH 3 corresponding to the second transitions observed by other techniques (Figure 2.5D). While no clear shift is visible at pH 4, pH 5 exhibits a transition at the temperature of protein aggregation. Biphasic transitions are visible at pH 6-8 in agreement with Trp fluorescence and CD thermal results.

SipD contains eleven Tyr, seven Phe (peaks not illustrated) and four Trp residues.[33] The Tyr/Trp peak at 279 nm manifests temperature-dependent blue shifts under most pH conditions suggesting movement to more polar environments (Figure 2.6A). Almost identical trends occur for the peaks at 285 and 291 nm with transitions to shorter wavelengths except at pH 4 and 5 (Figures 2.6B-C) in agreement with the other techniques. The $OD_{350\,nm}$ data shows the greatest aggregation at pH 5 with some occurring at pH 6 as well (Figure 2.6D). Unlike the right-angle light scattering results (Figure 2.5C), these is little increase in turbidity at pH 4.

2.3.4 LcrV

Far-UV CD spectra of LcrV at pH values from 3-8 show the characteristic negative peaks at 208 nm and 222 nm (not illustrated). This is again expected since the α-helical content estimated from a previous CD study is 68%.[14] CD spectra at pH 3 and 4 have more intense negative peaks implying greater secondary structure (see Figure 2.7A at 10 °C). The magnitudes of the peaks at pH 5-8 are within 0.5×10^{-9} deg cm^2/dmol of each other suggesting similar secondary structure content. The molar ellipticity of LcrV monitored at 222 nm from 10 to 85 °C shows transitions with onset temperatures which increase with increased pH with the exception of pH at 7 and 8 where the transition temperatures are nearly identical (Figure 2.7A). Only one transition appears at each pH from pH 5-8. At pH 3 and 4 however, some high temperature transitions may be occurring near 80 °C.

The intrinsic Trp fluorescence of LcrV as a function of temperature shows shifts to lower wavelengths in fluorescence peak position at all pH conditions accompanied by increased light scattering (Figures 2.7B-C). The blue shifts seen in Figure 2.7B mark significant divergence from trends in the first three tip proteins where such transitions generally only occurred at pH 5 and 6. The temperature of the transition rises with increased pH. While the transitions are occasionally difficult to see in Figure 2.7C, close inspection of the results at pH 3 and 8 indicate that these pH conditions follow the trends detected by the other techniques. The magnitude of the light scattering changes at pH 4-6 as well as the precipitation at pH 5 is explainable by the pI of 5.49. Unlike light scattering, $OD_{350\ nm}$ measurements only display clear

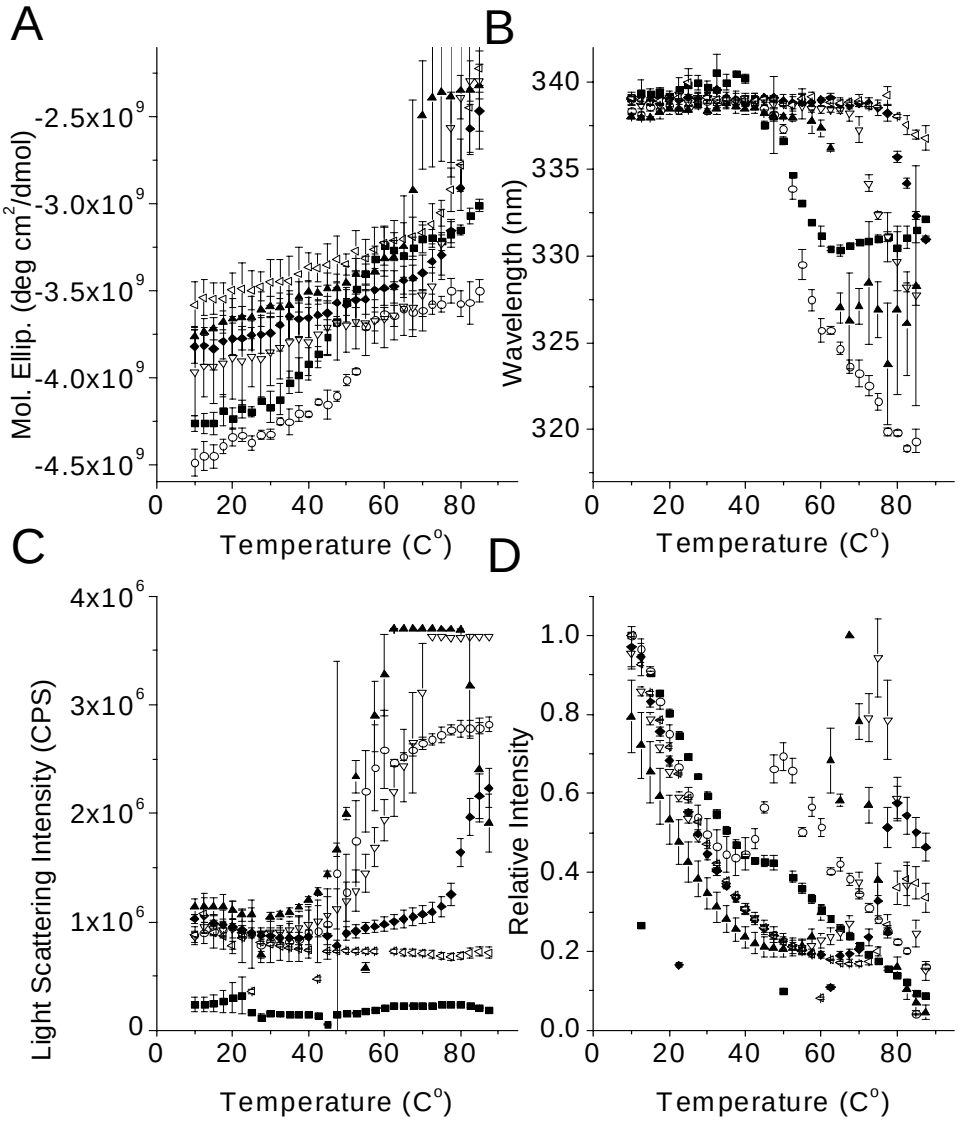

Figure 2.7. LcrV spectroscopic data. Far-UV CD molar ellipticity at 222 nm was monitored from 10 to 85 °C (A). Intrinsic Trp fluorescence emission peak position wavelength (B) and light scattering intensity at 295 nm (C) were measured from 10 to 87.5 °C. The excitation wavelength for Trp fluorescence is 295 nm. ANS fluorescence emission peak intensity (D) was measured from 10 to 87.5 °C. The excitation wavelength was 372 nm. ANS fluorescence peak intensity data were normalized to the intensity at 10 °C. Error bars are the standard deviation from at least three trials. ■, pH 3; ○, pH 4; ▲, pH 5; ▽, pH 6; ◆, pH 7; ◁, pH 8.

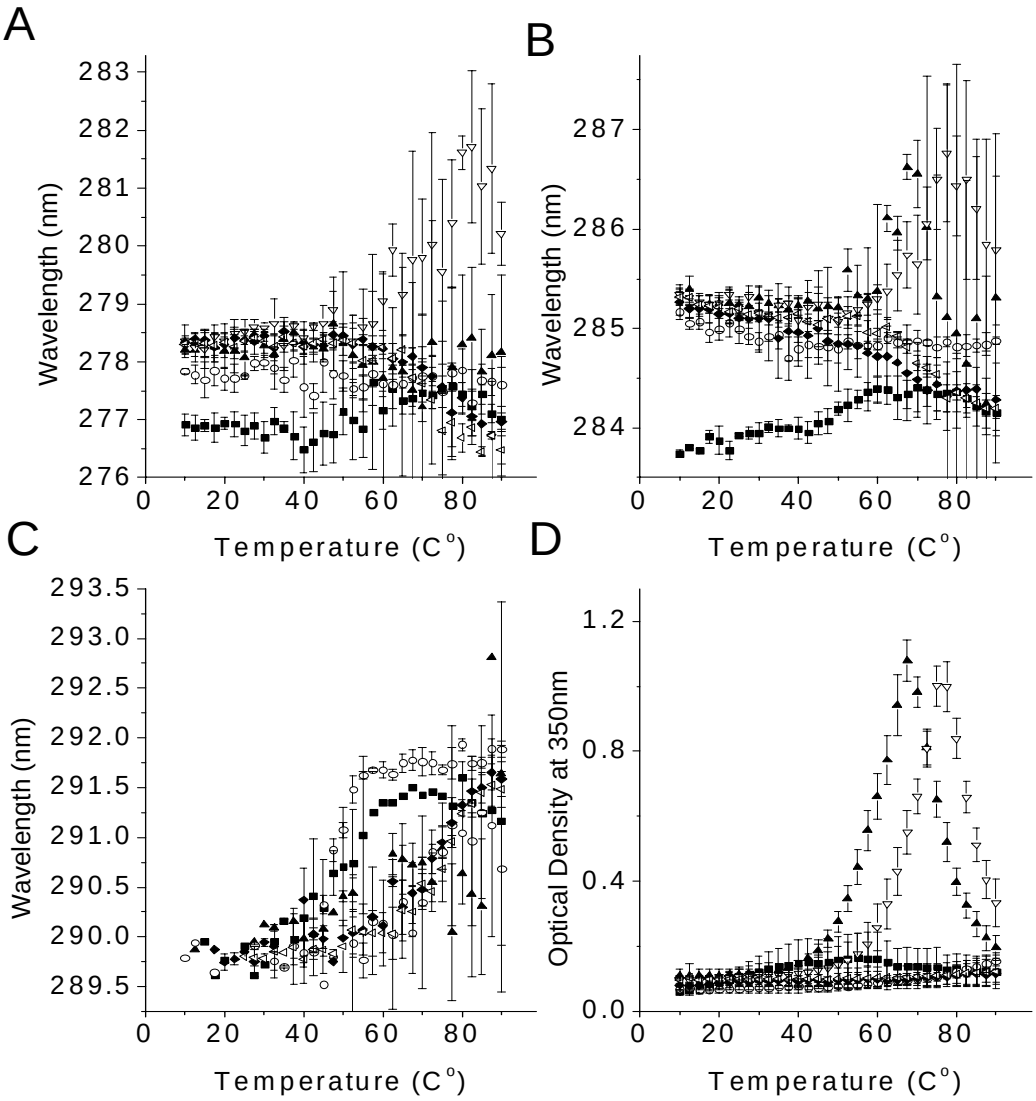

Figure 2.8. LcrV second derivative UV absorption spectroscopy. Absorption peak position minima centered around 279 nm (Tyr/Trp, A), 285 nm (Tyr, B) and 291 nm (Trp, C) are recorded as a function of temperature from 10 to 90 °C. Optical densities at 350 nm (D) are recorded over the same temperature range. Error bars are the standard deviation from at least three trials. ■, pH 3; ○, pH 4; ▲, pH 5; ▽, pH 6; ◆, pH 7; ◁, pH 8.

transitions at pH 5 and 6 (Figure 2.8D). Employing the ANS probe, the relative peak intensity data has the same temperature transition trends seen by the other techniques, except at pH 3 for which transitions occur later than pH 4 (Figure 2.7D).

Second derivative UV absorption spectroscopy of LcrV partially supports the trends seen in tertiary structure behavior by the fluorescence techniques (Figures 2.8A-C). LcrV contains a single Trp, eleven Phe (peaks not illustrated) and eleven Tyr residues.[34] The peak at 279 nm at pH 7 and 8 shows transitions to shorter wavelength (Figure 2.8A). The behavior of these transitions is not in complete agreement with the intrinsic Trp fluorescence or the Trp second derivative negative data near 290 nm (Figure 2.8C). The negative peak for Tyr at 285 nm also shows transitions to shorter wavelengths at pH 7 and 8 (Figure 2.8B). This is possible since residues may enter a more polar environment despite aggregation. The second derivative peak at 290 nm is, however, in direct agreement with the intrinsic fluorescence data. The turbidity results only show significant transitions at pH 5-6 (Figure 2.8D).

2.3.5 *PcrV*

The far-UV CD spectra of PcrV are similar to those of the other proteins (not illustrated). The low pH environments at 3 and 4 elicit the most intense negative peaks again suggesting increased helical content. The peaks at pH 6 are the least intense indicating far less secondary structure. Measuring the intensity of the negative peak at 222 nm as a function of temperature produces transitions which

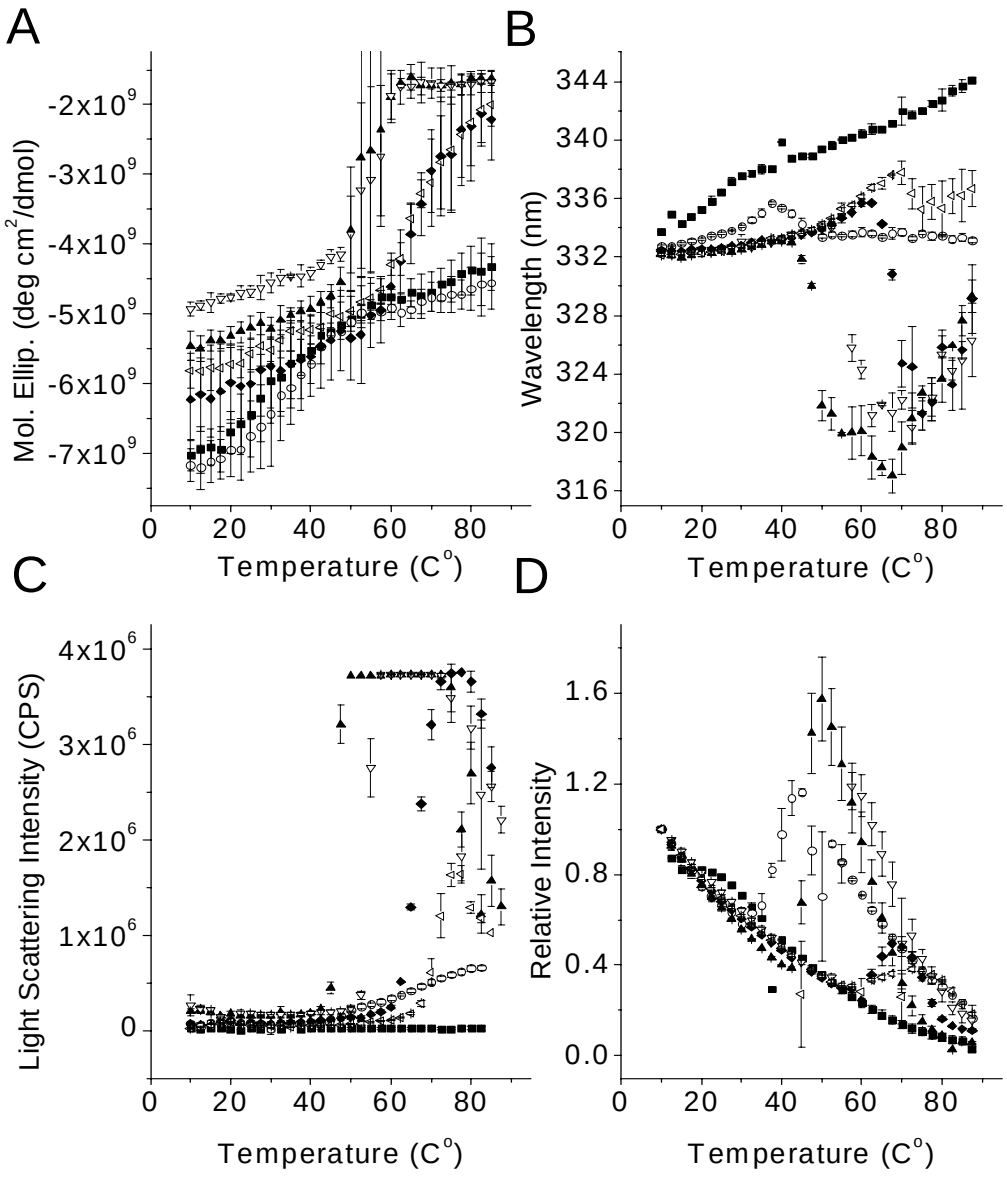

Figure 2.9. PcrV spectroscopic data. Far-UV CD molar ellipticity at 222 nm was monitored from 10 to 85 °C (A). Intrinsic Trp fluorescence emission peak position wavelength (B) and light scattering intensity at 295 nm (C) were measured from 10 to 87.5 °C. The excitation wavelength for Trp fluorescence is 295 nm. ANS fluorescence emission peak intensity (D) was measured from 10 to 87.5 °C. The excitation wavelength was 372 nm. ANS fluorescence peak intensity data were normalized to the intensity at 10 °C. Error bars are the standard deviation from at least three trials. ■, pH 3; (, pH 4; ▲, pH 5; ▽, pH 6; ◆, pH 7; ◁, pH 8.

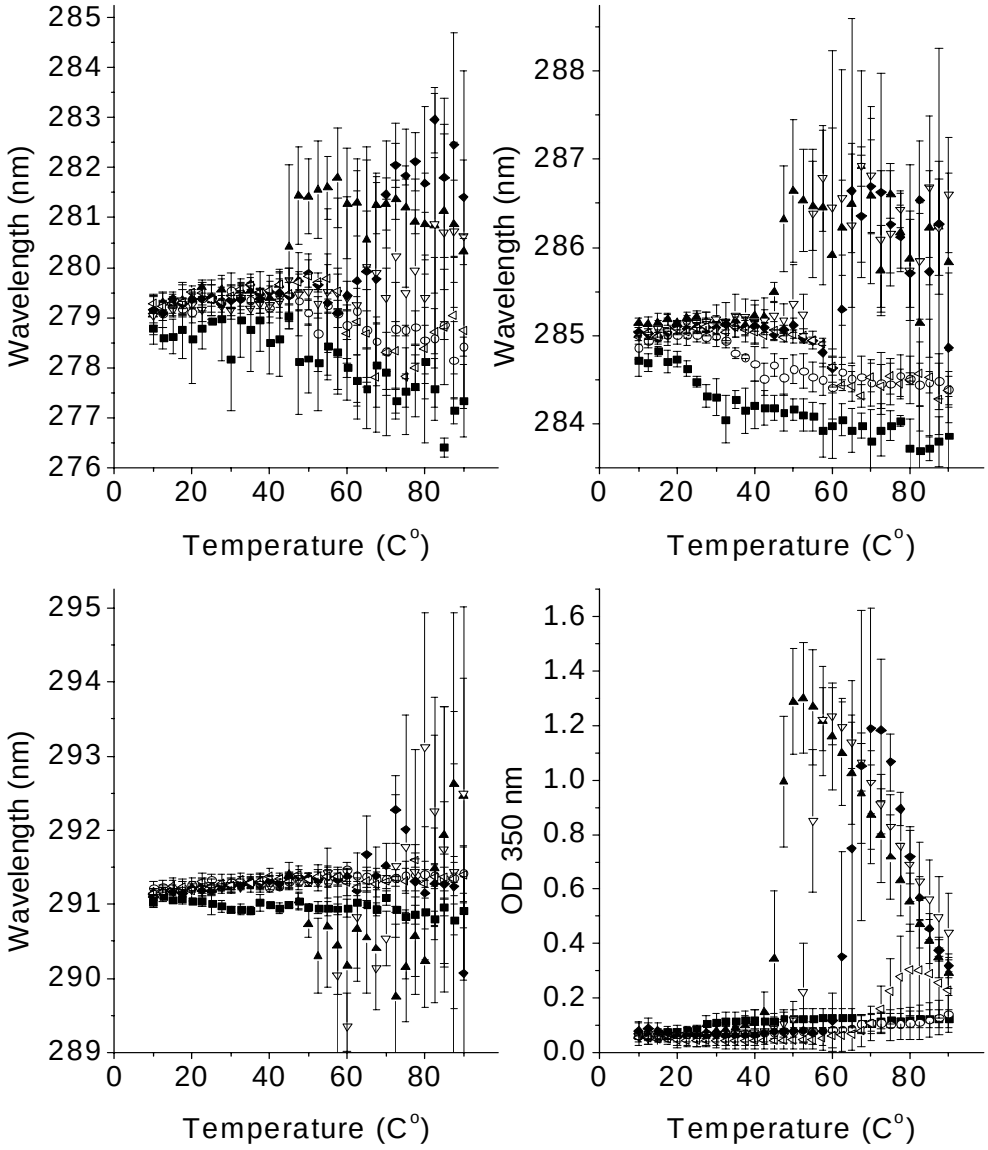

Figure 2.10. PcrV second derivative UV absorption spectroscopy. Absorption peak position minima centered around 279 nm (Tyr/Trp, A), 285 nm (Tyr, B) and 291 nm (Trp, C) are recorded as a function of temperature from 10 to 90 °C. Optical densities at 350 nm (D) are recorded over the same temperature range. Error bars are the standard deviation from at least three trials. ■, pH 3; ○, pH 4; ▲, pH 5; ▽, pH 6; ◆, pH 7; ◁, pH 8.

occur successively earlier as pH decreases (Figure 2.9A). The transitions at pH 5 and 6 are the sharpest with the onset temperature of pH 5 near 45 °C. The magnitude of the intensity change is comparable for all pH environments.

The intrinsic Trp fluorescence of PcrV displays different temperature/pH behavior than that seen for SipD, BipD or IpaD but very similar to trends exhibited by LcrV. At pH 3 and 4, low temperature transitions (about 20 and 27 °C, respectively) involve shifts to longer wavelengths although the early transition at pH 4 is followed by a shift to shorter wavelengths (Figure 2.9B). In the case of all other pH conditions, blue shifts occur indicating that the four Trp residues[35] move on average into a more non-polar environment. As observed with the far-UV CD results, higher transition temperatures appear to be directly related to increased pH. Light scattering (Figure 2.9C) shows the same pH/temperature relationship for pH 5-8 with some increase in light scattering also visible at pH 4 at higher temperatures. Extrinsic ANS fluorescence relative intensity in the presence of PcrV from 10 to 87.5 °C shows a small early shift at pH 3 (Figure 2.9D). The transitions in peak position for the other pH values vary directly with pH. This trend is in agreement with both far-UV CD and intrinsic Trp fluorescence temperature studies.

Second derivative UV absorption spectroscopy results for PcrV were not conclusive for all peaks (Figure 2.10A-C). PcrV contains three Trp, one Tyr and eight Phe (not illustrated) residues.[35] The peaks around 279 and 285 nm show similar trends (Figure 2.10A-B). Blue shifts are evident at pH 3 and 4 while red shifts appear to occur at pH 5-7. At pH 8, both peaks exhibit a transition to shorter wavelengths

implying movement into a more polar environment beginning at 55 °C. In the case of the Trp peak at 291 nm, no discernable transitions can be resolved (Figure 2.10C). At higher temperatures, the peak position appears to fluctuate erratically with sufficient error to make analysis of the average local environment of the 3 Trp residues impossible. Turbidity data measured by optical density at 350 nm agree well with the right-angle light scattering observed during the intrinsic Trp fluorescence studies (Figure 2.10E).

2.3.6 Empirical Phase Diagrams

An effective means to visually summarize data from a wide variety of different techniques into a single, intuitive form is by employing empirical phase diagrams (EPDs).[20,32,36-38] The EPDs presented here show the effects of pH and temperature on proteins expressed in the form of colored region as a function of temperature and pH. Each colored block is a vector representation of the results from all techniques at a given pH and temperature relative to the same measurements at all other temperature and pH conditions for the same protein. Colors that are identical (or nearly so) indicate structural similarity. Since these regions are empirically determined and no equilibrium is necessarily present between the different (non-thermodynamic) states of the protein, they are referred to as empirical or apparent phases. It should be noted that the colors in any particular phase diagram are arbitrarily selected because of the normalization process used to permit data comparisons and cannot be used to directly compare results between EPDs.

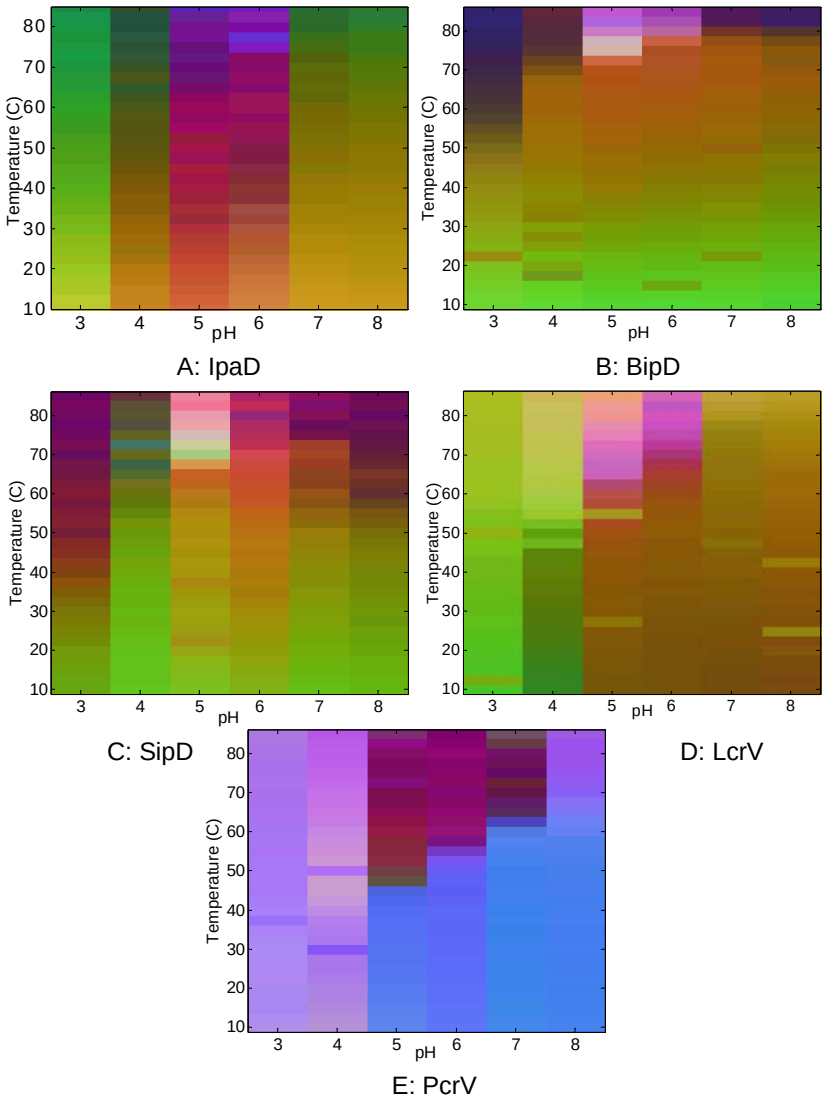

Figure 2.11. Empirical phase diagrams of five tip proteins. Empirical phase diagrams for IpaD (A), BipD (B) and SipD (C) show similar responses to pH and temperature. LcrV (D) and PcrV (E) phase diagrams exhibit similar trends as well. The empirical phase diagrams are created using all of the data presented in the previous figures.

An EPD for IpaD (Figure 2.11A) shows that the lower temperature regions at pH 4 and 7-8 have similar conformational states. At pH 7 two possible transitions appear with the initial change at about 35 °C and a second alteration at higher temperature. As the first transition is a less pronounced change in color, the trend at pH 7 could be considered as one broad transition from 35-70 °C however the results from intrinsic Trp fluorescence and CD suggest two thermal events are occurring. A transition begins at 25 °C at pH 4 and by 45 °C another conformation is evident. Even at low temperatures, the forms of IpaD at pH 5 and 6 are different from those at other pH values. Widely fluctuating colors at high temperatures are characteristic of aggregation and precipitation.[21,37]

The EPD for BipD displays an unexpected transition occurring under all pH conditions beginning at about 35 °C (Figure 2.11B). This transition is not directly observable in the data of the various techniques except perhaps in the ANS wavelength fluorescence experiments. When the ANS fluorescence data is removed however, the transition remains (not illustrated). It is therefore possible that this effect is an artifact of the intrinsic temperature effect on the CD and fluorescence peaks. Such results have been noted in studies of pure model amino acids using fluorescence and UV absorption spectroscopy and resultant temperature/pH EPDs.[21, unpublished results] As seen with IpaD, at higher temperatures there are clear conformational differences between pH 5-6 and lower and higher pH.

The empirical phase diagram for SipD shows evidence of conformational differences at pH 5 and 6 compared to the pH values at pH 4, 7 and 8 (Figure 2.11C).

As expected, at pH 3 the conformational state of SipD is also different. Two temperature transitions are visible for most pH conditions with aggregation occurring at pH 4-6. The transitions at pH 7 occur near 45 °C and 75 °C. The similarities in phase diagrams for IpaD and SipD indicate that both proteins respond analogously to pH and temperature. Indeed the similarities between these two tip proteins and also BipD suggest clear structural and presumably functional differences between them and LcrV and PcrV

The EPD for LcrV demonstrates fairly homogenous structural states at pH 5-8 at different forms at pH 3-4 (Figure 2.11D). As seen in the actual experimental data for the individual techniques, only a single temperature transition is visible which increases with increasing pH. Both the conformational continuity from pH 5-8 and the relationship between pH and protein stability distinguish the EPD of LcrV from those of the IpaD sub-family.

The EPD for PcrV, like that of LcrV, demonstrates a direct correlation between increasing pH and increasing transition temperature for pH values above pH 4 (Figure 2.11E). The multicolored regions at pH 5-7 are clear indicators of significant aggregation. Transitions are visible at pH 3 and 4 but are smaller than those seen at higher pH.

2.4 Discussion

In this study, the effects of pH and temperature on protein stability are probed by various spectroscopic techniques on a set of related proteins from pathogenic gram negative bacteria that are involved in regulating the activation of type III secretion. The large amount and complexity of the resultant data (not all shown) make simple interpretation difficult. The data were therefore combined to create empirical phase diagrams that summarize the behavior of the proteins as a function of pH and temperature. Based on both direct inspection of the spectroscopic data and the resultant phase diagrams, the five proteins appear to fall into two sub-families. IpaD, BipD, and SipD have similar stability and aggregation patterns as seen by most spectroscopic methods and their phase diagrams. In contrast, LcrV and PcrV show remarkably similar stability behavior, which are distinct from that of the IpaD sub-family. These results are not unexpected given the sequence homology shared by SipD, BipD and IpaD, especially near their C-termini.[14] LcrV and PcrV also share considerable sequence homology.[35] The empirical phase diagrams generated here illustrate the power of this form of data presentation in synthesizing information from a large number of disparate techniques in a form which provides clear, concise insight into shared protein temperature and pH stability behavior.

It was shown previously that IpaD and BipD possess N and C-terminal domains separated by a coiled coil which combine to form a dumbbell shaped structure.[13,17] The putative structure of SipD is therefore expected to be similar. For

IpaD and SipD at pH 7.4, the proteins are known to be comprised of two independently folding domains with the N-terminal domain more thermally labile.[14,17] Two thermal transitions are visible throughout much of the pH range used in this study for IpaD and SipD employing both CD and intrinsic Trp fluorescence spectroscopy. The two transitions are not seen in the phase diagrams at pH 3 but are clearly visible from pH 4 through 8. While there appear to be two transitions in the BipD phase diagram, the middle temperature range shows no major transitions in the individual spectroscopic data. Studies of model aromatic amino acids show clear changes as a function of temperature and pH that in phase diagram form are similar to those seen in BipD (unpublished data). The probable reason for the single transition seen in BipD is an unusually stable N-terminal domain. From x-ray diffraction structural analysis of BipD, the N-terminal region appears to have strong interaction with the coiled coil.[10] The effect of this has also been observed by FTIR with BipD's coil resembling a triple coiled coil.[14] Because of this interaction, the N-terminal domain is stabilized such that there is only one major unfolding event for this protein. This interaction is not present in IpaD and unlikely to be present in the putative structure of SipD.

The most striking feature of the three proteins in the IpaD sub-family is the pH dependent changes in structure. The proteins manifest three distinct structural forms from pH 3 through 8. The EPDs of IpaD and SipD at pH 5 and 6 show clear structural differences at all temperatures when compared to those seen at pH 4, 7 and 8. Less structural difference is observed for BipD at low temperatures, although

above approximately 45 °C a different structural form appears to be present. While this difference at pH 5 and 6 could reflect proximity to their pI, since this is not seen in the LcrV subfamily, this conserved pH dependence suggests some possible common mechanistic function in all three tip proteins. Little has been done previously with the TTSA to investigate possible pH effects. Given, however, the dramatic pH differences in the gastrointestinal tract which *S. flexneri* or *S. typhimurium* is expected to encounter, the pH effects observed on the tip proteins may play an important role. Additionally, a lower pH microenvironment often exists near cell membrane surfaces due to the negative surface charge attracting protons from the bulk solution.[18,19] Such microenvironments have been suggested to be involved in modulating conformational states in other systems.[19,39,40] Thus, these microenvironments might alter the structure of the IpaD sub-family in mechanistically significant ways as well.

Unlike the IpaD sub-family of proteins, LcrV and PcrV do not exhibit two distinct thermal transitions. The published LcrV crystal structure[16] shows the dumbbell shape which appears to be a common feature of all tip proteins.[10,13] Given the single observed temperature transition for LcrV and PcrV, the N-terminal region of these proteins is probably not an independently folding domain but rather its conformational integrity may be coupled to that of the C-terminal region.[14] In contrast to the IpaD subfamily where the N-terminal domain has been proposed to act as a self-chaperone for the coiled-coil, the LcrV subfamily proteins possess an independent chaperone (LcrG or PcrG) which appears to interact with the coiled-

coil.[41,42] No definitive function has yet been attributed to the N-terminal portion of the LcrV subfamily as would be expected if it behaved as a separable domain. Thus, the N-termini of the two different subfamilies may not have the same function.

Perhaps the most striking feature of these proteins is the pH dependence of their stability. For both Lcrv and PcrV, as pH increases from 4-8, the transition temperature increases as well. This trend leads to the characteristic stepped pattern present in the phase diagrams. While this dependence might have some effect on LcrV in *Y. enterocolitica* as it encounters different pH conditions in the gastrointestinal tract, its significance is unclear. Furthermore, as *P. aeruginosa* and *Y. pestis* (this species also possesses LcrV) invade through non-oral routes, the increase in stability with pH range may be more indicative of the advantage of greater stability for this sub-family near physiologic pH.

Empirical Phase diagrams have previously been used to demonstrate structural similarities between proteins of similar function despite differences in primary and tertiary structure.[21] LcrV and PcrV, known orthologs, also possess phase diagrams with very similar patterns. From pH 5-8 at low temperature, the conformations are invariant for each. At pH 3 and 4, their structures display large differences even at low temperature and from pH 5-8 they both aggregate with increasing pH and temperature. Most striking in this study is the clear difference between the phase diagrams of the IpaD sub-family to those of the LcrV sub-family. These differences, especially with regard to pH, suggest possible divergence in mechanisms between the sub-families.

2.5 References

1. Galan JE, Wolf-Watz H 2006. Protein delivery into eukaryotic cells by type III secretion machines. Nature 444(7119):567-573.
2. He SY, Nomura K, Whittam TS 2004. Type III protein secretion mechanism in mammalian and plant pathogens. Biochim Biophys Acta 1694(1-3):181-206.
3. Cossart P, Sansonetti PJ 2004. Bacterial invasion: the paradigms of enteroinvasive pathogens. Science 304(5668):242-248.
4. Espina M, Olive AJ, Kenjale R, Moore DS, Ausar SF, Kaminski RW, Oaks EV, Middaugh CR, Picking WD, Picking WL 2006. IpaD Localizes to the Tip of the Type III Secretion System Needle of *Shigella flexneri*. Infection and Immunity 74(8):4391-4400.
5. Blocker A, Gounon P, Larquet E, Niebuhr K, Cabiaux V, Parsot C, Sansonetti P 1999. The tripartite type III secreton of *Shigella flexneri* inserts IpaB and IpaC into host membranes. J Cell Biol 147(3):683-693.
6. Zychlinsky A, Prevost MC, Sansonetti PJ 1992. *Shigella flexneri* induces apoptosis in infected macrophages. Nature 358(6382):167-169.
7. Tran Van Nheiu G, Sansonetti PJ 1999. Mechanism of *Shigella* Entry into Epithelial Cells. Curr Opin Microbiol 2:51-55.
8. Mueller CA, Broz P, Mueller SA, Ringler P, Erne-Brand F, Sorg I, Kuhn M, Engel A, Cornelis GR 2005. The V-Antigen of *Yersinia* Forms a Distinct Structure at the Tip of Injectisome Needles. Science (Washington, DC, United States) 310(5748):674-676.
9. Goure J, Broz P, Attree O, Cornelis GR, Attree I 2005. Protective anti-V antibodies inhibit *Pseudomonas* and *Yersinia* translocon assembly within host membranes. J Infect Dis 192(2):218-225.
10. Johnson S, Roversi P, Espina M, Olive A, Deane JE, Birket S, Field T, Picking WD, Blocker AJ, Galyov EE, Picking WL, Lea SM 2006. Self-chaperoning of the type III secretion system needle tip proteins IpaD and BipD. J Biol Chem.
11. Kaniga K, Trollinger D, Galan JE 1995. Identification of two targets of the type III protein secretion system encoded by the *inv* and *spa* loci of *Salmonella typhimurium* that have homology to the *Shigella* IpaD and IpaA proteins. J Bacteriol 177(24):7078-7085.
12. Stevens MP, Haque A, Atkins T, Hill J, Wood MW, Easton A, Nelson M, Underwood-Fowler C, Titball RW, Bancroft GJ, Galyov EE 2004. Attenuated virulence and protective efficacy of a *Burkholderia pseudomallei bsa* type III secretion mutant in murine models of melioidosis. Microbiology 150(Pt 8):2669-2676.
13. Erskine PT, Knight MJ, Ruaux A, Mikolajek H, Sang NW, Withers J, Gill R, Wood SP, Wood M, Fox GC, Cooper JB 2006. High Resolution Structure of BipD: An Invasion Protein Associated with the Type III Secretion System of *Burkholderia Pseudomallei*. J Mol Biol 363(1):125-136.

14. Espina M, Ausar SF, Middaugh CR, Baxter MA, Picking WD, Picking WD 2007. Conformational stability and differential structural analysis of LcrV, PcrV, BipD, and SipD from type III secretion systems. Protein Sci 16(4):704-714.
15. Nanao M, Ricard-Blum S, Di Guilmi AM, Lemaire D, Lascoux D, Chabert J, Attree I, Dessen A 2003. Type III secretion proteins PcrV and PcrG from *Pseudomonas aeruginosa* form a 1:1 complex through high affinity interactions. BMC Microbiol 3:21.
16. Derewenda U, Mateja A, Devedjiev Y, Routzahn KM, Evdokimov AG, Derewenda ZS, Waugh DS 2004. The structure of *Yersinia pestis* V-antigen, an essential virulence factor and mediator of immunity against plague. Structure (Cambridge, MA, United States) 12(2):301-306.
17. Espina M, Ausar SF, Middaugh CR, Picking WD, Picking WL 2006. Spectroscopic and calorimetric analyses of invasion plasmid antigen D (IpaD) from *Shigella flexneri* reveal the presence of two structural domains. Biochemistry 45(30):9219-9227.
18. Eisenberg M, Gresalfi T, Riccio T, McLaughlin S 1979. Adsorption of monovalent cations to bilayer membranes containing negative phospholipids. Biochemistry 18(23):5213-5223.
19. van der Goot FG, Gonzalez-Manas JM, Lakey JH, Pattus F 1991. A 'molten-globule' membrane-insertion intermediate of the pore-forming domain of colicin A. Nature 354(6352):408-410.
20. Kueltzo LA, Ersoy B, Ralston JP, Middaugh CR 2003. Derivative absorbance spectroscopy and protein phase diagrams as tools for comprehensive protein characterization: A bGCSF case study. J Pharm Sci 92(9):1805-1820.
21. Fan H, Kashi RS, Middaugh CR 2006. Conformational lability of two molecular chaperones Hsc70 and gp96: effects of pH and temperature. Arch Biochem Biophys 447(1):34-45.
22. Marquart ME, Picking WL, Picking WD 1995. Structural analysis of invasion plasmid antigen D (IpaD) from *Shigella flexneri*. Biochem Biophys Res Commun 214(3):963-970.
23. Mach H, Middaugh CR, Lewis RV 1992. Statistical determination of the average values of the extinction coefficients of tryptophan and tyrosine in native proteins. Anal Biochem 200(1):74-80.
24. Hennessey JP, Jr., Johnson WC, Jr. 1981. Information content in the circular dichroism of proteins. Biochemistry 20(5):1085-1094.
25. Venkatesan MM, Buysse JM, Kopecko DJ 1988. Characterization of invasion plasmid antigen genes (*ipaBCD*) from *Shigella flexneri*. Proc Natl Acad Sci U S A 85(23):9317-9321.
26. Semisotnov GV, Rodionova NA, Razgulyaev OI, Uversky VN, Gripas AF, Gilmanshin RI 1991. Study of the "molten globule" intermediate state in protein folding by a hydrophobic fluorescent probe. Biopolymers 31(1):119-128.
27. Matulis D, Lovrien R 1998. 1-Anilino-8-naphthalene sulfonate anion-protein binding depends primarily on ion pair formation. Biophys J 74(1):422-429.

28. Mach H, Middaugh CR 1994. Simultaneous monitoring of the environment of tryptophan, tyrosine, and phenylalanine residues in proteins by near-ultraviolet second-derivative spectroscopy. Anal Biochem 222(2):323-331.
29. Mach H, Thomson JA, Middaugh CR, Lewis RV 1991. Examination of phenylalanine microenvironments in proteins by second-derivative absorption spectroscopy. Arch Biochem Biophys 287(1):33-40.
30. Ragone R, Colonna G, Balestrieri C, Servillo L, Irace G 1984. Determination of tyrosine exposure in proteins by second-derivative spectroscopy. Biochemistry 23(8):1871-1875.
31. Holden MT, Titball RW, Peacock SJ, Cerdeno-Tarraga AM, Atkins T, Crossman LC, Pitt T, Churcher C, Mungall K, Bentley SD, Sebaihia M, Thomson NR, Bason N, Beacham IR, Brooks K, Brown KA, Brown NF, Challis GL, Cherevach I, Chillingworth T, Cronin A, Crossett B, Davis P, DeShazer D, Feltwell T, Fraser A, Hance Z, Hauser H, Holroyd S, Jagels K, Keith KE, Maddison M, Moule S, Price C, Quail MA, Rabbinowitsch E, Rutherford K, Sanders M, Simmonds M, Songsivilai S, Stevens K, Tumapa S, Vesaratchavest M, Whitehead S, Yeats C, Barrell BG, Oyston PC, Parkhill J 2004. Genomic plasticity of the causative agent of melioidosis, *Burkholderia pseudomallei*. Proc Natl Acad Sci U S A 101(39):14240-14245.
32. Ausar SF, Foubert TR, Hudson MH, Vedvick TS, Middaugh CR 2006. Conformational stability and disassembly of Norwalk virus-like particles. Effect of pH and temperature. J Biol Chem 281(28):19478-19488.
33. Hermant D, Menard R, Arricau N, Parsot C, Popoff MY 1995. Functional conservation of the *Salmonella* and *Shigella* effectors of entry into epithelial cells. Mol Microbiol 17(4):781-789.
34. Price SB, Leung KY, Barve SS, Straley SC 1989. Molecular analysis of lcrGVH, the V antigen operon of *Yersinia pestis*. J Bacteriol 171(10):5646-5653.
35. Yahr TL, Mende-Mueller LM, Friese MB, Frank DW 1997. Identification of type III secreted products of the *Pseudomonas aeruginosa* exoenzyme S regulon. J Bacteriol 179(22):7165-7168.
36. Fan H, Ralston J, Dibiase M, Faulkner E, Middaugh CR 2005. Solution behavior of IFN-beta-1a: an empirical phase diagram based approach. J Pharm Sci 94(9):1893-1911.
37. Fan H, Li H, Zhang M, Middaugh CR 2006. Effects of solutes on empirical phase diagrams of human fibroblast growth factor 1. J Pharm Sci.
38. Ausar SF, Rexroad J, Frolov VG, Look JL, Konar N, Middaugh CR 2005. Analysis of the thermal and pH stability of human respiratory syncytial virus. Mol Pharm 2(6):491-499.
39. Bychkova VE, Dujsekina AE, Klenin SI, Tiktopulo EI, Uversky VN, Ptitsyn OB 1996. Molten globule-like state of cytochrome c under conditions simulating those near the membrane surface. Biochemistry 35(19):6058-6063.
40. Mach H, Ryan JA, Burke CJ, Volkin DB, Middaugh CR 1993. Partially structured self-associating states of acidic fibroblast growth factor. Biochemistry 32(30):7703-7711.

41. Lawton DG, Longstaff C, Wallace BA, Hill J, Leary SE, Titball RW, Brown KA 2002. Interactions of the type III secretion pathway proteins LcrV and LcrG from *Yersinia pestis* are mediated by coiled-coil domains. J Biol Chem 277(41):38714-38722.
42. Matson JS, Nilles ML 2002. Interaction of the Yersinia pestis type III regulatory proteins LcrG and LcrV occurs at a hydrophobic interface. BMC Microbiol 2:16.

Chapter 3

Immunogenicity of Recombinant TTSS Proteins

IpaD, MxiH, SipD and PrgI

3.1 Introduction

Gram-negative bacterial pathogens are responsible for millions of debilitating infections each year. For example, *Shigella flexneri* and *Salmonella* spp., account for upwards of 165 and 200 million cases annually, respectively [1,2]. The *Shigella* species primarily use fecal-oral transmission to invade human hosts, most commonly via contaminated food or water. Host-to-host spreading, however, has also been observed. As a result, densely populated regions lacking proper sanitation are among the most heavily impacted. Symptoms of infection include fever, vomiting, severe abdominal cramping and/or bleeding, diarrhea and dysentery. Immuno-compromised populations, including the young and elderly, are more susceptible to serious complications arising from infection, which may ultimately result in death. *Salmonella* spp. also infects via the fecal-oral route with symptoms similar to those of Shigella; however, select serotypes are also known to induce bacteremia [3]. While Shigella infections are more common in developing nations, high profile Salmonella outbreaks are increasingly frequent in the U.S [4,5]

Due to the frequency and severity of disorders caused by gram-negative bacteria, and their prevalence in the developing world, an inexpensive efficacious vaccine is a leading priority. This need is further emphasized by the emergence of antibiotic resistant strains over the last twenty years. For instance, in separate studies of *Shigella* outbreaks in Kenya and Chile, resistance to Ampicillan was more than 80% percent [6,7]. Also observed in Kenya, 47% of isolated *Salmonella* species were

resistant to at least 3 commonly used antibiotics [8]. In the developed world, drug resistance is also on the rise. In the United States, the number of drug-resistant strains has risen from 0.6% to 34% in a sixteen year period [9].

These two pathogens have in common Type Three Secretion Systems (TTSS) which facilitate host cell invasion. TTSS complexes are composed of more than 20 proteins organized in basal and extracellular regions which span the inner and outer bacterial membranes. They protrude approximately 60 nm from the bacterial surface [10,11]. The extracellular portion is commonly referred to as the 'needle' for its tubular geometry and involvement in transporting effector proteins directly from the bacterial interior to the host cell cytoplasm. The needle is primarily composed of approximately 120 copies of a repeating polymeric unit arranged in a helical array [10,11]. The subunit (MxiH, *Shigella flexneri* and PrgI, *Salmonella* spp.) is a small (9-10 kDa) protein composed largely of alpha helical structure. On the distal needle tip lies a multimer which regulates secretion of the effector proteins [12]. The monomer (IpaD, *Shigella flexneri* and SipD, *Salmonella* spp.) is a slightly acidic dumbbell shaped protein (35-37 kDa) with a coiled coil at its center [13,14].

Here the focus is on the needle (MxiH and PrgI) and tip (IpaD and SipD) proteins as potential vaccine antigens due to their surface exposure and essential function during infection. It is thought that antigens with repeating epitopes are more immunogenic than those possessing only a single recognition site [15]. Additionally, increased antigen size has been shown to increase immunogenicity. For this reason, a recombinant polymeric needle construct was chosen for formulation which mimics

the TTSS structure. This would be combined with tip proteins to create a vaccine with multi-valency and multi-epitope specificity.

Vaccine research directed toward these two pathogens has primarily focused on employing lipopolysaccharide (LPS) and attenuated bacteria, with limited success [16,17]. In general, vaccines for Salmonella have focused on prevention of enteric fevers such as typhoid, but little work has been done to combat non-typhoidal indications [16,18,19]. In the case of *Shigella*, both an attenuated form of the bacteria as well as a formulation containing an O-polysaccharide linked to a carrier protein have reached Phase III clinical trials, but have not yet attained approval [17]. Significant work has also been done on IpaD, the tip protein from the *Shigella* system. Several groups have shown IpaD to be immunogenic [20], and most recently that antibodies raised against IpaD neutralize host-cell invasion of Shigella in-vitro [12]. Furthermore, epitope mapping has been completed for IpaD, which indicates that immune responses are greater in the amino-terminal region [20]. In the same study, it was noted that the *Salmonella* analog, SipD, shares significant sequence homology with the C-terminal region of IpaD. Thus, it is possible that the epitopic response in these regions may provide a degree of cross-protection [20].

Another bacterium for which vaccine efforts have focused on TTSS components is *Yersenia pestis*. In this case, work has focused on subunit forms of the F1 capsular antigen and LcrV, the TTSS needle tip protein. Both have been proven immunogenic and protective, although development has been slowed by several factors including a demonstrated immuno-suppressive effect of LcrV on innate

immunity [21-24]. Regardless, it has been established that LcrV activates dendritic cells (DCs) [25]. Similar to the work indicated here, the needle component, YscF, has also been considered as a vaccine antigen for this species. The wild type needle protein was shown to elicit a strong antibody response, and provide a degree of protection (60%) upon challenge [26,27]. In contrast to the protective effect of antibodies to IpaD, anti-YscF does not inhibit translocation of effector proteins suggesting that its protective effect is probably due to opsinization and/or enhanced complement binding [26].

The work presented represents an initial attempt to develop human vaccines for two of these pathogens. To this end, an approved adjuvant, Alhydrogel, was included in the proposed recombinant subunit formulations.

3.2 Materials and Methods

3.2.1 Vaccine

Recombinant proteins were expressed in *E. coli* as described previously [28-31]. The needle proteins (MxiH and PrgI) were expressed with a five residue C-terminal truncation to prevent inherent polymerization and ensure monomeric behavior. Additionally, MxiH was expressed in its full length form, resulting in largely polymerized material referred to as 'Needle' hereafter (data not shown). All proteins were purified by means of a C-terminal His_6 tag, and dialyzed to 10 mM Histidine, 144 mM NaCl buffer at pH 6.0. Proteins were adsorbed to Alhydrogel, a positively charged aluminum salt adjuvant, at a concentration of 0.5 mg/mL aluminum by

stirring at 4 ^{o}C. In bivalent formulations, the solution materials were mixed, and the adsorption step was performed subsequent to mixing. Characterization and analysis of each formulation are documented in chapter 4. In all cases complete adsorption (>95%) of the antigens was observed.

3.2.2 Animals and Immunization

Animal studies were performed at the University of Kansas in accordance with regulations set forth by the Institutional Animal Care and Use Committee and guidelines of the Association for Assessment and Accreditation of Laboratory Animal Care. For all experiments, BALB/c mice were acquired from Charles River Breeding Laboratory (Wilmington, MA) and quarantined for 7 days prior to study start. Inoculations (100 μL) were administered intramuscularly on study days 1, 14 and 28 and mice were bled via the submandibular vein on days 0, 7, 21, 35 and 49.[32] Weights were recorded at each time-point and monitored for indications of adverse effects due to dosing, however none were observed. Mice were euthanized following the final bleed on day 49.

In the first study, each group contained 10 mice (5 female and 5 male) with the exception of the histidine buffer control group which contained only 7 mice. No significant differences were observed in end-point titers between male and female mice. Formulations containing only one antigen (MxiH or IpaD) were dosed at 1 (M1, D1), 10 (M10, D10) and 50 (M50, D50) μg/dose, while formulations containing both antigens (MD1, MD10 and MD50) were administered at the same total protein

concentration (1, 10 and 50 μg protein/dose); containing one-half the amount of each. The two control groups were dosed with either formulation buffer or 0.5 mg/mL Aluminum in formulation buffer.

Study 2 contained groups of 7 mice (female), and a single control group containing 5 mice (0.5 mg/mL Aluminum in isotonic His buffer). MxiH, MxiH Needle and IpaD were all dosed separately at 10 μg, both in the formulation buffer as well as adsorbed to Alhydrogel (M-Soln, M-His, N-Soln, N-His, D-Soln and D-His respectively). Bivalent formulations containing IpaD and either MxiH or Needle were administered adsorbed to Alhydrogel at total protein concentrations of 20 μg/mL (10 μg of each).

The third study, conducted concurrently with study 2, involved groups of 8 mice, and a control group of 5 mice (0.5 mg/mL Aluminum in isotonic His buffer). Monovalent formulations of both PrgI and SipD were administered at 1, 10 and 50 μg/dose (P1, P10, P50, S1, S10 and S50), while bivalent formulations were dosed at total protein concentrations of 2, 20 and 100 μg/dose (PS1, PS10 and PS50). Non-adsorbed formulations were also administered at 50 μg for PrgI, SipD and the bivalent combination (P50-Soln, S50-Soln and PS50-Soln).

3.2.3 IgG Detection in Serum Samples

Antigen specific IgG titers were determined for individual sera samples using a standard Enzyme Linked Immunosorbent Assay (ELISA). The optimal protocol differed for the needle (MxiH and PrgI) and tip (IpaD and SipD) proteins. Needle

proteins were adsorbed (100 µL) onto Nunc-Immuno™ MediSorp™ (Nalge Nunc International, Wiesbaden, Germany) 96-well plates at 10 µg/mL in carbonate buffer (pH 9.6) overnight at 4 ^{o}C. Plates were blocked with Superblock per product instructions. Sera dilutions (100 µL) were made using the blocking buffer and allowed to incubate on the plate for 2 h at RT. The plates were then washed 3 times using PBS buffer containing 0.05% Tween 20, and a final time with PBS buffer alone. HRP-conjugated Goat anti-Mouse Monoclonal Antibody (Sigma, St. Louis, MO) was diluted 1:500 in blocking buffer, plated (100 µL) and incubated for 1 h at RT. The plates were then washed as above, and 3,3'5,5'-TetraMethylBenzidine (TMB) substrate (100 µL) (Sigma, St. Louis, MO) was added. After 30 minutes at RT, 2 M HCl (100 uL) was added to quench the reaction and plates were read using a SpectraMax M5 plate reader (Molecular Devices, Sunnyvale, CA) at 450 nm.

Tip proteins were plated (100 µL) onto Costar® non-treated black with clear bottom plates (Corning Life Sciences, Lowell, MA) at 10 µg/ml in carbonate buffer overnight at 4 ^{o}C. Plates were blocked with casein buffer (pH 7.5) for 30 min. Subsequent steps were the same as those for the needle ELISA protocol with the exception that the casein buffer was used in place of the Superblock. In all cases, endpoint titers were determined as the inverse of the dilution with optical density at 450 nm greater than 3 times the negative control.

3.2.4 Statistical Analysis

The geometric mean was used to represent group responses, and error was determined as the standard deviation. Statistical significance was determined with Student's t-test using Microsoft Excel. Significance was determined as $p \leq 0.05$.

3.3 Results

Mice were intramuscularly immunized three times at two week intervals (study days 1, 14 and 28), and blood samples were collected on days 0, 7, 21, 35, and 49. For all cases, in which significant increases in IgG were observed, all mice had endpoint titers within two dilutions of the geometric mean. On day 0 of the first experiment, all mice had Anti-MxiH IgG titers near 128 (Figure 3.1A). Mice in the control group maintained a similar value throughout the study. Animals dosed with 1 µg of MxiH (M1) showed only a slight increase in antibody response throughout the study ($p<0.02$, day 49 compared to day 0), while those administered a 10 µg dose (M10) showed some response after the second booster compared to the control groups ($p<0.0015$). Mice who received the highest dose of 50 µg (M50) displayed an increase in serum IgG following the initial dose ($p=0.0002$), and continued to increase following the two booster injections. Those animals who received bivalent doses of 1 µg (MD1) did not show a significant increase in Anti-MxiH IgG during the experiment; however, when the dose was increased to 10 µg (MD10) an increased

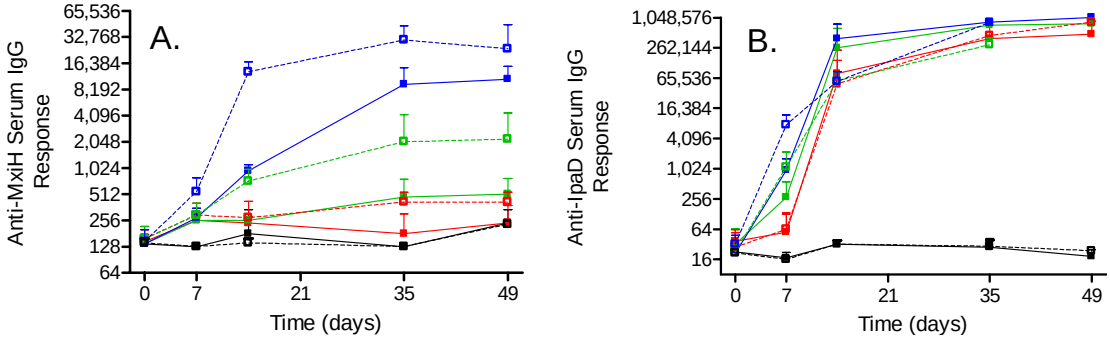

Figure 3.1. Anti MxiH (A) and IpaD (B) IgG serum responses following intramuscular injections on study days 1, 14, 28 of Control (■), M1/D1 (■), M10/D10 (■), M50/D50 (■),MD1 (□), MD10 (□), MD50 (□).

response relative to the control groups was observed after the initial dose and rose again following the first and second boosters. The largest bivalent dose of 50 μg (MD50) resulted in a dramatically increased response relative to the lower bivalent and all monovalent groups. In all cases, the responses observed following the second booster were sustained for three weeks after the last injection.

When assayed for Anti-IpaD antibodies at day 0, all mice had endpoint titers of approximately 32, and those mice in the control groups continued at a similar low level throughout the remainder of the experiment (Figure 3.1B). Mice which were injected with 1 μg of IpaD (D1) showed a slight increase in IpaD IgG following the first injection ($p<0.05$) followed by an increase of greater than 10 dilutions after the first booster. The 10 μg dose (D10) showed a larger increase in antibody titer compared to the 1 μg dose following the initial injection, and a similar increase following the first booster. The 50 μg dose (D50) followed the same trend with higher endpoints following the first two doses relative to the two lower dose groups. IgG titers for IpaD when administered in the presence of MxiH (MD 1, 10, 50) are analogous to those observed when IpaD was dosed alone. The only significant difference occurs following the initial injection, where the bivalent dosed mice have higher IgG titers than those who received IpaD alone. As seen with the MxiH IgG responses, those observed for IpaD following the second booster remained at a comparable level for all groups when sampled on study day 49.

The second and third studies followed the same immunization and blood collection schedule as the initial experiment. In the second study, all monovalent

doses were 10 μg while those containing both antigens had 10 μg of each included. Similar to the initial experiment, all mice had Anti-MxiH IgG endpoint titers of approximately 256 on day 0, and the control group maintained similar values throughout the study (Figure 3.2A). Those animals who received a 10 μg dose of MxiH in formulation buffer (M-Soln) did not show a significant response throughout the entire study. When the same dose was administered adsorbed to Alhydrogel (M-Al), again no response was observed. In the presence of IpaD, however, an increase in Anti-MxiH IgG was observed following the second booster ($p<0.0001$). A significant Anti-MxiH IgG response was observed following the initial injection and further increased following the first booster when mice were inoculated with the polymerized form of MxiH in solution (N-Soln.). The responses observed following the second booster increased only slightly ($p<0.05$). When the same dose was administered adsorbed to the adjuvant (N-Al), a similar trend was observed with increased magnitude. In the presence of IpaD, the response was identical to that in its absence with the exception of the response following the initial injection which was slightly higher in the presence of IpaD.

The anti-IpaD endpoint dilution for all mice prior to the first injection of study 2 as well as mice in the control group throughout was 32 (Figure 3.2B). Mice inoculated with a 10 μg dose of IpaD in solution (D-Soln) displayed a significant response following the first and second injections and maintained the IgG titer thereafter. When adsorbed to Alhydrogel (D-Al), the same response trend was observed but with a higher titer ($p<0.004$, day 49). In the presence of monomeric

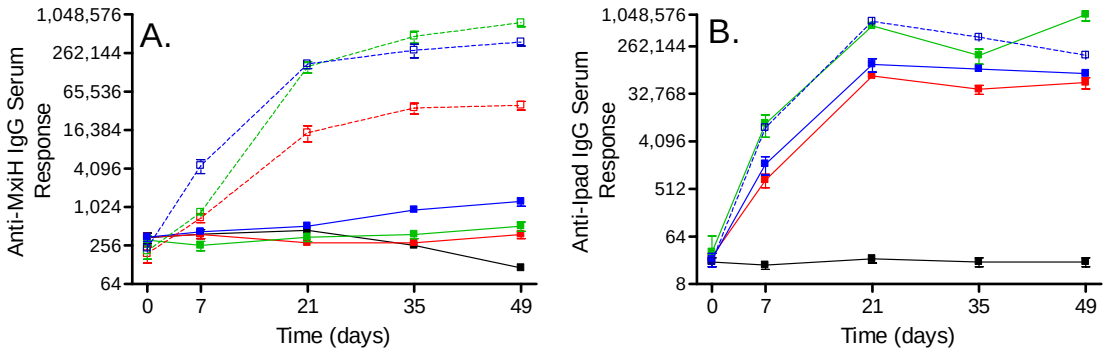

Figure 3.2. Anti MxiH (A) and IpaD (B) IgG serum responses following intramuscular injections on study days 1, 14, 28 Control (■), M-Soln/D-Soln (■), M-Al/D-Al (■), MD-Al (■), N-Soln (□), N-Al (□), and ND-Al (□).

MxiH (MD-Al), the initial dose elicited a slightly lower response than that of adsorbed IpaD alone ($p<0.01$), and the bivalent formulation did not reach the same endpoint titer following the boost injections. Mice given the bivalent formulation containing the polymerized MxiH displayed an identical profile to that of D-Al with the exception of the final time-point where the response was slightly lower ($p<0.01$).

The final study involved analogous needle and tip proteins from *Salmonella spp.* At the study start, all mice displayed PrgI specific IgG endpoint titers of approximately 64 (Figure 3.3A). The control group displayed a similar value throughout the study. Mice given the 1 μg dose of PrgI (P1) demonstrated an increase in titer over the course of the experiment ($p<0.005$, day 49 compared to day 0). The mice inoculated with 10 μg (P10) displayed an increase following the first dose, and levels rose somewhat during the remainder of the experiment. The mice in the highest Alhydrogel adsorbed dose group (P50), had increasing titers following each injection, while in the absence of Alhydrogel (P50-Soln), the response was comparable to that of P1 and P10. When dosed in the presence of SipD, the response to 1 μg (PS1) is slightly higher at day 21 ($p<0.05$), but similar thereafter to P1. At 10 μg (PS10), the PrgI IgG endpoints mirrored that of the antigen in the absence of SipD. At the highest dose level (PS50), the response followed a similar trend to that of the P50 treated mice, although the level was not as great following the second boost injection. The bivalent 50 μg solution dose (PS50-Soln) had similar values to that of the monovalent solution dose (P50-Soln) with the exception of day 7 where P50-Soln mice were slightly higher than PS50-Soln ($p<0.05$).

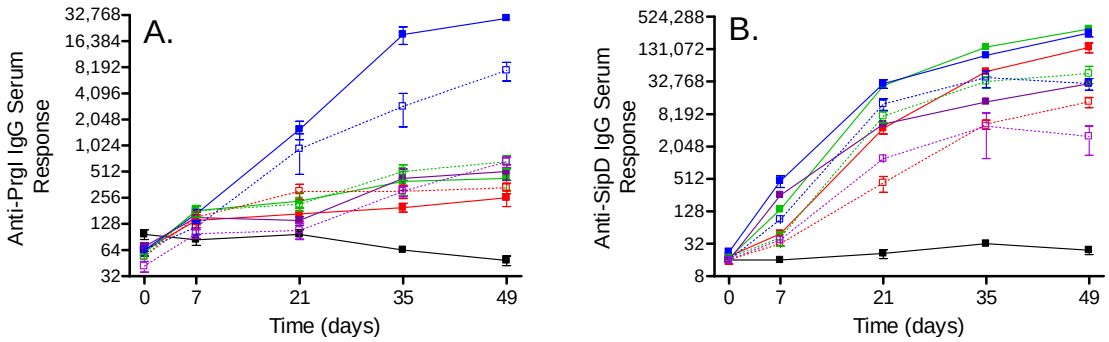

Figure 3.3: Anti PrgI (A) and SipD (B) IgG serum responses following intramuscular injections on study days 1, 14, 28 of Control (■), P1/S1 (■), P10/S10 (■), P50/S50 (■), P50-Soln/S50-Soln (■), PS1 (□), PS10 (□), PS50 (□) and PS50-Soln (□).

The endpoint titers in the SipD groups of Study 3 were roughly 16 prior to injections (Figure 3.3B). Mice given 1 μg doses of SipD (S1) demonstrated a slightly elevated endpoint after the first injection, but experienced a boost of more than 5 dilutions following the second dose. Mice in the 10 μg dose (S10) group followed a similar trend with increased endpoint titers at each time-point. The 50 μg (S50) dose did not elicit a significant difference in antibody response compared to that of S10 treated mice with the exception of day 7 where S50 was greater ($p<0.01$). When no Alhydrogel was present (S50-Soln), the response to the initial injection was comparable to that observed for S10 and S50. Following the booster doses, however, the increase in antibody levels was not as great. The 1 μg bivalent formulation (PS1) followed the trend observed for the monovalent (S1) formulation, but with lower antibody values. The 10 and 50 μg combination doses (PS10 and PS50) also behaved similarly to their monovalent analogues, S10 and S50, but with lower titers at all time-points. When the bivalent formulation was injected in the absence of Alhydrogel (PS50-Soln), the observed response was lower than that of the S50-Soln group throughout the study.

3.4 Discussion

In the present study, the immunogenicity of TTSS needle and tip proteins both in monovalent and bivalent formulations has been demonstrated. Additionally, no adverse effects were observed throughout the dosing regimen as indicated by normal

weight gain patterns (data not shown). In all studies where increases in specific antibody titers were observed, there were no non-responders suggesting that the formulations may be efficacious if IgG levels are predictive of protection.

MxiH monomer has shown to be weakly immunogenic and dose dependent, requiring fairly high doses of antigen, multiple boosts and the presence of an adjuvant to elicit a strong response. When administered in the presence of IpaD, however, the Anti-MxiH specific IgG was significantly boosted. This enhanced response does not appear to be the result of physical interaction between the two proteins when combined in solution (data not shown.) It is possible however that the presence of Alhydrogel provides a platform for interaction between the two. It is also possible that IpaD has inherent adjuvant-like properties as evidenced by its sizeable immunogenicity when dosed alone in the absence of an adjuvant.

The polymerized form of the needle protein, expressed without the C-terminal truncation, is drastically more immunogenic than the monomeric version. There exists a well established correlation between antigen size and immune response [15]. Thus, it is possible that the increase observed here is a result of the increased size of the polymeric version of the needle monomer. Another possibility is the existence of repeating epitopes in the polymeric unit which has also been shown to greatly increase immunogenicity. Finally, it is also possible that the 5 residue C-terminal region which is absent in the monomeric form constitutes a potent epitope. Similar to the monomeric version, the response of the polymerized form is further boosted by adsorption to an adjuvant.

The tip protein from the *Shigella* system is shown here to be highly immunogenic in agreement with previous work [20]. In contrast to the needle monomer MxiH, IpaD does not show significant dose-dependent behavior when administered in a multi-dose regimen; however there does appear to be an indication of dose-dependency following the first inoculation. As stated above, it is possible that due to its potent immunogenicity, IpaD may act as an adjuvant in multivalent formulations. While IpaD is strongly immunogenic alone, it does benefit from adsorption to Alhydrogel.

Antigens from the *Salmonella* system also appear to elicit substantial immune responses. Similar to the results observed for the *Shigella* system, the monomeric needle protein PrgI is less immunogenic than the tip protein SipD. PrgI displays dose dependent behavior, and titers increase markedly when booster doses are administered. As one would expect, IgG responses to PrgI are enhanced when the antigen is adsorbed to Alhydrogel. Contrary to the immune response to MxiH seen in the presence of the analogous tip protein, however; PrgI does not produce higher antibody levels in the presence of SipD.

Mice injected with SipD had high antibody titers following the first dose and were relatively dose independent after the first booster injection. This trend is similar to that observed for IpaD, but in all cases, responses to SipD were lower in magnitude. Additionally, where IpaD was boosted slightly by the presence of MxiH, SipD titers appear to be reduced when administered in the presence of PrgI. This

observation agrees with the documented immuno-suppressing activity associated with LcrV, the tip protein of *Yersinia pestis* [24].

While the studies presented here support further vaccine development utilizing TTSS needle and tip proteins, further work is clearly necessary. Additional studies will focus on tailoring the formulation to elicit an appropriate response based on the pathogenesis of each species to ensure protection. *Salmonella* spp. bacterial infections often result in systemic invasion, which are responsible for some of the most severe symptoms [3]. Preventing a systemic infection may be possible using versions of the formulation studied here which was dosed intramuscularly. While no data is currently available to definitively associate the presence of PrgI/SipD specific IgG with protection, needle proteins have been shown to enhance well-established opsinization phenomenon and *in-vitro* studies suggest that tip protein antibodies prevent host-cell invasion [12].

In contrast, *Shigella* infections generally involve the epithelial cells of the intestines and do not commonly result in septicemia. This suggests that a vaccine will need to protect the mucosal surfaces to be effective. It is not yet certain whether the current formulation will meet this requirement. To explore this question, it will be necessary to conduct additional immunogenicity experiments focusing on IgA levels. Other tests which may be necessary include evaluation of cellular responses and associated adjuvants and the effect of the route of administration. In this study, an aluminum salt adjuvant was chosen because it is currently the only FDA approved

vaccine adjuvant. Novel adjuvants are now becoming available, however, and they will need to be examined in this system [33-36].

As previously stated, the main purpose of the work presented here is to establish the antigenic potential of TTSS needle and tip proteins. This chapter shows that administration of these proteins results in robust humoral immune responses. Based on previous work, this may be sufficient for protection. While some bivalent formulations did not have a synergistic effect, it is proposed that the multivalent approach may be advantageous for several reasons including increased likelihood of protection across populations and potential cross-protection among similar species. In summary, this chapter supports the development of TTSS proteins as antigens in multivalent subunit vaccines.

3.5 References

1. 2005. World Health Organiation Drug-Resistant *Salmonella.*, ed.
2. 2009. *Shigella*. ed.
3. S.M. G 2002. Salmonellosis in children in developing and developed countries and populations. Curr Opin Infect Dis 15(5):507-512.
4. 2008. *Salmonella Saintpaul* Outbreak. ed.
5. 2008. Peanut Product Recalls: *Salmonella Typhimurium*. ed.
6. Brooks JT, Shapiro RL, Kumar L, Wells JG, Phillips-Howard PA, Shi Y-P, Vulule JM, Hoekstra RM, Mintz E, Slutsker L 2003. Epidemiology of Sporadic Bloody Diarrhea in Rural Western Kenya. Am J Trop Med Hyg 68(6):671-677.
7. Fulla N, Prado V, Duran C, Lagos R, Levine M 2005. Surveillance for Antimicrobial Resistance Profiles Among Shigella Species Isolated from a Semirural Community in the Northern Administrative Area of Santiago, Chile. Am J Trop Med Hyg 72(6):851-854.

8. Kariaki S, Gilks C, Corkill J, Kimari J, Benea A, Waiyaki P, Hart CA 1996. Multi-drug resistant non-typhi salmonellae in Kenya. J Antimicrob Chemother 38(3):425-434.
9. Glynn MK, Bopp C, Dewitt W, Dabney P, Mokhtar M, Angulo FJ 1998. Emergence of Multidrug-Resistant Salmonella enterica SerotypeTyphimurium DT104 Infections in the United States. N Engl J Med 338(19):1333-1339.
10. Deane JE, Roversi P, Cordes FS, Johnson S, Kenjale R, Daniell S, Booy F, Picking WD, Picking WL, Blocker AJ, Lea SM 2006. Molecular model of a type III secretion system needle: Implications for host-cell sensing. Proc Natl Acad Sci USA 103(33):12529-12533.
11. Kubori T, Matsushima Y, Nakamura D, Uralil J, Lara-Tejero M, Sukhan A, Gal, aacute, n JE, Aizawa S-I 1998. Supramolecular Structure of the *Salmonella typhimurium* Type III Protein Secretion System. Science 280(5363):602-605.
12. Espina M, Olive AJ, Kenjale R, Moore DS, Ausar SF, Kaminski RW, Oaks EV, Middaugh CR, Picking WD, Picking WL 2006. IpaD Localizes to the Tip of the Type III Secretion System Needle of *Shigella flexneri*. Infect Immun 74(8):4391-4400.
13. Espina M, Ausar SF, Middaugh CR, Picking WD, Picking WL 2006. Spectroscopic and Calorimetric Analyses of Invasion Plasmid Antigen D (IpaD) from Shigella flexneri Reveal the Presence of Two Structural Domains. Biochemistry 45(30):9219-9227.
14. Johnson S, Roversi P, Espina M, Olive A, Deane JE, Birket S, Field T, Picking WD, Blocker AJ, Galyov EE, Picking WL, Lea SM 2006. Self-chaperoning of the type III secretion system needle tip proteins IpaD and BipD. J Biol Chem:M607945200.
15. Dintzis RZ, Okajima M, Middleton MH, Greene G, Dintzis HM 1989. The immunogenicity of soluble haptenated polymers is determined by molecular mass and hapten valence. J Immunol 143(4):1239-1244.
16. Guzman CA, Borsutzky S, Griot-Wenk M, Metcalfe IC, Pearman J, Collioud A, Favre D, Dietrich G 2006. Vaccines against typhoid fever. Vaccine 24(18):3804-3811.
17. Levine MM, Kotloff KL, Barry EM, Pasetti MF, Sztein MB 2007. Clinical trials of *Shigella* vaccines: two steps forward and one step back on a long, hard road. Nat Rev Micro 5(7):540-553.
18. Boyle EC, Bishop JL, Grassl GA, Finlay BB 2007. Salmonella: from Pathogenesis to Therapeutics. J Bacteriol 189(5):1489-1495.
19. Plotkin SA, Orenstein WA. 2004. Typhoid Fever Vaccines. In Levine MM, editor Vaccines, 4 ed., Philadelphia: Elsevier, Inc. p 1057-1093.
20. Turbyfill KR, Mertz JA, Mallett CP, Oaks EV 1998. Identification of Epitope and Surface-Exposed Domains of *Shigella flexneri* Invasion Plasmid Antigen D (IpaD). Infect Immun 66(5):1999-2006.
21. Hill J, Leary SE, Griffin KF, Williamson ED, Titball RW 1997. Regions of *Yersinia pestis* V antigen that contribute to protection against plague identified by passive and active immunization. Infect Immun 65(11):4476-4482.

22. Williamson ED, Eley SM, Stagg AJ, Green M, Russell P, Titball RW 2000. A single dose sub-unit vaccine protects against pneumonic plague. Vaccine 19(4-5):566-571.
23. Williamson ED, Vesey PM, Gillhespy KJ, Eley SM, Green M, Titball RW 1999. An IgG1 titre to the F1 and V antigens correlates with protection against plague in the mouse model. Clin Exp Immunol 116(1):107 - 114.
24. Brubaker RR 2003. Interleukin-10 and Inhibition of Innate Immunity to *Yersiniae*: Roles of Yops and LcrV (V Antigen). Infect Immun 71(7):3673-3681.
25. Kingston R, Burke F, Robinson JH, Bedford PA, Jones SM, Knight SC, Williamson ED 2007. The fraction 1 and V protein antigens of *Yersinia pestis* activate dendritic cells to induce primary T cell responses. Clinical and Experimental Immunology 149(3):561-569.
26. Matson J, Durick K, Bradley D, Nilles M 2005. Immunization of mice with YscF provides protection from *Yersinia pestis* infections. BMC Microbiology 5(1):38.
27. Swietnicki W, Powell BS, Goodin J 2005. *Yersinia pestis* Yop secretion protein F: Purification, characterization, and protective efficacy against bubonic plague. Protein Expression and Purification 42(1):166-172.
28. Darboe N, Kenjale R, Picking WL, Picking WD, Middaugh CR 2005. Physical characterization of MxiH and PrgI, the needle component of the type III secretion apparatus from *Shigella* and *Salmonella*. Protein Sci 15(3):543-552.
29. Espina M, Ausar SF, Middaugh CR, Baxter MA, Picking WD, Picking WL 2007. Conformational stability and differential structural analysis of LcrV, PcrV, BipD, and SipD from type III secretion systems. Protein Sci 16(4):704-714.
30. Kenjale R, Wilson J, Zenk SF, Saurya S, Picking WL, Picking WD, Blocker A 2005. The Needle Component of the Type III Secreton of *Shigella* Regulates the Activity of the Secretion Apparatus. J Biol Chem 280(52):42929-42937.
31. Marquart ME, Picking WL, Picking WD 1995. Structural Analysis of Invasion Plasmid Antigen D (Ipad) from *Shigella flexneri*. Biochemical and Biophysical Research Communications 214(3):963-970.
32. Golde WT, Gollobin P, Rodriguez LL 2005. A rapid, simple, and humane method for submandibular bleeding of mice using a lancet. Lab Anim (NY) 34(9):39-43.
33. Aguilar JC, Rodríguez EG 2007. Vaccine adjuvants revisited. Vaccine 25(19):3752-3762.
34. Ott G, Radhakrishnan R, Fang JH, Hora M. 2001. The adjuvant MF59: a ten year perspective Vaccine Adjuvants: Preparation Methods and Research Protocols, ed., Totowa, N.J.: Humana Press. p 211-228.
35. Skene CD, Sutton P 2006. Saponin-adjuvanted particulate vaccines for clinical use. Methods 40(1):53-59.
36. Wikman M, Friedman M, Pinitkiatisakul S, Andersson C, LÃ¶vgren-Bengtsson K, LundÃ©n A, StÃ¥hl S 2006. Achieving directed immunostimulating complexes incorporation. Expert Review of Vaccines 5(3):395-403.

Chapter 4

Formulation of a Potential Multivalent TTSS Tip Protein Vaccine

4.1 Introduction

Despite modern advances, gram-negative bacterial pathogens continue to persist as serious health risks for humans, particularly in the developing world. These agents cause diseases such as bacillary dysentery (*Shigella flexneri*), septicemia (*Salmonella typhi, Burkholderia pseudomallei* and *Yersinia pestis*), gastroenteritis (*Salmonella typhimurium, Yersinia enterocolitica*) and chronic infections in compromised individuals *(Pseudomonas aeruginosa). Shigella* alone is estimated to cause 165 million infections each year worldwide with over a million deaths.[1] The severity and frequency of such infections highlights the need for safe, efficacious vaccines that can be inexpensively produced and administered anywhere in the world. This need has increased in the last 20 years with the emergence of antibiotic resistant strains for many of the pathogens mentioned above.[2-5]

Proteins from the type III section system (TTSS) of important pathogens have been selected for the development of targeted subunit vaccines. The TTSS plays an integral role in the pathogenesis of these bacteria either by facilitating host cell invasion or by preventing macrophage phagocytosis.[6,7] The type III secretion apparatus (TTSA) is comprised of a basal body and needle, which together span the inner and outer bacterial membrane and extend into the extracellular space.[6-8] The overall complex is composed of more than 20 proteins and functions to translocate effector proteins from the bacterial cytoplasm into the membrane and cytoplasm of a host cell.

A specific class of protein has recently been shown to localize to the extracellular end of the TTSA needle where it functions to regulate the secretion of other proteins passing through the TTSA.[9-12] Due to the location and function of these so called tip proteins, it is anticipated that they would be effective antigens in a sub-unit vaccine. The five tip proteins selected for this vaccine formulation study are IpaD from *S. flexneri*, BipD of *B. pseudomallei*, SipD of *Salmonella* spp., LcrV of *Yersinia* spp. and PcrV of *P. aeruginosa*. These proteins, ranging in size from 32 to 37 kDa, possess primarily α-helical secondary structure and are dumbbell shaped with a central coiled coil separating the N and C terminal domains.[10,13-17] It has previously been established that, in animal models, these prospective antigens are highly immunogenic and provide at least a degree of protection.[18-21] Furthermore, in the case of *Shigella*, experiments have demonstrated that *in vitro*, anti-IpaD IgG neutralized host cell invasion in model systems.[9]

While the tip proteins show promise in eliciting an appropriate, protective immune response, it is important that any formulation involving these antigens be sufficiently stable to permit distribution to regions of the world lacking reliable refrigerated storage.[22] This requirement demands any such product possess greater stability than is often expected for marketing in developed countries. Until now, little attention has been given to formulation considerations for these tip proteins. This chapter describes studies to systematically ascertain optimal formulation compositions and conditions. This has been done with the ultimate goal of combining

these antigens into a single multivalent vaccine. As such, a single formulation is sought which stabilizes all of the antigens.

An adjuvant is often necessary for subunit vaccines to increase the immune response.[23] This boost in immunogenicity is accomplished by a variety of mechanisms ranging from activation of Toll-like receptors on antigen presenting cells to creating an antigen depot.[23-25] The adjuvant selected for this project is the aluminum salt Alhydrogel®. The mechanism of action of this crystalline substance has not been fully elucidated.[26-30] Nevertheless, due to its excellent safety record, inclusion in many FDA approved commercial vaccines and the pI's of the tip protein (all between ~5 and 5.5 which facilitates electrostatic interactions with the positively charged adjuvant) it is the obvious choice.[30-33] Adsorption and desorption studies were conducted to elucidate the nature of protein-Alhydrogel® interactions.

4.2 Materials and Methods

4.2.1 Materials

Recombinant proteins were expressed and purified as described previously.[15,34,35] All proteins were dialyzed into 20 mM citrate/phosphate buffer at pH 7 and stored at -80 C°. For the final formulation, a 10 mM histidine buffer was selected containing 5 mM phosphate. Phosphate was included to exchange some of the exposed aluminum hydroxide to aluminum phosphate, thus lowering the pH microenvironment at the adjuvant/protein interface. All buffer components were purchased from Sigma-Aldrich (St. Louis, Mo).

4.2.2 Excipient Screening

A high throughput screening method was devised to identify additives that could serve as stabilizers in a pharmaceutical formulation. Previous work indicted that all of the putative antigens aggregated significantly at pH 5 and 6 at elevated temperatures. This physical degradation pathway was selected because it could be easily adapted for high throughput screening.[17] An assay was developed employing 96 well plates at 55 °C using a SpectraMax plate reader (Molecular Devices, Sunnyvale, CA) measuring time-dependent optical density at 360 nm. Samples were analyzed in duplicate with a negative control containing buffer and excipient on the same 96 plate. Measurements were taken at 2 min intervals for a period of 2 h. The effectiveness of each additive was quantified by percent inhibition of aggregation. The value of this parameter was calculated using the following equation:

$$\%Inhibition = \left(1 - \frac{\Delta OD_{360}(E)}{\Delta OD_{360}(A)}\right) \times 100$$

where $\Delta OD_{360}(E)$ change in optical density over the course of the experiment of the protein with excipient present and $\Delta OD_{360}(A)$ represents the same measurement without excipient.

To create the appropriate sample conditions, protein stock solutions were diluted to 0.2 mg/ml in 20 mM citrate phosphate buffer at pH 5. All excipients tested belong to the GRAS (generally regarded as safe) library of compounds which includes a selection of amino acids, antioxidants, cyclodextrans, surfactants,

carbohydrates, polyols and proteins among other agents (see results section). These GRAS additives have proven track-records in pharmaceutical formulations.

4.2.3 Intrinsic Trp Fluorescence

The environment of Trp residues was monitored using fluorescence to measuring tertiary structural stability in the presence and absence of promising stabilizers. Samples, excited at 295 nm, had emission monitored from 300 to 400 nm using a 0.5 s integration time and a resolution of 1 nm. Emission was measured 90° from the direction of the incident beam with a PTI QM-1 spectrofluorometer with a four position rotating turret (Brunswick, NJ). Quartz cuvettes with a 1 cm pathlength were used and were filled to a volume of 1 ml. In the case of samples containing Alhydrogel®, front face fluorescence was employed after permitting samples to settle overnight.[29] Samples were measured from 10 to 85 °C in 2.5 °C increments where temperature was controlled using a water bath cooled peltier system. Peak positions were determined using Origin® software by fitting the data to a 2° polynomial followed by first derivative analysis. Where possible, a sigmoidal function was fit to the data to estimate T_m values.

In addition to thermal stress studies, long term stability of the final formulations was also monitored by Trp fluorescence using the instrument settings described above. Temperature conditions equivalent to the long term stability storage temperature were used for measurements. Disposable Brand UV semi-micro cuvettes (1-3 mL) purchased from Sigma were using for these studies.

4.2.4 Adjuvant Binding Studies

The aluminum hydroxide product Alhydrogel® was selected due to its zero point charge (approximately 11) which suggests it could potentially form desirable ionic interactions with the tip proteins. For binding assays, Alhydrogel® was diluted to 0.5 mg/ml while the protein concentration was varied from approximated 0.1 mg to 0.7 mg in a solution totaling 1 ml. A 10 mM Histidine/5 mM phosphate buffer was selected since this buffer was the initial choice for final formulation based on earlier studies.[17] The concentration of the proteins prior to adjuvant addition was confirmed with an Agilent 8453 diode array spectrophotometer by measuring ultraviolet (UV) absorption spectra from 200-400 nm. Concentrations were calculated from the absorbance at 280 nm. Adjuvant was added and the samples were tumbled on an end-over-end tube rotor at 4 °C for 1 h to ensure steady state was reached. Adjuvant was then pelleted by centrifugation at 14,000g for 1 min. The UV Absorbance of the supernatant was recorded to ascertain the concentration of free protein. From the initial and supernatant protein amounts, mass balance calculations gave bound protein values.

Protein desorption from Alhydrogel® was explored using compounds known to frequently disrupt specific binding mechanisms. These include sodium chloride (2M), sodium phosphate (1M) and sodium citrate (1M). Samples containing 0.1 mg of protein were pelleted as described above and the supernatants were replaced with an equal volume of one of the potentially protein-adjuvant disrupting solutions. After reconstitution, samples were tumbled for 1 h and the adjuvant was again centrifuged

to pellet the adjuvant. Concentrations of protein in the supernatant were determined as described previously.

4.2.5 Long Term Stability Studies

Potential formulations were tested for long term stability at 25 °C for each of the five sub-unit vaccine candidates. Formulations consisted of 1 mL samples of 0.1 mg protein and 0.5 mg Alhydrogel® in solutions containing 10% sucrose and 5% dextrose. Positive controls containing no excipient and negative controls lacking tip proteins were included in the study. Chemical stability was quantified by desorbing the proteins from the adjuvant after 40 days at 40 °C with 1 M sodium phosphate. Samples were subjected to trypsin digestion (0.05mg/ml trypsin for 8 hrs at 37 °C) and subjected to capillary liquid chromatography-mass spectrometry (LC-MS). The capillary liquid chromatography column was directly connected to a LTQ-FT Ultra Hybrid Mass Spectrometer (ThermoFinnigan) as described [36]. MS/MS results were processed using TurboSequest batch search in BioWorks 3.2 software. After subsequent data analysis with an in house Perl script, the Mascot (v2.2, Matrix Science) database-searching program was used to identify the peptides and proteins. All major protein degradation pathways were explored during this process. Results were imported into Scaffold 2.2.03 software (Proteome Software Inc.) for viewing and Xcaliber® was used for quantitative analysis in concert with Scaffold 2.2.03.

4.3 Results and Discussion

4.3.1 Excipient Screening and Optimization in Solution

To increase the stability of proteins in solution, a variety of compounds and polymers are typically included in commercial formulations. In this case, a library of GRAS (generally regarded as safe) compounds was tested for stabilizing effects. Components of this library include amino acids, antioxidants, cyclodextrans, carbohydrates, surfactants, polyols and proteins (see Table 4.1 for further examples) which potentially stabilize through a variety of mechanisms. Based on previous work in Chapter 2, one of the tip proteins' major degradations pathways at elevated temperatures was aggregation. Therefore turbidity was chosen to identify potential stabilizers.[17] Turbidity was monitored as the optical density at 360 nm as the samples were incubated at 55 °C in the presence excipients.

Results of excipient screening are shown in Table 4.1 where the average percent inhibition has been used to rank order the stabilizers. Only excipients which had an average positive percent inhibition are shown. Individual percent inhibition values varied by no more than ± 5% except in cases of greater than 50% negative inhibition where error was often as large as the absolute values of the results shown. Based on this study, sugars and polyols appear to have the greatest stabilizing effects on the proteins with dextrose inhibiting aggregation to the greatest extent. Interestingly, the ability of dextrose to stabilize is effectively invariant to its

Excipients	Concentration	IpaD	BipD	SipD	LcrV	PcrV	Average
Dextrose	20.00%	79	45	69	86	95	75
Sucrose	20.00%	83	44	53	84	89	71
Dextrose	10.00%	74	51	65	70	73	67
Sorbitol	20.00%		35	63	73	92	66
Lactose	20.00%	66	33	76	61	91	65
Glycerol	20.00%	76	39	38	58	87	60
2-OH propyl γ-CD	10.00%	21	60	56	64	49	50
Mannitol	10.00%	56	19	49	53	69	49
Sucrose	10.00%	55	35	38	39	67	47
Lactose	10.00%	47	24	53	52	57	47
Trehalose	10.00%	54	0	53	58	61	45
Trehalose	20.00%	79	64	-114	92	78	40
Glycerol	10.00%	47	9	16	39	57	34
Arginine	0.3 M	64	38	11	28	22	33
2-OH propyl β-CD	10.00%	-52	5	32	66	46	19
Sodium Citrate	0.1 M	48	15	12	45	-23	19
α Cyclodextrin	2.50%	25	-67	-1	92	32	16
Sorbitol	10.00%	62	-2	-97	35	77	15
Guanidine	0.3 M	53	60	-16	37	-74	12
Pluronic F-68	0.01%	-4	-26	95	-8	-11	9
Sodium Citrate	0.2 M	69	56	26	45	-177	4
2-OH propyl γ-CD	5.00%	-27	37	12	47	-66	1

Table 4.1. Percent Inhibition of Aggregation. High throughput excipient screening expressed in terms of Percent Inhibition of aggregation. Samples were incubated for a period of 2 h at 55 °C at pH 5. Uncertainties are approximately 5 % with the exception of the highly negative numbers where error may equal the absolute value of the percent inhibition.

concentration (compare 20% to 10% w/v) for IpaD, BipD and SipD. Many of the compounds screened stabilized one or two of the proteins while behaving like chaotropic agents with others. This trend did not follow protein sub-family classifications. Prior biophysical characterization and primary sequence information suggested that IpaD, BipD and SipD were more homologous, forming one sub-family while LcrV and PcrV belonged in another.[17] The additives which most stabilized the tip proteins presumably do so through the well known mechanism of preferential exclusion.[37-40] Preferential exclusion occurs when the compounds are excluded from the protein surface which ultimately favors a smaller surface area and therefore increases the free energy of unfolding.[38-40]

After some additional screening of the best stabilizers from Table 4.1, a formulation containing 10% sucrose and 5% dextrose was identified as most potent in inhibiting aggregation. To determine whether the stabilizing mechanism of the formulation was due to increased conformational stability or to an excipient/protein interaction that directly blocked protein association, tertiary structural stability was measured by intrinsic Trp fluorescence. Fluorescence emission peak position was monitored as a function of temperature from 10 to 85 °C at pH 5 (not illustrated) and subsequently at pH 7 (Figure 4.1). In agreement with previous results, IpaD and SipD (Figure 4.1A,C) display biphasic transitions indicative of two independent folding domains.[15-17] The calculated transition midpoint (T_m) for the first transition is increased by more than 2 °C for both proteins in the sucrose/dextrose formulation.

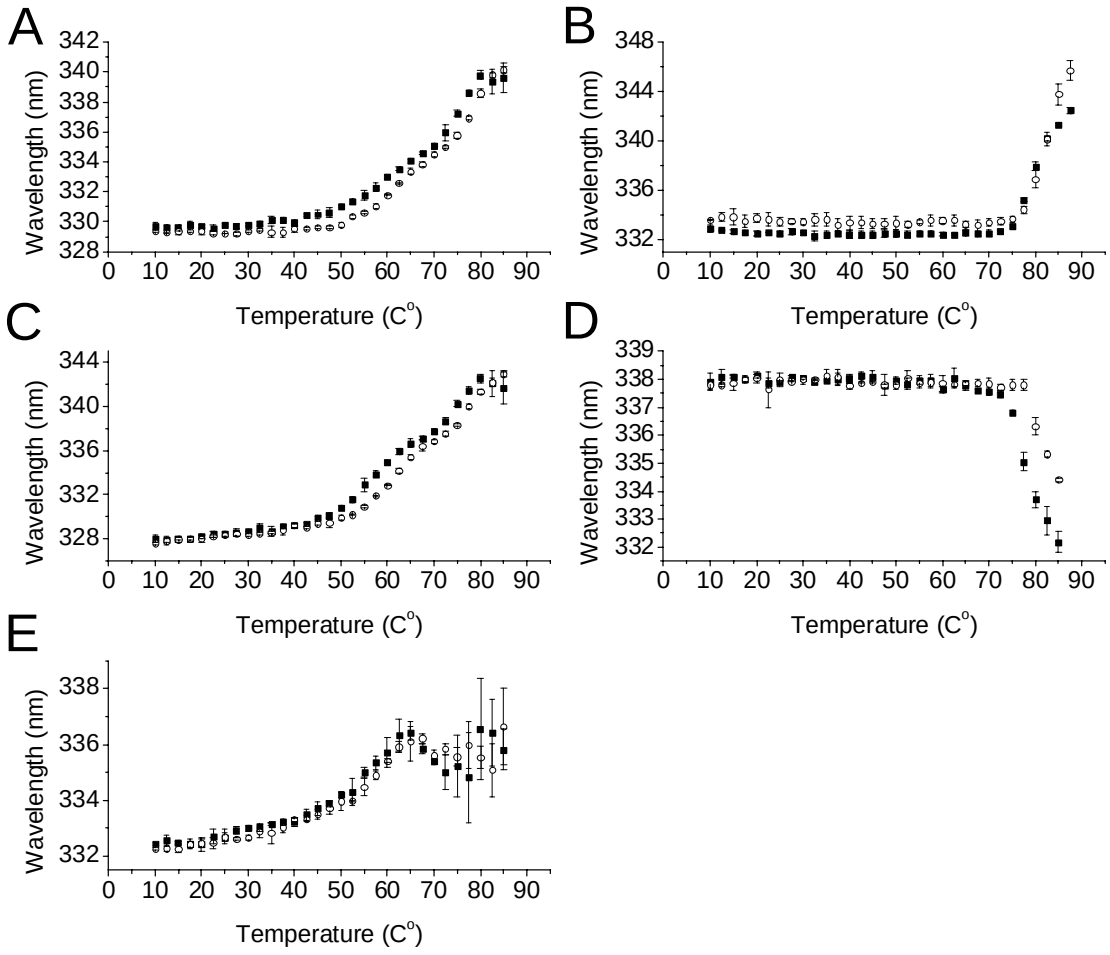

Figure 4.1: Intrinsic Trp fluorescence peak position measured from 10 to 85 °C for IpaD (A), BipD (B), SipD (C), LcrV (D) and PcrV (E). The excitation wavelength was 295 nm. The proteins were monitored in the absence (■) and presence (○) of sucrose 10% and dextrose 5%. Error bars are the standard deviation from at least three trials.

BipD, the other member of the subfamily, appears to have less labile tertiary structure with a T_m occurring without excipients at nearly 80 °C and rising above 82 °C in their presence. Transition midpoints for BipD were calculated based on the assumption that the curves are beginning to curve towards upper asymptotes. Estimates of the onset of temperature transition (T_0) resulted in similar conclusions.

Unlike the other tip proteins, transitions for LcrV in the presence and absence of excipient shift to shorter wavelengths indicating that the Trp residue is moving into a more apolar environment. Transition onsets for LcrV increase by nearly 5 °C in the formulation. Unlike LcrV which exhibited blue shifts in agreement with previous work, PcrV shifts to longer wavelengths in this study. This possibly occurs due to the change in buffer system from 20 mM citrate/phosphate to 10 mM histidine/5 mM phosphate. Interestingly, initial emission wavelengths (10°C) and static light scattering transitions are similar in either buffer system (not illustrated), suggesting that interactions with either the citrate or histidine effect PcrV unfolding, but perhaps not its initial conformation nor its propensity to aggregate. PcrV's T_m is increased by more than 2 °C in the presence of the excipients.

4.3.2 Adjuvant Binding

To quantify the extent of tip protein adsorption to Alhydrogel®, adsorption isotherms were created by incubating known concentrations of the proteins with adjuvant at 4 ° C and measuring the unbound protein in the supernatant after

centrifugation (Figure 4.2). Simple mass balance calculations were then used to produce the plots shown here. Conditions were sought under which the antigens are at least 95% adsorbed based on the idea that an enhanced immune response is dependent on a high degree of antigen adorption.[23] In a 1 ml solution containing 0.5 mg aluminum hydroxide, up to 0.65 mg of IpaD are bound (Figure 4.2A). LcrV has comparable adsorption properties to IpaD and is highly bound throughout the experimental range. BipD and PcrV show less affinity to aluminum hydroxide and have similar binding curves to each other. SipD adsorbs the least, falling below 95% adsorption at 0.15 mg.

It is possible that there is some difference in the mechanism of adsorption for BipD, SipD and PcrV compared to LcrV and IpaD. The most direct evidence for this, besides the differences in the adsorption isotherms discussed above, is the adsorption properties of the proteins in the presence of the excipients (10% sucrose and 5% dextrose). In studies conducted for the proteins at 0.4 mg (except SipD which because of its low binding was tested at 0.15 mg), the highly adsorbed IpaD and LcrV have unchanged properties, however, the remaining three proteins show a reduction in binding (Figure 4.3). Upon addition of the formulation stabilizers, the amount of protein adsorbed for BipD and SipD is reduced by more than 30% and PcrV adsorption is reduced approximately 10%. Even when the amount of protein added is significantly reduced (halved for BipD and PcrV), the percentage of protein adsorbed in the presence of the excipients does not reach the levels of protein and adjuvant

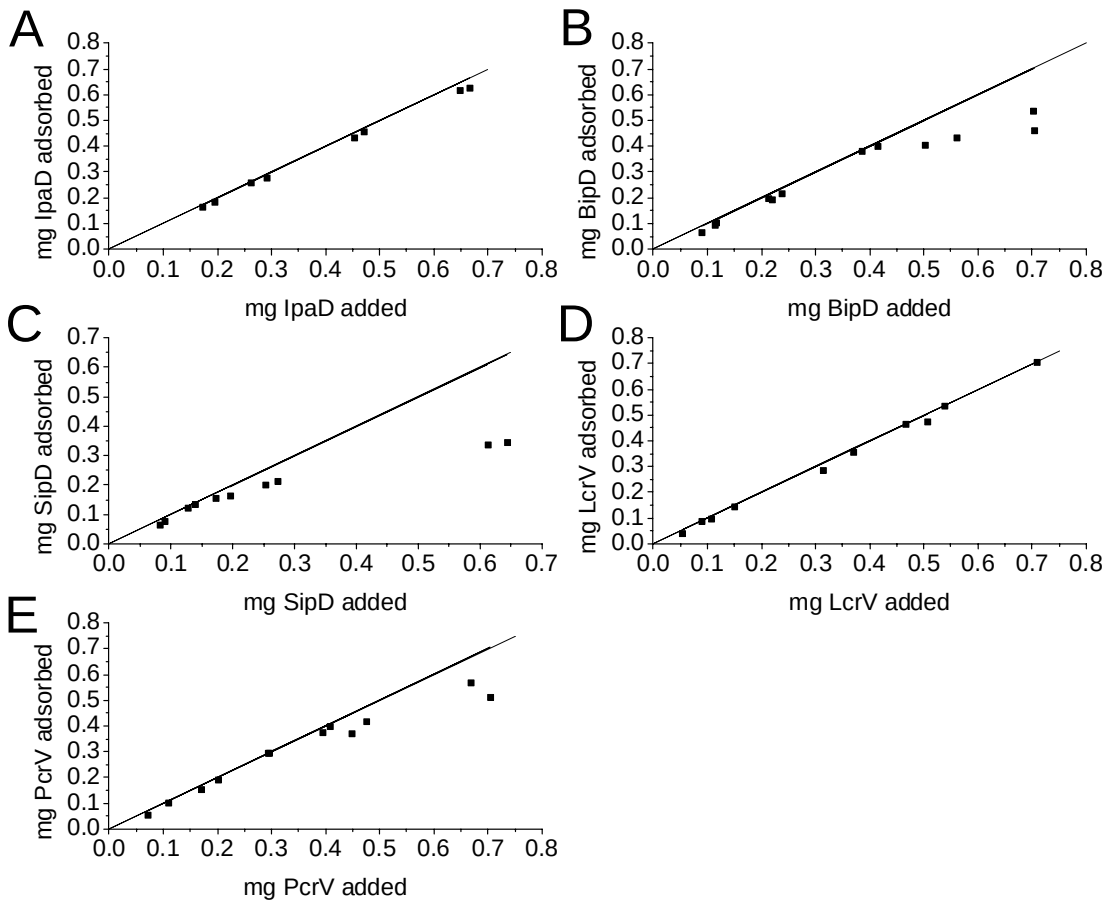

Figure 4.2: Adsorption isotherms of IpaD (A), BipD (B), SipD, (C), LcrV (D) and PcrV (E) to Alhydrogel® at 4 °C. The aluminum amount was 0.5 mg in all cases. Solid lines represent 100% adsorption.

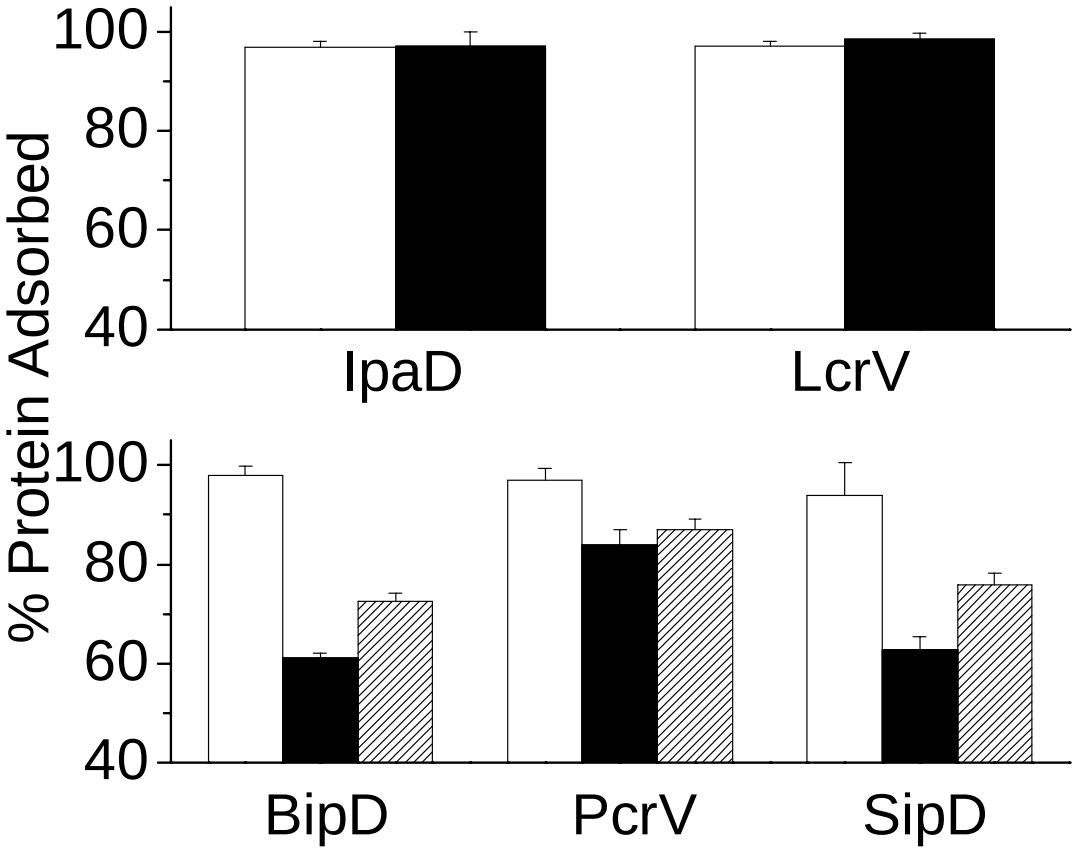

Figure 4.3: Percent of protein adsorbed to 0.5 mg Alhydrogel® in absence (□) and presence (■) of 10% sucrose 5% dextrose. Protein content is 0.4 mg for (■,□) and 0.2 mg for the crosshatched bar with the exception of SipD where the amounts are 0.15 mg and 0.1 mg respectively.

alone. This phenomenon was observed regardless of the order of addition of the components.

The cause of the reduced adsorption is not completely clear since desorption studies of the individual tip proteins give different results (not illustrated). Three different compounds were evaluated (sodium chloride, sodium phosphate and sodium citrate) based on their ability to disrupt the protein-aluminum hydroxide interaction. Addition of 2 M sodium chloride did not desorb more than 11 % of any of the proteins (the highest was SipD), suggesting that the interaction between the antigens and the Alhydrogel® is not primarily ionic. Addition of 1 M sodium phosphate, which exchanges hydroxide ions with phosphate, released at least half of IpaD, BipD and LcrV but had less effect on SipD and PcrV. Finally, citrate which partially dissolves aluminum hydroxide had results nearly identical to those seen for phosphate addition for all of the proteins. Based on these results it appears that the interaction between the proteins and the adjuvant is perhaps a mixture of hydrogen bonding and Van der Waals forces, although the relative importance of each may vary by protein. While the results from Figure 4.3 would suggest that BipD, SipD and PcrV have similar adsorption mechanisms, the other additive studies suggest that BipD is more similar to IpaD and LcrV. The results for BipD may highlight the difference in its structure compared to the other proteins. While the other four tip proteins are dumbbell shaped with a coiled-coil in the middle, BipD possess a triple coiled-coil which may effect its interaction with the adjuvant .[10,14]

Intrinsic Trp fluorescence data suggest that the chosen excipient combination increased protein tertiary structural stability in solution, however, it is important to also monitor Trp fluorescence when the antigens are adsorbed to Alhydrogel®. Samples were therefore thermally stressed from 10 to 85 °C when bound to the adjuvant using front surface Trp fluorescence to minimize light scattering problems and T_m values were calculated (Table 4.2). When comparing the adsorbed proteins to those in solution, nearly all samples manifested lower T_m values upon adsorption with the exception of IpaD. The decreased transition temperatures are indicative of destabilization of the proteins' tertiary structures when adsorbed to aluminum hydroxide. IpaD displays a biphasic transition in solution. Its first T_m is displayed in Table 4.2, however, only a single transition is observed upon adsorption to the adjuvant. Since the second thermal transition is higher than the T_m in the presence of Alhydrogel® it may also be that IpaD is less stable on the adjuvant surface.

Statistically significant increases in stability are observed when the optimized excipient combination is introduced to the adjuvant system, again with the exception of IpaD where no change occurs. Since the concentration of protein in these studies is 0.1 mg/ml with over 95% of the protein adsorbed, this suggests that the stabilization effect does not reflect the behavior of the free antigen. While little is known about how excipients effect the stability of adsorbed proteins, it seems likely that preferential exclusion continues to play a role.[37,39,40] It is unclear why IpaD does not exhibit increased stability in the presence of sucrose and dextrose in this case. One would predict that IpaD would exhibit increased stability like its counterparts.

	Solution	Adsorbed to Alhydrogel®	Complete Formulation
IpaD	60.4 ± 0.5	64.4 ± 1.4	64.0 ± 4.8
BipD	79.7 ± 0.2	73.7 ± 0.8	78.1 ± 0.3
SipD	56.6 ± 0.4	48.1 ± 0.6	59.6 ± 0.6
LcrV	72.0 ± 0.3	66.7 ± 0.2	70.5 ± 1.1
PcrV	57.2 ± 1.7	54.3 ± 1.0	57.2 ± 1.7

Table 4.2: Transition midpoints calculated from intrinsic Trp fluorescence measurement from 10 to 85 °C. The solution column provides values for protein alone (0.1 mg/ml), the second column shows protein adsorbed to the aluminum adjuvant (0.5 mg/ml) and the final column for adsorbed protein in 10% sucrose and 5% dextrose.

Therefore, it is possible that there is some change in either the behavior of the excipient or the protein upon adsorption. It is also possible, however, that IpaD is sufficiently structurally disrupted in the presence of Alhydrogel® that preferential hydration simply has no stabilizing effect.

4.3.3 Long Term Stability

While thermally stressing the prospective vaccines from 10 to 85 °C is useful in predicting stability, it is important to confirm those results with long term experiments. Stability studies were conducted to monitor changes in tertiary structure of the proteins adsorbed to Alhydrogel® in the presence and absence of the optimized excipient combination at 25 °C. This was accomplished by measuring peak position using intrinsic Trp fluorescence at three to four day intervals for a period of 100 days. Data indicate that there is no significant change in fluorescence emission peak position in the prospective vaccine during this time (data not shown). Tip proteins adsorbed to adjuvant in the absence of the excipients also showed no statistically significant variance in fluorescence emission. These results indicate that either the proteins possess physical stability for greater than three months or that intrinsic Trp fluorescence is not sensitive to the tertiary structural changes that occur over time. UV spectroscopy was used to measure possible desorption of proteins or protein fragments. No such events were observed, suggesting that the physical interactions responsible for adsorption are unchanged and possibly enhanced over time.

Capillary liquid chromatography and mass spectrometry (LC-MS) analysis provided information on possible chemical degradation. Proteins in the potential final formulations as well as proteins adsorbed to adjuvant alone were stored at 40 °C for 40 days. The incubated proteins were desorbed from adjuvant using 1 M sodium phosphate and then digested using trypsin. As a negative control, fresh samples were also analyzed. Asn deamidation was the predominant degradation pathway and is shown Table 4.3 (in the case of SipD some Gln degradation was also observed). Analysis of LcrV samples did not reveal chemical modifications under any circumstances. Primary sequence data for IpaD revealed three Asn residues followed by Gly which are especially susceptible to deamidation and consequently even fresh samples showed some deamidation of Asn (Table 4.3).[41,42] IpaD also experienced deamidation in the presence of 10% sucrose and 5% dextrose, but much more extensive degradation occurred in their absence. For SipD Asn^{88} and PcrV Asn^{252}, deamidation events observed with protein and adjuvant alone were undetectable in the final formulation. In the case of BipD, however, the second residue deamidated completely under either incubation condition. Interestingly, a small amount of deamidation was observed in the fresh sample at Asn^{270} but not seen in incubated samples. It is possible that adsorption to the adjuvant alters the secondary or tertiary structure such that the Asn^{270} Φ and Ψ angles no longer permit facile deamidation.

If one assumes that the secondary and tertiary structure of these proteins is stabilized in long term stability conditions in the presence of the optimized excipient combination, as would be predicted based on T_m data from Table 4.2, then the

IpaD			
AA #	Fresh	A	+E
48	10	20	9
107	0	3	0
241	0	100	100
266	65	100	100
305	7	50	0

BipD			
AA #	Fresh	A	+E
2	0	100	100
270	2	0	0

SipD			
AA #	Fresh	A	+E
88	1	2	0

PcrV			
AA #	Fresh	A	+E
252	2	30	0

Table 4.3. Percent deamidation of tip proteins Asn residues. Only Asn residues which displayed significant degradation are shown. The initial column for each protein lists the primary sequence number. This is followed by results for fresh protein subjected to tryptic digest. The A and +E columns represent samples incubated at 40 °C for 40 days in the absence and presence of excipients respectively. Error for all values shown is less than 5%.

chemical degradation results observed for most proteins is not surprising. There is mounting evidence that proteins are in general more chemically stable when a high degree of secondary and tertiary structure exists.[43-49] Indeed, even the deamidation in BipD does not refute this explanation. Since the Asn residue is second in the primary sequence, it is probably not part of any rigid structural feature that would inhibit the formation of the critical cyclic-imide intermediate.

4.4 Conclusions

Subunit vaccines containing multiple antigens offer many advantages including increased patient compliance and cost, but finding formulation conditions appropriate for all antigens is often difficult. The purpose of this chapter was to show how biophysical methods can be used to methodically expedite formulation even in complex systems. Choosing aggregation as the degradation pathway to monitor, high throughput screening of a GRAS library of compounds was accomplished for all five TTSA needle tip proteins. Following additional analysis, an optimized excipient combination (10% sucrose and 5% dextrose) was identified. This excipient combination was shown to stabilize the proteins both in solution and when adsorbed to Alhydrogel® under thermal stress studies. Adsorption isotherms and desorption experiments were conducted to characterize the nature of the interaction of the proteins with aluminum hydroxide. IpaD and LcrV have the strongest interaction with Alhydrogel. This interaction is not affected by the inclusion of excipients. Long

term stability studies at 25 °C established that the tip proteins' intrinsic Trp fluorescence peak position remains unchanged for over three months. Initial chemical stability data indicate that 10% sucrose and 5% dextrose generally inhibit degradation of the proteins. In the future, additional long term stability and chemical stability studies are needed for the five antigens in combination.

4.5 References

1. WHO. 2009. *Shigella*. ed.
2. Brooks JT, Shapiro RL, Kumar L, Wells JG, Phillips-Howard PA, Shi YP, Vulule JM, Hoekstra RM, Mintz E, Slutsker L 2003. Epidemiology of sporadic bloody diarrhea in rural Western Kenya. Am J Trop Med Hyg 68(6):671-677.
3. Graham SM 2002. Salmonellosis in children in developing and developed countries and populations. Curr Opin Infect Dis 15(5):507-512.
4. Levy SB, Marshall B 2004. Antibacterial resistance worldwide: causes, challenges and responses. Nat Med 10(12 Suppl):S122-129.
5. Fulla N, Prado V, Duran C, Lagos R, Levine MM 2005. Surveillance for antimicrobial resistance profiles among *Shigella* species isolated from a semirural community in the northern administrative area of Santiago, Chile. Am J Trop Med Hyg 72(6):851-854.
6. Cossart P, Sansonetti PJ 2004. Bacterial invasion: the paradigms of enteroinvasive pathogens. Science 304(5668):242-248.
7. Galan JE, Wolf-Watz H 2006. Protein delivery into eukaryotic cells by type III secretion machines. Nature 444(7119):567-573.
8. He SY, Nomura K, Whittam TS 2004. Type III protein secretion mechanism in mammalian and plant pathogens. Biochim Biophys Acta 1694(1-3):181-206.
9. Espina M, Olive AJ, Kenjale R, Moore DS, Ausar SF, Kaminski RW, Oaks EV, Middaugh CR, Picking WD, Picking WL 2006. IpaD Localizes to the Tip of the Type III Secretion System Needle of *Shigella flexneri*. Infection and Immunity 74(8):4391-4400.
10. Johnson S, Roversi P, Espina M, Olive A, Deane JE, Birket S, Field T, Picking WD, Blocker AJ, Galyov EE, Picking WL, Lea SM 2006. Self-chaperoning of the type III secretion system needle tip proteins IpaD and BipD. J Biol Chem.

11. Mueller CA, Broz P, Mueller SA, Ringler P, Erne-Brand F, Sorg I, Kuhn M, Engel A, Cornelis GR 2005. The V-Antigen of *Yersinia* Forms a Distinct Structure at the Tip of Injectisome Needles. Science (Washington, DC, United States) 310(5748):674-676.
12. Picking WL, Nishioka H, Hearn PD, Baxter MA, Harrington AT, Blocker A, Picking WD 2005. IpaD of *Shigella flexneri* is independently required for regulation of Ipa protein secretion and efficient insertion of IpaB and IpaC into host membranes. Infect Immun 73(3):1432-1440.
13. Derewenda U, Mateja A, Devedjiev Y, Routzahn KM, Evdokimov AG, Derewenda ZS, Waugh DS 2004. The structure of *Yersinia pestis* V-antigen, an essential virulence factor and mediator of immunity against plague. Structure (Cambridge, MA, United States) 12(2):301-306.
14. Erskine PT, Knight MJ, Ruaux A, Mikolajek H, Sang NW, Withers J, Gill R, Wood SP, Wood M, Fox GC, Cooper JB 2006. High Resolution Structure of BipD: An Invasion Protein Associated with the Type III Secretion System of *Burkholderia Pseudomallei*. J Mol Biol 363(1):125-136.
15. Espina M, Ausar SF, Middaugh CR, Baxter MA, Picking WD, Picking WD 2007. Conformational stability and differential structural analysis of LcrV, PcrV, BipD, and SipD from type III secretion systems. Protein Sci 16(4):704-714.
16. Espina M, Ausar SF, Middaugh CR, Picking WD, Picking WL 2006. Spectroscopic and calorimetric analyses of invasion plasmid antigen D (IpaD) from *Shigella flexneri* reveal the presence of two structural domains. Biochemistry 45(30):9219-9227.
17. Markham AP, Birket SE, Picking WD, Picking WL, Middaugh CR 2008. pH sensitivity of type III secretion system tip proteins. Proteins 71(4):1830-1842.
18. Turbyfill KR, Mertz JA, Mallett CP, Oaks EV 1998. Identification of epitope and surface-exposed domains of *Shigella flexneri* invasion plasmid antigen D (IpaD). Infect Immun 66(5):1999-2006.
19. Anderson GW, Jr., Leary SE, Williamson ED, Titball RW, Welkos SL, Worsham PL, Friedlander AM 1996. Recombinant V antigen protects mice against pneumonic and bubonic plague caused by F1-capsule-positive and -negative strains of *Yersinia pestis*. Infect Immun 64(11):4580-4585.
20. Leary SE, Williamson ED, Griffin KF, Russell P, Eley SM, Titball RW 1995. Active immunization with recombinant V antigen from *Yersinia pestis* protects mice against plague. Infect Immun 63(8):2854-2858.
21. Holder IA, Neely AN, Frank DW 2001. PcrV immunization enhances survival of burned *Pseudomonas aeruginosa*-infected mice. Infect Immun 69(9):5908-5910.
22. Brandau DT, . JLS, C.M. W, C. R, Middaugh CR 2003. Thermal stability of vaccines. Journal of Pharmaceutical Sciences 92(2):218-231.
23. WHO. 1976. World Health Organization technical report series no. 595. ed., Geneva: World Health Organization. p 5-6.
24. Cox JC, Coulter AR 1997. Adjuvants--a classification and review of their modes of action. Vaccine 15(3):248-256.

25. Akira S, Takeda K, Kaisho T 2001. Toll-like receptors: critical proteins linking innate and acquired immunity. Nat Immunol 2(8):675-680.
26. Lindblad EB 2004. Aluminium compounds for use in vaccines. Immunol Cell Biol 82(5):497-505.
27. Lindblad EB 2004. Aluminium adjuvants--in retrospect and prospect. Vaccine 22(27-28):3658-3668.
28. Johnston CT, Wang SL, Hem SL 2002. Measuring the surface area of aluminum hydroxide adjuvant. J Pharm Sci 91(7):1702-1706.
29. Jones LS, Peek LJ, Power J, Markham A, Yazzie B, Middaugh CR 2005. Effects of adsorption to aluminum salt adjuvants on the structure and stability of model protein antigens. J Biol Chem 280(14):13406-13414.
30. Gupta RK 1998. Aluminum compounds as vaccine adjuvants. Adv Drug Deliv Rev 32(3):155-172.
31. Singh M, O'Hagan DT 2002. Recent advances in vaccine adjuvants. Pharm Res 19(6):715-728.
32. Seeber SJ, White JL, Hem SL 1991. Predicting the adsorption of proteins by aluminium-containing adjuvants. Vaccine 9(3):201-203.
33. Vogel FR, Powell MF 1995. A compendium of vaccine adjuvants and excipients. Pharm Biotechnol 6:141-228.
34. Marquart ME, Picking WL, Picking WD 1995. Structural analysis of invasion plasmid antigen D (IpaD) from *Shigella flexneri*. Biochem Biophys Res Commun 214(3):963-970.
35. Nanao M, Ricard-Blum S, Di Guilmi AM, Lemaire D, Lascoux D, Chabert J, Attree I, Dessen A 2003. Type III secretion proteins PcrV and PcrG from *Pseudomonas aeruginosa* form a 1:1 complex through high affinity interactions. BMC Microbiol 3:21.
36. Ikehata K, Duzhak TG, Galeva NA, Ji T, Koen YM, Hanzlik RP 2008. Protein Targets of Reactive Metabolites of Thiobenzamide in Rat Liver in Vivo. Chemical Research in Toxicology 21(7):1432-1442.
37. Gekko K, Timasheff SN 1981. Mechanism of protein stabilization by glycerol: preferential hydration in glycerol-water mixtures. Biochemistry 20(16):4667-4676.
38. Kendrick BS, Chang BS, Arakawa T, Peterson B, Randolph TW, Manning MC, Carpenter JF 1997. Preferential exclusion of sucrose from recombinant interleukin-1 receptor antagonist: role in restricted conformational mobility and compaction of native state. Proc Natl Acad Sci U S A 94(22):11917-11922.
39. Lee JC, Timasheff SN 1981. The stabilization of proteins by sucrose. J Biol Chem 256(14):7193-7201.
40. Timasheff SN 1993. The control of protein stability and association by weak interactions with water: how do solvents affect these processes? Annu Rev Biophys Biomol Struct 22:67-97.
41. Patel K, Borchardt RT 1990. Chemical pathways of peptide degradation. III. Effect of primary sequence on the pathways of deamidation of asparaginyl residues in hexapeptides. Pharm Res 7(8):787-793.

42. Patel K, Borchardt RT 1990. Chemical pathways of peptide degradation. II. Kinetics of deamidation of an asparaginyl residue in a model hexapeptide. Pharm Res 7(7):703-711.
43. Robinson AB, Rudd CJ 1974. Deamidation of glutaminyl and asparaginyl residues in peptides and proteins. Curr Top Cell Regul 8(0):247-295.
44. Wearne SJ, Creighton TE 1989. Effect of protein conformation on rate of deamidation: ribonuclease A. Proteins 5(1):8-12.
45. Xie M, Schowen RL 1999. Secondary structure and protein deamidation. J Pharm Sci 88(1):8-13.
46. Xie M, Shahrokh Z, Kadkhodayan M, Henzel WJ, Powell MF, Borchardt RT, Schowen RL 2003. Asparagine deamidation in recombinant human lymphotoxin: hindrance by three-dimensional structures. J Pharm Sci 92(4):869-880.
47. Kosky AA, Razzaq UO, Treuheit MJ, Brems DN 1999. The effects of alpha-helix on the stability of Asn residues: deamidation rates in peptides of varying helicity. Protein Sci 8(11):2519-2523.
48. Chu JW, Yin J, Brooks BR, Wang DI, Ricci MS, Brems DN, Trout BL 2004. A comprehensive picture of non-site specific oxidation of methionine residues by peroxides in protein pharmaceuticals. J Pharm Sci 93(12):3096-3102.
49. Pan B, Abel J, Ricci MS, Brems DN, Wang DI, Trout BL 2006. Comparative oxidation studies of methionine residues reflect a structural effect on chemical kinetics in rhG-CSF. Biochemistry 45(51):15430-15443.

Chapter 5

Biophysical Characterization of *Chlamydia trachomatis* CT584: A Newly Discovered Putative TTSS Tip Protein

5.1 Introduction

Chlamydia infections are common throughout the world and cause a range of diseases including pneumonia, atherosclerosis, pelvic inflammatory disease, reproductive sterility and blindness.[1,2] *Chlamydia trachomatis* alone is responsible for an estimated 92 million sexually transmitted infections a year.[3] Despite this prevalence, much is still unknown about the pathogenesis of these obligate intracellular pathogens. *Chlamydia* invade eukaryotic cells as a metabolically inactive elementary body (EB) and form an inclusion which evades fusion with the late endosome/lysosome endocytic vescicles.[4-7] In this compartment, EB convert into metabolically active reticulate bodies (RB) which replicate by binary fission.[4] After approximately 18 hrs, RB begin differentiating back into EB and are eventually exocytosed to repeat the infection cycle. The pathogens are also known to exist in a persistent form inside host cells presumably to evade immune system responses.[2,8,9]

Like many pathogenic Gram-negative bacteria, *Chlamydia* use type III secretion systems (T3SS) to facilitate infection and exploitation of eukaryotic cells.[10-14] In particular, the T3SS of *Chlamydia* is implicated in host cell invasion, intracellular trafficking, and maintenance of the unique intracellular niche of *Chlamydia*. Early evidence for the T3SS in these bacteria was based primarily on genetic information and electron microscopy where protrusions observed on the bacterial surface are presumed to be T3SS needles.[13-16] The lack of a system for genetic exchange in *C. trachomatis* has hampered functional studies of T3SS

components. Numerous proteins, however, have been demonstrated to be secreted in heterologous systems (e.g. *Shigella*) in a T3SS dependent manner and/or are present in the cytosol (or cytosolic face of inclusion) of *Chlamydia* infected cells, providing support for identification of effector molecules and utility of the T3SS in *Chlamydia*.[17-23] Unlike most bacteria possessing T3SSs, Chlamydial T3SS genes are found at multiple loci throughout the genome which has made identification of functional components more difficult.[10,24]

T3SS are composed of a basal body and a needle which is responsible for the translocation of effector proteins from the bacterial cytosol to the surface of a host cell or into its cytoplasm.[12,25,26] This secretion apparatus is comprised of more than 20 distinct proteins and has a possible evolutionary relationship to bacterial flagella. One class of protein in this system of particular interest is the tip protein which is so named for its propensity to localize to the extracellular needle tip.[27-30] These proteins have been shown to regulate secretion of the other effector proteins and thus play a pivotal role in the pathogenesis of the bacteria.[27] Furthermore, T3SS needle tip proteins, such as LcrV from *Yersinia pestis*, have been demonstrated to be excellent protective vaccinogens.[31-33] In addition, some tip proteins, such as IpaD from *Shigella flexneri*, may have additional roles though these functions are not fully understood.

In Chapter 2, biophysical tools were employed to understand the characteristics of T3SS needle tip proteins from proteobacteria. This work revealed protein sub-families based on their response to pH and temperature.[34,35] These

distinctions were made after creating Empirical phase diagrams (EPDs) which provide a global description of results from disparate techniques.[36,37] Furthermore, the utility of EPDs in highlighting structure/function similarities in proteins with little primary sequence homology has been established.[38]

The identity of the T3SS needle tip protein is presently unknown for *Chlamydia*. As presented here, computational structure prediction and homology search indicates that a *Chlamydia trachomatis* ORF (CT584), a protein with no primary sequence homology to any other protein with a determined function, exhibits predicted structural homology to T3SS needle tip proteins. In this chapter, we hypothesize that CT584 is a functional T3SS needle tip protein. To test this hypothesis, biophysical analyses of CT584 are employed to compare pH/temperature responses to the previously analyzed T3SS needle tip proteins.

5.2 Materials and Methods

5.2.1 CT584 cloning, expression, and purification

CT584 was PCR amplified from *C. trachomatis* (L2/434/Bu) using primers 5'- GGA ATT CCA TAT GAC GAC GAA ACC CAA AAC TC and 5'- CGC CGG CCG CCA CAG ATT TCG TTA ATT CTT C (Integrated DNA technologies, Coralville, IA). Purified amplicons were restriction enzyme digested (NdeI and EagI) and ligated into pET21b (Novagen). Isogenic transformants were selected and propagated in *E. coli* TOP10 (Invitrogen, Carlsbad, CA). Plasmid constructs were confirmed via DNA sequencing (University of Kansas, DNA Sequencing Facility).

For protein expression, plasmids containing CT584 were freshly transformed into BL21(DE3) *E. coli* (Bioline, Boston, MA) and grown at 37°C in 1 L of Luria-Bertani broth with 100 μg/mL ampicillin. Cells were grown to an OD_{600} 0.7 prior to 1 mM of isopropyl-β-D-thiogalactopyranoside being added. After 4 h of induction, cells were centrifuged and pellets frozen. Thawed cells were resuspended and lysed using sonication in a Tris Buffer (40mM Tris, 500mM NaCl, and 5% Glycerol pH 8.0). 6XHis-tagged CT584 was purified using a cobalt metal affinity resin (Talon beads; Pierce) and gravity filtration column. Protein was eluted in Tris buffer containing 500mM Imidizole and affinity purified CT584 was applied to a Superdex 200 gel filtration column (GE Healthcare) employing an ÄKTA FPLC (GE Healthcare) in Tris buffer. Protein containing fractions were collected at approximately 150 kDa. Coomassie stained SDS-PAGE of the protein sample revealed the expected 21 kDa monomer at >95% purity.

5.2.2 Ultraviolet Absorption Spectroscopy

Spectra for each protein were analyzed from 200-400 nm with an Agilent 8453 diode-array spectrophotometer equipped with a peltier temperature controller. The experimental spectral resolution was 1 nm and the integration time was set to 25 seconds. Spectra were recorded from 10-90 °C in 2.5 °C increments with a 5 min equilibration time at each temperature. The resultant absorbance data were analyzed using Agilent UV-visible ChemStation™ software by fitting spectra to a fifth degree Savitzky-Golay polynomial followed by a second derivative calculation. The

derivative spectra were subjected to a 99 point interpolation which produces an effective resolution of 0.01 nm.

5.2.3 Far-UV Circular Dichroism

Circular dichroism (CD) spectra were recorded from 190-260 nm with a 1 nm resolution at 20 °C. Spectra were obtained with a Jasco J-720 spectrometer equipped with a Peltier controlled sample holder (Tokyo, Japan). For thermal stress experiments, CD data were acquired at 222 nm from 10-85 °C at a rate of 15 °C/hr. This wavelength was chosen to monitor changes in the protein's α-helical content. CD signals were converted to molar ellipticity using the Jasco software.

5.2.4 Fluorescence Spectroscopy

A PTI QM-1 spectrophotometer was used to collect fluorescence data. For intrinsic Tyr fluorescence, the excitation wavelength was 275 nm and emission was recorded from 280-380 nm in 1 nm increments with a 0.5 s integration time. In the case of ANS fluorescence, samples were excited at 372 nm with emission spectra acquired from 400-600 nm in 2 nm intervals. ANS was added from a 2 mg/ml ethanol solution to CT584 to obtain a 10:1 molar ANS/protein ratio. In both cases, emission was recorded by a photomultiplier tube (PMT) 90° from the angle of incident light. Approximately 1 ml of the samples were pipetted into a 1 cm pathlength quartz cuvette and data were collected from 10-85 °C in 2.5 °C increments. Light scattering was recorded simultaneously with the intrinsic

fluorescence acquisition with a second photomultiplier tube located 180° to the emission acquisition at 275 nm. Blank solutions containing all of the chemical components except protein were also measured and the resultant spectra were subtracted from the protein emission spectra. Peak positions were calculated in Origin® by fitting the data to a 2° polynomial curve followed by a first derivative calculation.

5.2.5 Empirical Phase Diagrams

Data from all the techniques described above were combined to create empirical phase diagrams (EPD). The underlying theory and mathematics employed have been described in detail previously.[37] In brief, data from the biophysical studies were formed into vectors with each vector representing a distinct pH/temperature setting. A density matrix is formed by assembling these vectors which can be manipulated to calculate eigenvalues. The three largest eigenvalues are selected and employed to create new eigenvectors which expand a truncated version of the data set in three dimensions. Each dimension is assigned a color (red, green, and blue) and the data are expressed in an EPD by plotting these color assignments. Thus, color assignments are arbitrary. Not equilibria are implied across "apparent" phase boundaries and these are therefore not thermodynamic phase diagrams but are empirical in nature.

5.2.6 Fourier Transform Infrared Spectroscopy

A Bruker (Billerica, MA) Tensor™ 27 FTIR spectrometer equipped with a ZnSe attenuated total reflectance (ATR) plate (Pike Technologies, Madison, WI) was used to collect Fourier transform infrared (FTIR) spectra at room temperature 25 °C. Data were collected over 256 composite scans with a resolution of 4 cm^{-1}. The samples were analyzed in 20 mM citrate/phosphate buffer at 1.8 mg/ml. Water spectra were subtracted with the OPUS spectroscopy software associated with the spectrometer and data were further analyzed using GRAMS/AI software (Galactic, Inc.). The baseline was corrected between 1800 and 2400 cm^{-1} and the spectra were then smoothed using a 5 point Savitsky-Golay function. Following Fourier self deconvolution, the Amide I/II bands of the spectrum (1500-1700 cm^{-1}) were decomposed using a peaks fitting tool which employs Gaussian band profiles. The second derivative spectra from 1500-1700 cm^{-1} provided the initial peak positions for fitting.

5.2.7 Analytical Ultracentrifugation

Protein molecular weight and oligomerization state were assessed using a Beckman Coulter XL-I analytical ultracentrifuge (Palo Alto, CA) in both sedimentation velocity and equilibrium modes. For sedimentation velocity, CT584 was diluted to 0.2 and 0.5 mg/ml in citrate phosphate buffer and injected into two channel, 12 mm optical path length cells. A four-hole An60Ti rotor at 10 °C housed the cells and samples were run in triplicate at 36,000 rpm for 8 hrs. Sedimentation

velocity analysis was conducted using SEDFIT (version 11.71) which was developed at the NIH by Peter Schuck. Continuous c(s) distribution analysis was employed and both the Simplex and Marquardt-Levenberg models were tested to ensure the final fit was in a global minimum. Both time and radial invariant noise were removed. In equilibrium mode, the same settings were used as before except 6 channel centerpieces were included in the assembly and the rotor speed was 17,000 RPM with 5 measurements taken hourly after a 12 hr delay. Data were analyzed using SEDPHAT (version 6.21) with a monomer n-mer Self Association model giving the best fit both for global reduced Chi² and local RMSD values.

5.3 Results

5.3.1 Computational Structure Prediction and Homology Comparison

Identifying candidate T3SS needle tip proteins using primary sequence homology has not proven useful in *Chlamydia*. To identify potential T3SS needle tip candidates, computational structure prediction followed by a structural homology search was employed. I-TASSER is a hierarchal protein structure, molecular modeling program that incorporates a secondary-structure enhanced Profile-Profile Alignment and iterative implementation of the Threading Assembly Refinement program.[39] This computational modeling program has proven to be the most effective program at accurately predicting protein 3D-structure blindly from primary sequence.[40,41] Using this program, predicted structures of proteins with unknown function can then be used for comparison to structures of proteins for which the

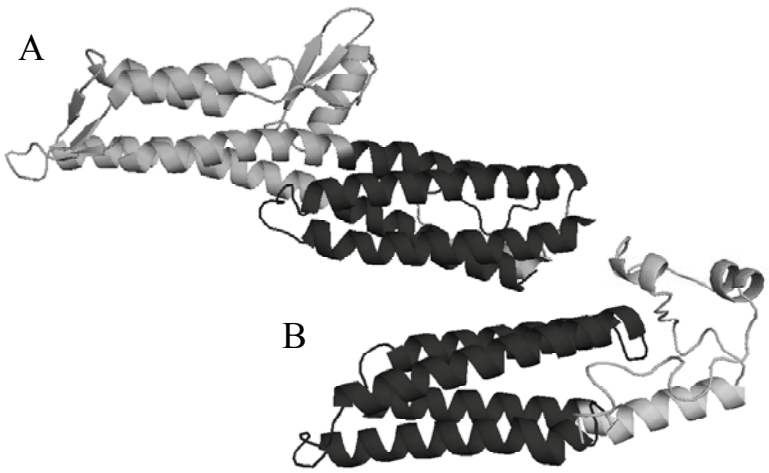

Figure 5.1. Protein Ribbon Structure of IpaD and I-TASSER Predicted Structure of *C. trachomatis* CT584. (A) IpaD from *Shigella flexneri* (PDB:2J0O) and (B) I-TASSER structural prediction of CT584. Region of shared structural similarity is indicated in dark grey.

function has previously been determined. Similar to primary sequence homology BLAST analysis, this approach can provide candidates for subsequent functional analysis.

One of the *C. trachomatis* proteins that exhibited predicted structural similarity to other T3SS needle tip proteins was ORF CT584. The I-TASSER predicted structure of CT584 was compared pairwise (DaliLite) to each of the three determined T3SS needle tip protein structures known: IpaD (2J0O), BipD (2IXR), and LcrV (1R6F).[42] This pairwise analysis will generate a Z-score indicative of the measure of quality for the alignment, with scores between 8-20 supporting an intermediate level of confidence that two proteins are homologous. For reference, comparison of IpaD and BipD structures return a relatively high Z-score of 17.3 with 220 amino acids aligned despite only 27% sequence identity. In contrast, IpaD or BipD compared to LcrV results in a very low Z-score < 3.9, reflecting the structural differences between these functionally similar proteins. Comparison of the predicted structure of CT584 to the structure of IpaD revealed an intermediate Z-score of 8.4. Only 108 amino acids of the predicted CT584 structure (of 184 total) were aligned to IpaD, although the aligned region is structured very similarly (Figure 5.1). Given the structural homology between IpaD and BipD, it was expected that a pairwise comparison of CT584 with BipD should show some homology. This analysis resulted in a Z-score of 6.9 and a region of structural similarity of 119 amino acids. In contrast to the results observed for IpaD and BipD, the Z-score for the LcrV

comparison to the predicted structure of CT584 was 2.1, close to a no confidence score (< 2.0).

Overall, structural prediction of CT584 and comparison to known T3SS needle tip protein structures provided an intermediate level of confidence that CT584 has structural similarity to T3SS needle proteins, specifically IpaD and BipD. The predicted structure of CT584 forms two alpha-helical coil-coiled domains. While this is a widely distributed structural feature, needle tip proteins share this structure.[29,43,44] Size exclusion chromatography indicated that CT584 is forming a higher order complex (~150 kDa), possibly a hexamer or heptamer. This molecular weight is very similar to that observed for natively purified T3SS needle tip proteins, including IpaD.[29,45] To provide further support for the hypothesis that CT584 is a *Chlamydia* T3SS needle tip protein, biophysical characterization of this protein was performed and compared to prior studies that revealed protein sub-families based on their response to pH and temperature.[34,35,46].

5.3.2 Far-UV Circular Dichroism

To characterize the secondary structure of CT584, circular dichroism (CD) and FTIR spectroscopy were employed Both of these techniques permit quantitation of α-helical and β-sheet content in addition to turns and disordered structural elements.[47,48] Circular dichroism spectra from 190 to 260 nm at 10 °C in pH 7 buffer indicate that, under physiologic conditions, the protein has primarily α-helical structure (Figure 5.2A). This conclusion is based on the presence of two negative

peaks located at 208 and 222 nm. Secondary structure analysis using the program Dichroweb estimates that the protein is 55% α-helical. CD spectra were measured from pH 3 to 8 and the strongest minima were recorded at pH 3 suggesting that maximum secondary structure exists under more acidic condition. In contrast, pH 6 possessed the least α-helical content while pH 8 had minima nearly as strong as pH 3 (not illustrated).

In addition to acquiring full length spectra at 10 °C, the intensity of the minimum at 222 nm was monitored as a function of temperature from 10 to 85 °C in 2.5 °C increments (Figure 5.2B). By thermally stressing the protein in this manner, the relative stability of the secondary structure can be ascertained. CT584 shows only small changes in secondary structure at pH 3 and 6 compared to other conditions. Transitions from pH 4-8 show increasing transition onsets ($T_{0)}$ with T_0 occurring near 20 °C at pH 4 and at approximately 42 °C in the pH 8 environment. The most distinctive trend is at pH 5 where there appears to be a biphasic transition initiating at 27 °C. This suggests the possible existence of at least two independently folding domains.

5.3.3 FTIR

Fourier transform infrared spectroscopy (FTIR) provides an orthogonal method with which to measure protein secondary structure and was performed here at pH 7 and 25 °C. Estimation of secondary structural elements is possible by deconvoluting the Amide I band (Figure 5.3).[48] Decomposition of the Amide I and II

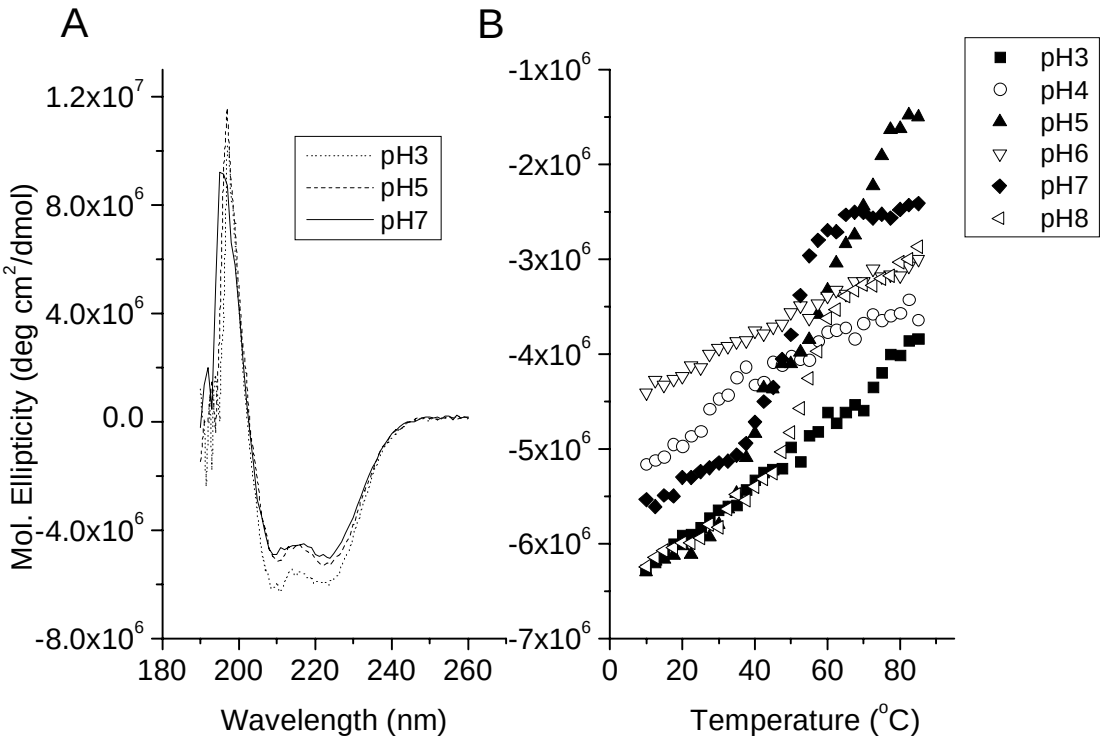

Figure 5.2. Far-UV Circular Dichroism. Spectra from 190 to 260 nm expressed in terms of molar ellipticity (A) and pH versus temperature trends at 222 nm monitored from 10 to 85 °C (B). Error bars not shown. ■, pH 3; ○, pH 4; ▲, pH 5; ▽, pH 6; ◆, pH 7; ◁, pH 8.

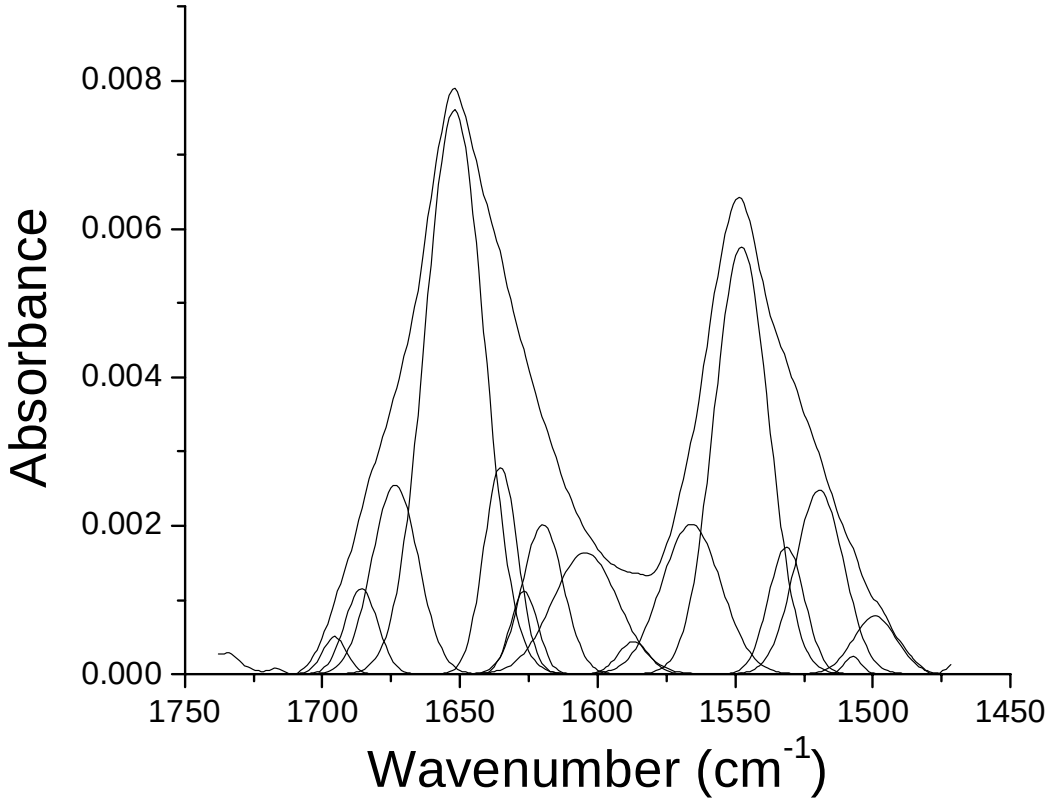

Figure 5.3. Deconvoluted Amide I and II bands in solution measured by ATR-FTIR at 1.8 mg/ml and pH 7. The Fourier self-deconvolution bandwidth and enhancement parameters were 21 and 2.5 respectively. Six peaks were identified as secondary structure elements at 1695.5, 1683.7, 1674.2, 1652.9, 1635.9 and 1625.5 cm^{-1}.

bands was accomplished using Fourier self-deconvolution with the second derivative trace of the spectra guiding initial peak position estimates. From this analysis 6 peaks were clearly identified at 1695.5, 1683.7, 1674.2, 1652.9, 1635.9 and 1625.5 cm^{-1}. The first two peaks are generally associated with β-turns, while peaks at 1674.7 cm-1 and the two below 1650 cm^{-1} are attributed to β-sheet.[48] The dominant peak, located at 1652.9 cm^{-1} and can be assigned to α-helical content. Based on the relative areas, helix comprises 60 % of the of the protein's secondary structure which is within 5% of estimates from CD spectra. β-sheet contribution to the Amide I peak is estimated to be approximately 30 % which compares with only 17% in CD analysis.

5.3.4 Second Derivative UV Absorption Spectroscopy

Tertiary structure can be monitored through a variety of spectroscopic techniques including intrinsic fluorescence, near-UV CD and second derivative UV absorption spectroscopy. Intrinsic fluorescence is not useful here due to the insensitivity of Tyr residues to changes in environment. Second derivative UV absorption spectroscopy provide a fairly global picture of tertiary structure changes since all three aromatic amino acid residues can be simultaneously monitored.[49,50] CT584 has 13 Phe, 1 Tyr and no Trp residues. Representative second derivative negative peaks are shown in Figure 5.4 near 253, 259, and 265 nm. These correspond to Phe and a final peak at 269 nm which arises from the lone Tyr residue. The shallow slope seen at lower temperatures in all pH environments is not due to alterations in tertiary structure but rather to dynamic aspects of the proteins behavior

and suggests burial and immobilization of the Phe residues. This phenomenon is discussed in detail elsewhere (in publication). Initial peak positions are nearly identical under all pH conditions and are slightly longer (~0.5-1 nm) than observed in the free amino acid indicating that on average the aromatic residues are buried.[37,49] For the Phe negative peaks (Figure 5.4A-C), there is little change at pH 8 except in the peak centered at 265 nm where two or more transitions to longer wavelengths occur (the largest of which starts at 52 °C). CT584 exhibits red shifts at pH 7 which manifest high error associated with aggregation. Confirmation of this protein association is present in light scattering and turbidity data (Figure 5.5C-D). At pH 5 and 6, initial blue shifts lead to erratic data with large error which again is undoubtedly the result of protein aggregation. The two most acidic pH environments examined for CT584 display less variation with temperature with the greatest changes occurring in the peak centered near 265 nm where a broad transition to longer wavelength takes place. The Tyr peak centered around 269 nm again displays little discernable transition at pH 3 and 4 but distinct blue shifts accompanied by larger error are present at pH 5 and 6. These shifts to shorter wavelength indicate a more solvent exposed state for the Tyr residue. Aggregation, which coincides with this transition, again accounts for the increased variability. Red shifts appear at pH 7 and 8 with greater variability observed at pH 7.

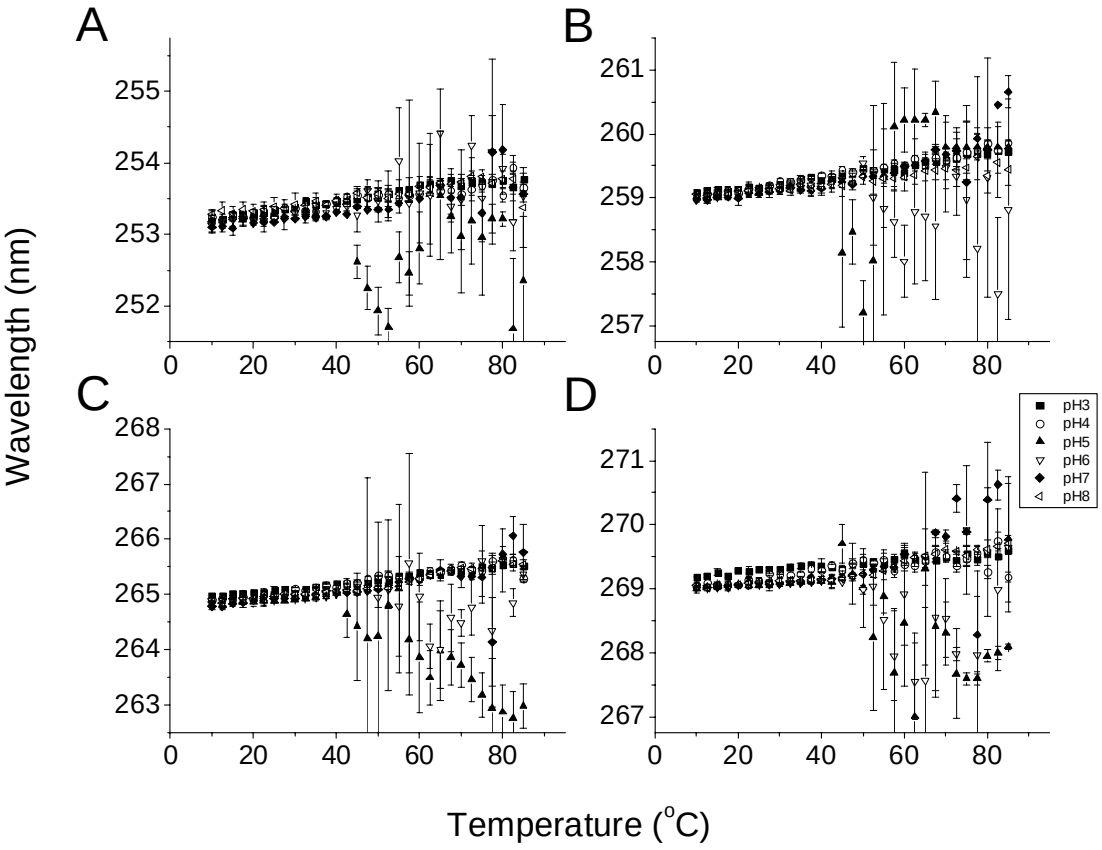

Figure 5.4. Second derivative UV absorption spectroscopy. Absorption peak position minima centered around 253 nm (Phe, A), 259 nm (Phe, B), 265 nm (Phe, C) and 269 nm (Tyr, D) are presented as a function of temperature from 10 to 85 °C. Error bars are the standard deviation from at least three trials. ■, pH 3; ○, pH 4; ▲, pH 5; ▽, pH 6; ◆, pH 7; ◁, pH 8.

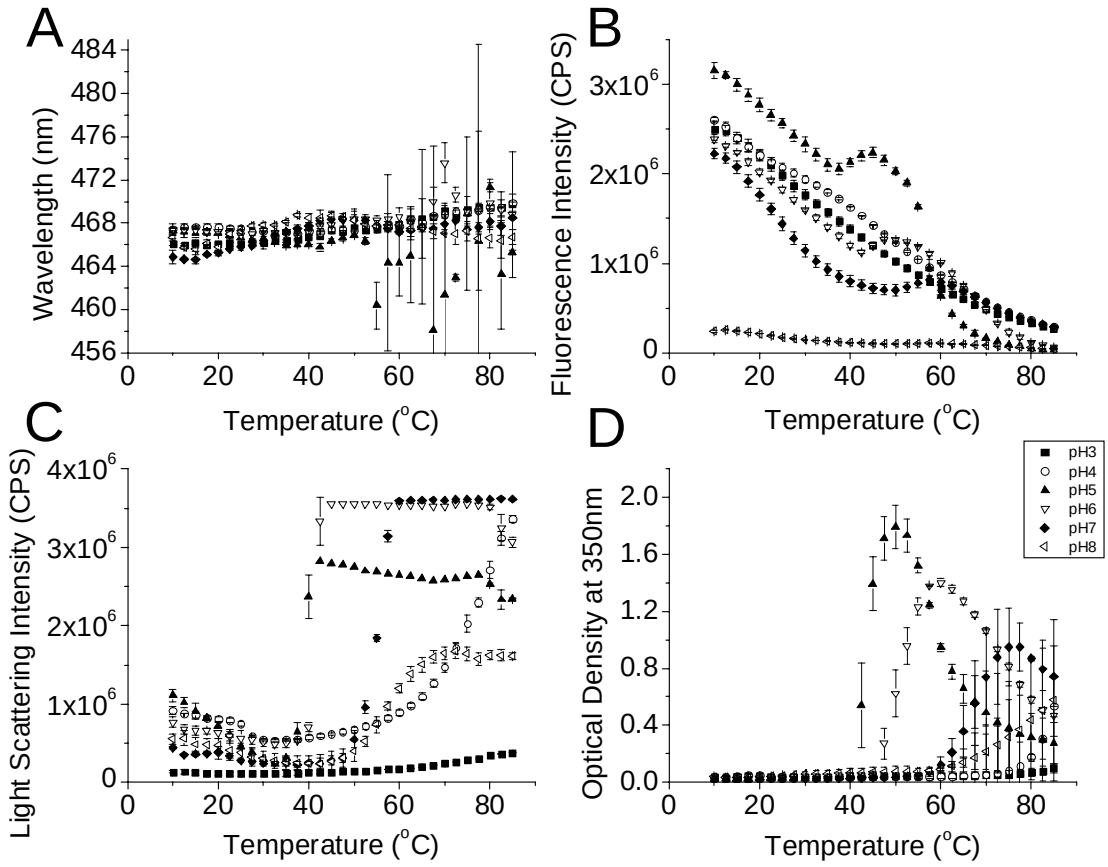

Figure 5.5. IpaD ANS and light scattering studies. ANS fluorescence wavelength peak position (A) and intensity (B) was monitored from 10 to 85 °C. Light scattering intensities at 275 nm (C) and optical densities at 350 nm were measured under the same conditions. Error bars are the standard deviation from at least three trials. ■, pH 3; ○, pH 4; ▲, pH 5; ▽, pH 6; ◆, pH 7; ◁, pH 8.

5.3.5 Extrinsic Fluorescence-ANS

Extrinsic fluorescence using ANS as a probe was performed to monitor the appearance of apolar binding sites in CT584 with respect to both temperature and wavelength. Initial peak positions are nearly identical at pH 4-6 but occur at shorter wavelengths under more acidic or basic conditions (Figure 5.5A). Results at pH 7 and 8 display low temperature red shifts which begin at ~15 °C and are followed by transitions to shorter wavelengths at midrange temperatures. Trends in the middle range of pH (pH 4-6) manifest less pronounced blue shifts at lower temperatures. Peak position wavelength trends are less revealing at high temperatures where error, particularly at pH 5 and 6, precludes definitive conclusions. In contrast, at pH 3 the general trend reveals a biphasic red shift suggesting the existence of two independent domains.

Structural changes in CT584 can also be observed through examination of the fluorescence intensity of the ANS molecule. ANS interacts strongly with apolar regions in proteins. As the structure of a protein begins to loosen, the dye partitions into the apolar core causing an increase in its fluorescence quantum yield.[51] Due to the negative charge of ANS in solution, there may also be some ionic interactions which might be expected more under acidic circumstances.[52] Only broad, comparatively small transitions are observable below pH 5. From pH 5-8, however, transitions occur at increasing temperature with respect to alkalinity (Figure 5.5B). T_0 in the pH 8 environment, the most stable condition observed, begins at approximately 50 °C. The initial fluorescence signal is highest at pH 5 indicating a

more disrupted three dimensional structure. In contrast, the fluorescence intensity at pH 8 is nearly an order of magnitude lower than any other condition. This lower quantum yield may be due in part to the pI of the protein (5.61) which would cause it to be more negatively charged in an alkaline environment. Specifically, this pH is sufficiently far from the pKa of the 4 His residues and sufficiently close to the pKa of the 3 Cys to expect a significant alteration in charge state compared to even pH 7. Even with such a change in ionization state, however, it is likely that the tertiary structure at pH 8 is adequately compact to preclude the level of ANS binding observed in more acidic conditions.

5.3.6 Aggregation

In addition to secondary and tertiary structure changes, the stability of proteins can also be measured in terms of their aggregation behavior. Light scattering provides insights into the formation of higher order aggregates and is more sensitive than turbidity measurements. Alterations in static light scattering intensity may in some cases be the result of variation in the refractive index of scatterers. Increases in scattering are, however, most often a consequence of a change in association behavior. In this case, transition temperatures in light scattering data increase with respect to pH with the exception of pH 3 and 4 (Figure 5.5C). At pH 3, the initial light scattering signal is less than half that observed under other conditions and remains lower than the decrease in intensity seen at ~ 40 °C at higher pH. The initial decrease in intensity observed at pH 4-8 is probably due to changes in the

oligomerization behavior discussed in the analytical ultracentrifugation results section below (Figure 5.6). Optical density data, recorded at 350 nm during the UV absorption experiments, also indicate increasing transition temperature occurring with higher pH (Figure 5.5D). The exception again is environments below pH 5. The OD transition onsets for all pH conditions begin at higher temperatures compared to the right angle light scattering results. This phenomenon is attributed to the fact that light scattering is a more sensitive measure of aggregation.

5.3.7 Analytical Ultracentrifugation

To gain a better understanding of the presence or absence of self-association events that may be occurring in CT584, the protein was analyzed using analytical ultracentrifugation (AUC) at 10 °C. Some tip proteins are known to oligomerize in their native state and are reported to form pentamers or hexamers when localized to the needle tip.[29,45,53,54] Samples of CT584 were examined in both sedimentation velocity and equilibrium modes using interference and absorption optical systems. Samples were run at 36,000 RPM at 0.5 and 1.0 mg/ml in velocity runs. In Figure 5.6A, the results from a continuous c(s) distribution analysis are shown at 0.5 mg/ml. The peak at 1.6 S corresponds to approximately 32 kDa, while the peak at 3.1 S is just over 88 kDa. When the concentration was doubled to 1 mg/ml, the size of the first peak fell to 29 kDa while the sizes of the higher order species were also altered. Since the size of monomeric CT584 is just over 21.1 kDa and there is a change in the apparent size of species when concentration is varied, the oligomerization kinetics

must be fast on the time scale of sedimentation.[55] Fast kinetics skews the apparent sizes of the species of interest in velocity analysis. For this reason, CT584 was analyzed using sedimentation equilibrium as well.

Equilibrium runs were conducted at 0.5 mg/ml at 10 °C with a rotor speed of 17,000 RPM. The data were fit to multiple models. Despite the complex self-association phenomenon observed, the best fits occurred with the monomer-n-mer self-association model (Figure 5.6B). A larger non-participating species set at the size of the smallest higher order aggregate (4.3 S) was included in this analysis to improve the fit. The result shown in Figure 5.6B is monomer to pentamer with the residuals shown below. The data were fit to four different equilibrium conditions and the global reduced Chi² was 1.4. The pentameric and hexameric models both gave good fits. Based the size of the second peak in the sedimentation velocity analysis, however, it is most likely that the correct model is monomer in equilibrium with pentamer with small amounts of higher order aggregation occurring.

5.3.8 Empirical Phase Diagram

Empirical phase diagrams (EPDs) provide an effective way to summarize data from multiple techniques and enable one to get a more global picture of the effect of temperature and pH on protein structure.[36-38,56] In addition, proteins with similar function but little sequence homology generally have similar EPDs which highlights the utility of this technique in considering structure/function relationships.[38,46] In the case of CT584, even at low temperatures (i.e. 10°C), there are conformational

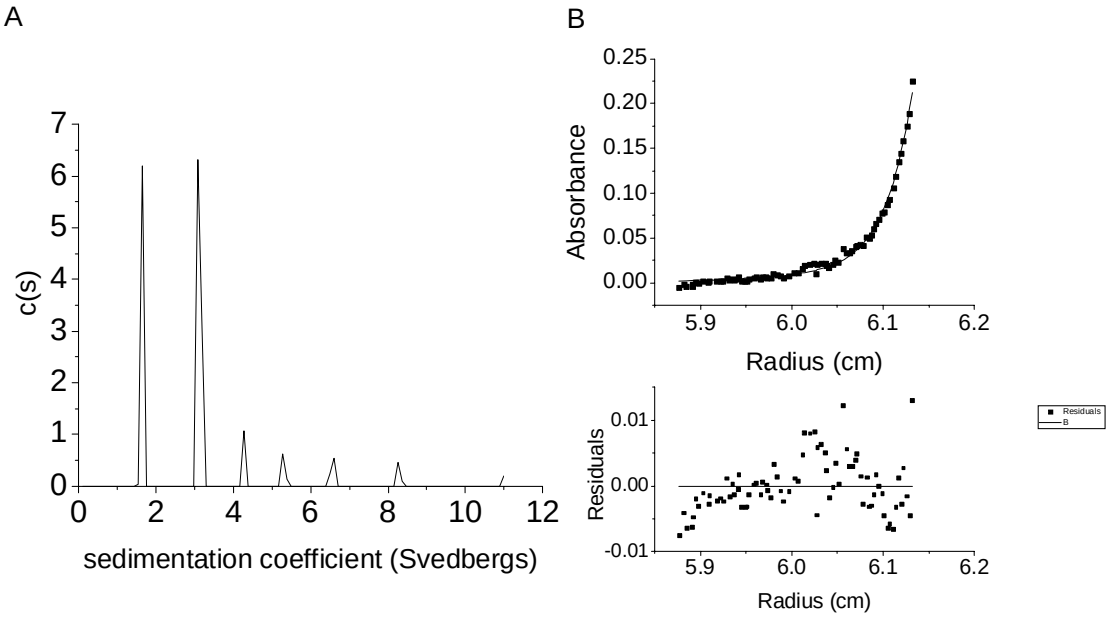

Figure 5.6. Analytical Ultracentrifugation. Sedimentation velocity analysis for CT584 at 0.5 mg/ml and 36,000 RPM at 10°C using a continuous c(S) distribution model from SEDFIT (A). Sedimentation equilibrium results 10 °C at 18,000 RPM using a monomer to pentamer self-association model in SEDPHAT (B).

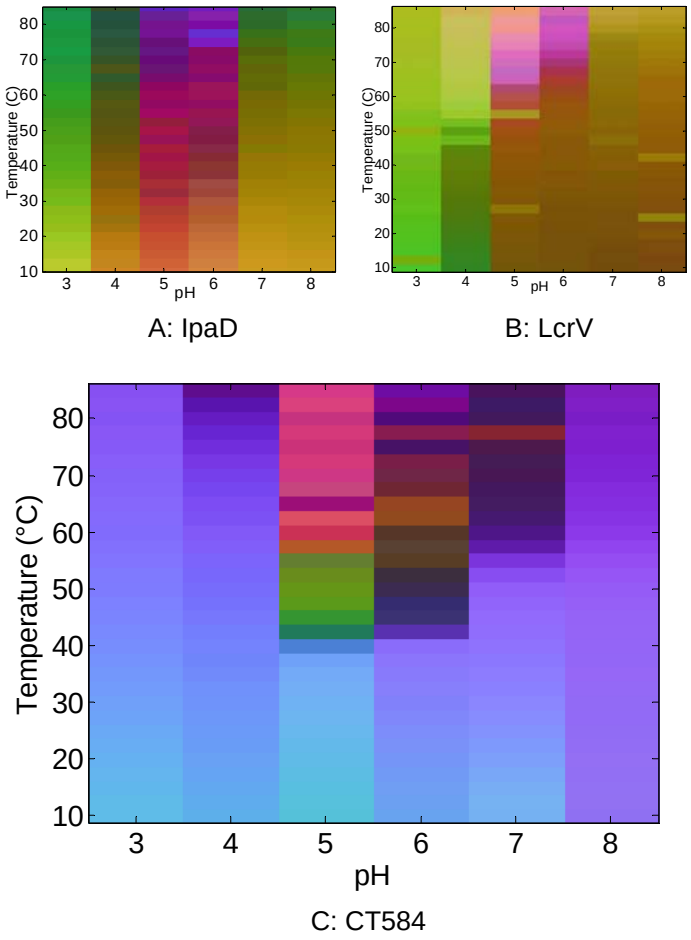

Figure 5.7. Empirical phase diagrams. The empirical phase diagram is a way of summarizing data from different techniques and was created using all of the data biophysical techniques. The empirical phase diagrams shown here are from IpaD (A), LcrV (B) and CT584 (C).

differences from pH 6-8 (Figure 5.7C). The difference between pH 7 and 8 is primarily due to ANS intensity data while pH 6 differs because of the CD results. A small transition occurs at pH 7 near 15 °C which arises from a red shift in ANS wavelength peak position. Ignoring this smaller transition, the trend of increasing stability with respect to pH above pH 4 is in agreement among the multiple techniques. Acidic environments (pH 3 and 4) display more subtle changes in the empirical phase diagram. At pH 3, for example, the greater amount of secondary structure and the more buried aromatic residues seen in UV absorption data suggest that pH 3 may be more stable than any other condition. The dramatic changes in color seen at high temperatures near the protein pI are generally indicative of aggregation and are in agreement with the parent data.

5.4 Discussion

One reason for this biophysical characterization of CT584 is to explore the possibility that it functions as the tip protein in the T3SS of *Chlamydia trachomatis*. Tip proteins from other T3SSs have been thoroughly examined with biological assays,[27,28,30,57-64] crystallographic methods,[29,43,44] biophysical characterization and a number of other techniques.[34,35,46] This work however, represents the first biophysical exploration of CT584 and one of the first studies of any kind of this protein. As such, the data presented above should be compared to CT584 putative functional homologs.

Previous work with EPDs has highlighted their utility in revealing structure/function relationships between proteins with minimal sequence homology.[38,46] The tip proteins IpaD (*Shigella flexneri*), BipD (*Burkholderia pseudomallei*), SipD (*Salmonella* spp.), LcrV (*Yersinia* spp.) and PcrV (*Pseudomonas aeruginosa*) were compared in Chapter 2 and were shown to fall into two distinct sub-families.[46] The first sub-family (IpaD, BipD and SipD) produced EPDs that manifested different structures at pH 6 and 7 even at 10 °C (see example in Figure 5.7A). The physical states of the proteins were the same at pH 7 and above and, in general, were disrupted under acidic conditions below pH 5. The second sub-family's hallmark was nearly identical conformations at low temperatures from pH 5 to 8 with stability increasing in response to higher pH (see example in Figure 5.7B). CT584's phase diagram is similar to all of the tip proteins mentioned above in that there is a dramatic difference in protein structure (conformation) above and below pH 5. This difference was associated with a disrupted physical structure in acidic media with the other T3SS proteins but may be a region of greater stability for CT584. Defining which sub-family the *Chlamydia* protein most resembles is more challenging since it appears to posses one or more of the defining characteristics of each group. Like the IpaD sub-family, CT584 displays conformational differences at low temperatures between pH 6 and 7 with the EPD color shift arising from changes in secondary structure. The observed increasing stability as a function of rising pH, however, would place it in the LcrV subfamily. It is tempting to speculate based on these two observations that, since *Chlamydia trachomatis* belongs to a different phylum than

the other bacteria mentioned, similarities to both sub-families trace it back to a common ancestor prior to the split in the protein family.

While EPD similarities to known tip proteins is not sufficient evidence to establish CT584's function, the protein has other properties described here that strengthen the possibility. Many of the T3SS tip proteins have been shown to oligomerize *in vitro* and *in vivo* and it is believed that, on the needle tip, they are pentamers or hexamers.[29,45,53,54] AUC Sedimentation velocity and equilibrium analysis demonstrate that in aqueous solution, CT584 oligomerizes most probably to a pentamer with some higher order aggregates present. If this self-association occurs in more biologically relevant situations, it suggests a similar role for the protein to other tip proteins. Light scattering displayed an initial drop in intensity from 10 to 37 °C at pH 7 and additional work is needed to ascertain if this change is due to an alteration in oligomerization properties or perhaps due to the formation of less dense particles.

Biphasic transitions are visible under various conditions as a function of temperature for CT584. Circular dichroism traces at pH 5 and 6 as well as ANS peak position transitions in several environments display this behavior which suggests the presence of two independent folding domains. This response to temperature is significant because IpaD and SipD have similar biphasic transitions and have been shown to possess N-terminal and C-terminal domains which have differences in thermal stability.[34,35,46]

Fourier transform infrared spectroscopy de-convolution results agree with the general conclusion from circular dichroism spectra that the secondary structure of CT584 is primarily α-helical. FTIR secondary structural analysis, however, of most of the tip proteins from proteobacteria listed above revealed three predominate bands of nearly equal intensity which is indicative of coiled-coil structure.[34,35,65,66] This structure has been confirmed by crystallographic studies of IpaD, BipD and LcrV.[29,43,44] In the case of CT584, however, there is little evidence from spectroscopic data of a coiled-coil domain. This does not, of course, completely preclude the possibility that some other intramolecular interaction is interfering with its detection. For example, BipD's trimeric coiled-coil alters its FTIR spectrum such that the bands are not longer equal in intensity.

This study provides the first detailed biophysical study of the putative *Chlamydia trachomatis* T3SS tip protein, CT584. Secondary structural analysis reveals that the protein contains primarily α-helical structure, although not necessarily in the form of a coiled-coil. The EPD of CT584 has characteristics in common with both sub-families of tip proteins previously subjected to this analysis.[46] From pH 5 through 8, the putative tip protein shows increased stability as a function of pH in most spectroscopic measurements. Like other tip proteins, CT584 has complex oligomerization properties probably forming a pentamer with small amounts of higher order species also observed. While much work remains, this study represents a first step in ascertaining the function of this newly discovered protein.

5.5 References

1. Schachter J. 1999. Infection and disease epidemiology. In Stephens RS, editor *Chlamydia*: Intracellular biology, pathogenesis and immunity, ed., Washington D.C: American Society for Microbiology. p 139-169.
2. Brunham RC, Rey-Ladino J 2005. Immunology of *Chlamydia* infection: implications for a *Chlamydia trachomatis* vaccine. Nat Rev Immunol 5(2):149-161.
3. WHO. 2001. Global Prevalence and Incidence of Selected Curable Sexually Transmitted Infections: Overview and Estimates. ed.: World Health Organization.
4. Bedson SP, Bland JOW 1932. A morphological study of psittacosis virus with the description of a developmental cycle. Brit J Exptl Pathol 13:461-466.
5. Byrne GI, Moulder JW 1978. Parasite-specified phagocytosis of *Chlamydia psittaci* and *Chlamydia trachomatis* by L and HeLa cells. Infect Immun 19(2):598-606.
6. Hackstadt T, Rockey DD, Heinzen RA, Scidmore MA 1996. *Chlamydia trachomatis* interrupts an exocytic pathway to acquire endogenously synthesized sphingomyelin in transit from the Golgi apparatus to the plasma membrane. Embo J 15(5):964-977.
7. Scidmore MA, Rockey DD, Fischer ER, Heinzen RA, Hackstadt T 1996. Vesicular interactions of the *Chlamydia trachomatis* inclusion are determined by chlamydial early protein synthesis rather than route of entry. Infect Immun 64(12):5366-5372.
8. Beatty WL, Morrison RP, Byrne GI 1994. Persistent chlamydiae: from cell culture to a paradigm for chlamydial pathogenesis. Microbiol Rev 58(4):686-699.
9. Hogan RJ, Mathews SA, Mukhopadhyay S, Summersgill JT, Timms P 2004. Chlamydial persistence: beyond the biphasic paradigm. Infect Immun 72(4):1843-1855.
10. Hueck CJ 1998. Type III protein secretion systems in bacterial pathogens of animals and plants. Microbiol Mol Biol Rev 62(2):379-433.
11. Galan JE, Collmer A 1999. Type III secretion machines: bacterial devices for protein delivery into host cells. Science 284(5418):1322-1328.
12. Galan JE, Wolf-Watz H 2006. Protein delivery into eukaryotic cells by type III secretion machines. Nature 444(7119):567-573.
13. Hsia RC, Pannekoek Y, Ingerowski E, Bavoil PM 1997. Type III secretion genes identify a putative virulence locus of Chlamydia. Mol Microbiol 25(2):351-359.
14. Stephens RS, Kalman S, Lammel C, Fan J, Marathe R, Aravind L, Mitchell W, Olinger L, Tatusov RL, Zhao Q, Koonin EV, Davis RW 1998. Genome sequence of an obligate intracellular pathogen of humans: *Chlamydia trachomatis*. Science 282(5389):754-759.

15. Matsumoto A 1981. Isolation and electron microscopic observations of intracytoplasmic inclusions containing *Chlamydia psittaci*. J Bacteriol 145(1):605-612.
16. Matsumoto A 1982. Surface projections of *Chlamydia psittaci* elementary bodies as revealed by freeze-deep-etching. J Bacteriol 151(2):1040-1042.
17. Clifton DR, Fields KA, Grieshaber SS, Dooley CA, Fischer ER, Mead DJ, Carabeo RA, Hackstadt T 2004. A *chlamydial* type III translocated protein is tyrosine-phosphorylated at the site of entry and associated with recruitment of actin. Proc Natl Acad Sci U S A 101(27):10166-10171.
18. Fields KA, Hackstadt T 2000. Evidence for the secretion of *Chlamydia trachomatis* CopN by a type III secretion mechanism. Mol Microbiol 38(5):1048-1060.
19. Ho TD, Starnbach MN 2005. The *Salmonella enterica* serovar typhimurium-encoded type III secretion systems can translocate *Chlamydia trachomatis* proteins into the cytosol of host cells. Infect Immun 73(2):905-911.
20. Hower S, Wolf K, Fields KA 2009. Evidence that CT694 is a novel *Chlamydia trachomatis* T3S substrate capable of functioning during invasion or early cycle development. Mol Microbiol.
21. Kleba B, Stephens RS 2008. *Chlamydial* effector proteins localized to the host cell cytoplasmic compartment. Infect Immun 76(11):4842-4850.
22. Peters J, Wilson DP, Myers G, Timms P, Bavoil PM 2007. Type III secretion a la *Chlamydia*. Trends Microbiol 15(6):241-251.
23. Subtil A, Delevoye C, Balana ME, Tastevin L, Perrinet S, Dautry-Varsat A 2005. A directed screen for *chlamydial* proteins secreted by a type III mechanism identifies a translocated protein and numerous other new candidates. Mol Microbiol 56(6):1636-1647.
24. Hefty PS, Stephens RS 2007. Chlamydial type III secretion system is encoded on ten operons preceded by sigma 70-like promoter elements. J Bacteriol 189(1):198-206.
25. Cossart P, Sansonetti PJ 2004. Bacterial invasion: the paradigms of enteroinvasive pathogens. Science 304(5668):242-248.
26. He SY, Nomura K, Whittam TS 2004. Type III protein secretion mechanism in mammalian and plant pathogens. Biochim Biophys Acta 1694(1-3):181-206.
27. Espina M, Olive AJ, Kenjale R, Moore DS, Ausar SF, Kaminski RW, Oaks EV, Middaugh CR, Picking WD, Picking WL 2006. IpaD Localizes to the Tip of the Type III Secretion System Needle of *Shigella flexneri*. Infection and Immunity 74(8):4391-4400.
28. Goure J, Broz P, Attree O, Cornelis GR, Attree I 2005. Protective anti-V antibodies inhibit *Pseudomonas* and *Yersinia* translocon assembly within host membranes. J Infect Dis 192(2):218-225.
29. Johnson S, Roversi P, Espina M, Olive A, Deane JE, Birket S, Field T, Picking WD, Blocker AJ, Galyov EE, Picking WL, Lea SM 2006. Self-chaperoning of the type III secretion system needle tip proteins IpaD and BipD. J Biol Chem.

30. Mueller CA, Broz P, Mueller SA, Ringler P, Erne-Brand F, Sorg I, Kuhn M, Engel A, Cornelis GR 2005. The V-Antigen of *Yersinia* Forms a Distinct Structure at the Tip of Injectisome Needles. Science (Washington, DC, United States) 310(5748):674-676.
31. Frank DW, Vallis A, Wiener-Kronish JP, Roy-Burman A, Spack EG, Mullaney BP, Megdoud M, Marks JD, Fritz R, Sawa T 2002. Generation and characterization of a protective monoclonal antibody to *Pseudomonas aeruginosa* PcrV. J Infect Dis 186(1):64-73.
32. Holder IA, Neely AN, Frank DW 2001. PcrV immunization enhances survival of burned *Pseudomonas aeruginosa*-infected mice. Infect Immun 69(9):5908-5910.
33. Une T, Brubaker RR 1984. Roles of V antigen in promoting virulence and immunity in *yersiniae*. J Immunol 133(4):2226-2230.
34. Espina M, Ausar SF, Middaugh CR, Baxter MA, Picking WD, Picking WD 2007. Conformational stability and differential structural analysis of LcrV, PcrV, BipD, and SipD from type III secretion systems. Protein Sci 16(4):704-714.
35. Espina M, Ausar SF, Middaugh CR, Picking WD, Picking WL 2006. Spectroscopic and calorimetric analyses of invasion plasmid antigen D (IpaD) from *Shigella flexneri* reveal the presence of two structural domains. Biochemistry 45(30):9219-9227.
36. Fan H, Ralston J, Dibiase M, Faulkner E, Middaugh CR 2005. Solution behavior of IFN-beta-1a: an empirical phase diagram based approach. J Pharm Sci 94(9):1893-1911.
37. Kueltzo LA, Ersoy B, Ralston JP, Middaugh CR 2003. Derivative absorbance spectroscopy and protein phase diagrams as tools for comprehensive protein characterization: A bGCSF case study. J Pharm Sci 92(9):1805-1820.
38. Fan H, Kashi RS, Middaugh CR 2006. Conformational lability of two molecular chaperones Hsc70 and gp96: effects of pH and temperature. Arch Biochem Biophys 447(1):34-45.
39. Zhang Y 2008. I-TASSER server for protein 3D structure prediction. BMC Bioinformatics 9:40.
40. Battey JN, Kopp J, Bordoli L, Read RJ, Clarke ND, Schwede T 2007. Automated server predictions in CASP7. Proteins 69 Suppl 8:68-82.
41. Zhang Y 2007. Template-based modeling and free modeling by I-TASSER in CASP7. Proteins 69 Suppl 8:108-117.
42. Holm L, Park J 2000. DaliLite workbench for protein structure comparison. Bioinformatics 16(6):566-567.
43. Derewenda U, Mateja A, Devedjiev Y, Routzahn KM, Evdokimov AG, Derewenda ZS, Waugh DS 2004. The structure of *Yersinia pestis* V-antigen, an essential virulence factor and mediator of immunity against plague. Structure (Cambridge, MA, United States) 12(2):301-306.
44. Erskine PT, Knight MJ, Ruaux A, Mikolajek H, Sang NW, Withers J, Gill R, Wood SP, Wood M, Fox GC, Cooper JB 2006. High Resolution Structure of BipD: An Invasion Protein Associated with the Type III Secretion System of *Burkholderia Pseudomallei*. J Mol Biol 363(1):125-136.

45. Caroline G, Eric F, Bohn YS, Sylvie E, Attree I 2008. Oligomerization of PcrV and LcrV, protective antigens of *Pseudomonas aeruginosa* and *Yersinia pestis*. J Biol Chem 283(35):23940-23949.
46. Markham AP, Birket SE, Picking WD, Picking WL, Middaugh CR 2008. pH sensitivity of type III secretion system tip proteins. Proteins 71(4):1830-1842.
47. Hennessey JP, Jr., Johnson WC, Jr. 1981. Information content in the circular dichroism of proteins. Biochemistry 20(5):1085-1094.
48. Byler DM, Susi H 1986. Examination of the secondary structure of proteins by deconvolved FTIR spectra. Biopolymers 25(3):469-487.
49. Mach H, Middaugh CR 1994. Simultaneous monitoring of the environment of tryptophan, tyrosine, and phenylalanine residues in proteins by near-ultraviolet second-derivative spectroscopy. Anal Biochem 222(2):323-331.
50. Mach H, Thomson JA, Middaugh CR, Lewis RV 1991. Examination of phenylalanine microenvironments in proteins by second-derivative absorption spectroscopy. Arch Biochem Biophys 287(1):33-40.
51. Semisotnov GV, Rodionova NA, Razgulyaev OI, Uversky VN, Gripas AF, Gilmanshin RI 1991. Study of the "molten globule" intermediate state in protein folding by a hydrophobic fluorescent probe. Biopolymers 31(1):119-128.
52. Matulis D, Lovrien R 1998. 1-Anilino-8-naphthalene sulfonate anion-protein binding depends primarily on ion pair formation. Biophys J 74(1):422-429.
53. Broz P, Mueller CA, Muller SA, Philippsen A, Sorg I, Engel A, Cornelis GR 2007. Function and molecular architecture of the *Yersinia* injectisome tip complex. Mol Microbiol 65(5):1311-1320.
54. Veenendaal AK, Hodgkinson JL, Schwarzer L, Stabat D, Zenk SF, Blocker AJ 2007. The type III secretion system needle tip complex mediates host cell sensing and translocon insertion. Mol Microbiol 63(6):1719-1730.
55. Dam J, Velikovsky CA, Mariuzza RA, Urbanke C, Schuck P 2005. Sedimentation velocity analysis of heterogeneous protein-protein interactions: Lamm equation modeling and sedimentation coefficient distributions c(s). Biophys J 89(1):619-634.
56. Fan H, Li H, Zhang M, Middaugh CR 2006. Effects of solutes on empirical phase diagrams of human fibroblast growth factor 1. J Pharm Sci.
57. De Geyter C, Wattiez R, Sansonetti P, Falmagne P, Ruysschaert JM, Parsot C, Cabiaux V 2000. Characterization of the interaction of IpaB and IpaD, proteins required for entry of *Shigella flexneri* into epithelial cells, with a lipid membrane. Eur J Biochem FIELD Full Journal Title:European journal of biochemistry / FEBS 267(18):5769-5776.
58. Fields KA, Nilles ML, Cowan C, Straley SC 1999. Virulence role of V antigen of *Yersinia* pestis at the bacterial surface. Infect Immun 67(10):5395-5408.
59. Hermant D, Menard R, Arricau N, Parsot C, Popoff MY 1995. Functional conservation of the *Salmonella* and *Shigella* effectors of entry into epithelial cells. Mol Microbiol 17(4):781-789.
60. Lawton DG, Longstaff C, Wallace BA, Hill J, Leary SE, Titball RW, Brown KA 2002. Interactions of the type III secretion pathway proteins LcrV and LcrG from

Yersinia pestis are mediated by coiled-coil domains. J Biol Chem 277(41):38714-38722.
61. Marquart ME, Picking WL, Picking WD 1995. Structural analysis of invasion plasmid antigen D (IpaD) from *Shigella flexneri*. Biochem Biophys Res Commun 214(3):963-970.
62. Nanao M, Ricard-Blum S, Di Guilmi AM, Lemaire D, Lascoux D, Chabert J, Attree I, Dessen A 2003. Type III secretion proteins PcrV and PcrG from *Pseudomonas aeruginosa* form a 1:1 complex through high affinity interactions. BMC Microbiol 3:21.
63. Stevens MP, Wood MW, Taylor LA, Monaghan P, Hawes P, Jones PW, Wallis TS, Galyov EE 2002. An *Inv*/Mxi-*Spa*-like type III protein secretion system in *Burkholderia pseudomallei* modulates intracellular behaviour of the pathogen. Mol Microbiol 46(3):649-659.
64. Venkatesan MM, Buysse JM, Kopecko DJ 1988. Characterization of invasion plasmid antigen genes (*ipaBCD*) from *Shigella flexneri*. Proc Natl Acad Sci U S A 85(23):9317-9321.
65. Heimburg T, Schuenemann J, Weber K, Geisler N 1996. Specific recognition of coiled coils by infrared spectroscopy: analysis of the three structural domains of type III intermediate filament proteins. Biochemistry 35(5):1375-1382.
66. Heimburg T, Schunemann J, Weber K, Geisler N 1999. FTIR-Spectroscopy of multistranded coiled coil proteins. Biochemistry 38(39):12727-12734.

Chapter 6

Summary and Conclusions

6.1 Overview

The bacterial pathogens discussed here are responsible for some of the most serious epidemics in the world. Many gram-negative bacteria employ type III secretion systems (TTSS) to facilitate interactions with eukaryotic organisms as symbionts or pathogens.[1,2] The TTSS apparatus is comprised of a basal body which spans the inner and outer bacterial membranes and a needle through which effector proteins translocate to subvert normal host cell functions. A protein located at the needle tip regulates the secretion of other effectors.[3,4] Due to its location and function, these so called tip proteins are excellent antigen candidates for sub-unit vaccines.

Previously, it was shown that these tip proteins possess a central coiled coil flanked by N and C-terminal domains.[5-7] This structure appears to be dumbbell in shape. The tip proteins discussed in Chapters 1 through 4 exhibit pI's between 4.8 and 5.5 with molecular weights between 33 and 37 kDa. These proteins are predicted to oligomerize when interacting with the TTSS needle complex and possibly associate in other environments as well.[7-9]

Chapter 2 presents the biophysical characterization of the tip proteins IpaD from *Shigella flexneri*, BipD of *Burkholderia pseudomallei*, SipD of *Salmonella* spp., LcrV of *Yersinia* spp. and PcrV of *Pseudomonas aeruginosa*. The conformational stability of these proteins was characterized as a function of pH and temperature. Secondary and tertiary structural changes were monitored using the spectroscopic techniques of far-UV circular dichroism, Trp fluorescence, ANS fluorescence and

ultraviolet absorption spectroscopy. Optical density and right angle scattering measurements were also used to evaluate protein association/dissociation. Finally data were combined and summarized using empirical phase diagrams (EPD).[10,11]

Responses of these tip proteins to pH and temperature reveal two distinct sub-families. The first is that of IpaD, BipD and SipD which reveal low temperature conformational differences at pH 5 and 6. Many reasons may exist for these differences in conformation. One interesting possibility is that the more acidic pH microenvironments present near host cell membranes may induce a functionally relevant conformational change in these proteins perhaps triggering the translocation of other effectors.[12-14] The second sub-family includes LcrV and Pcrv and is characterized by increasing temperature transitions with higher pH.

Chapter 3 establishes the antigenicity of two of the TTSS tip proteins, IpaD and SipD. Administration of these proteins adsorbed to aluminum salt adjuvant elicits a robust humoral immune response. IpaD does not show significant dose-dependent behavior when administered in a multi-dose regimen. There appears, however, to be an initial dose-dependency following the first inoculation. In the absence of Alhydrogel®, anti-IpaD IgG endpoint titers were reduced but still displayed values well above the titers of adjuvant alone. The needle monomer MxiH antibody response was boosted when co-administered with IpaD. The increased anti-MxiH titers suggest that IpaD may possess some adjuvant like properties. The SipD antibody response was also higher in the presence of the adjuvant. The final endpoint titers of SipD antibodies were invariant relative to the amount of antigen injected.

In Chapter 4, formulation experiments were conducted on the five tip proteins discussed in the second chapter. After excipient screening and subsequent optimization experiments, 10% sucrose and 5% dextrose was selected as the optimal excipient combination. Adsorption isotherms and desorption experiments were conducted to understand the nature of the interaction between the proteins and aluminum hydroxide adjuvant. Based on these experiments, the interaction between the proteins and the adjuvant is probably a mixture of hydrogen bonding and Van der Waals forces although the relative importance of each varies by protein. Excipients increased the transition midpoints of the tip proteins when adsorbed to Alhydrogel® in thermal stress studies conducted from 10 to 85 °C. In long term stability experiments at 25 °C, intrinsic Trp fluorescence peak positions remained unchanged for a period of three months. The excipient combination also inhibited chemical degradation at 40 °C compared to antigen adsorbed to aluminum hydroxide adjuvant alone. The work in this chapter defines a formulation which, based on preliminary stability results, increases the stability of the tip proteins. More long term experiments will be necessary to confirm this stabilizing capacity.

Chapter 5 presents the biophysical characterization of a putative tip protein (CT584) from Chamydiae. Spectroscopic techniques were employed to measure conformational changes with respect to pH and temperature. An EPD of CT584 revealed possible structure/function characteristics in common with both sub-families explored in Chapter 2.[10] In addition, analytical ultracentrifugation, in both velocity and sedimentation equilibrium modes, established that CT584 oligomerizes (most

likely to a pentamer). Since other tip proteins are believed to pentamerize when associated with the needle complex, this suggests that CT584 may have a similar function.[7,9,15,16]

6.2 Future Work

Animal studies and formulation experiments outlined in Chapters 3 and 4 present evidence that a successful multivalent vaccine is possible. More experiments, however, are necessary before such a vaccine becomes reality. Animal challenge studies are needed to ascertain whether the tip proteins in the presence of immunopotentiators like aluminum hydroxide adjuvant protect for all the bacterial species against relevant challenges. Specifically, no data exist on the protective effects of IpaD, BipD or SipD adsorbed to aluminum salt adjuvants in their individual systems. Murine models exist for *Yersinia pestis*, some *Salmonella enterica* serovars, *Burkholderia pseudomallei* and *Pseudomonas aeruginosa*.[17-20] *Shigella flexneri*, however, requires work in primates since the disease state currently can only be induced in that model.[21]

Additional long term stability studies need to confirm that the excipients identified increase both physical and chemical stability. In particular, studies at 25 °C conducted for longer than three months (24-36 months) are necessary to ascertain the extent of conformational stability. Ongoing studies at 4 °C also require additional measurements and analysis. Chemical stability studies would be useful at lower

temperatures and longer times to confirm the results at 40 °C and to discover if chemical degradation pathways or their kinetics are altered under those conditions. If alternative stability monitoring methods are required, standard ELISA protocols similar to those in Chapter 3 may yield useful information. Additionally, effects of extended storage on potency should also be explored. After shelf life has been estimated by conformational and chemical stability studies, administration of the vaccine formulation to animals is needed to confirm retention of potency.

Another possible direction for future work involves synthesizing a sub-unit vaccine more analogous to the TTSS. This would be accomplished by combining the tip proteins discussed here with their polymerized needle counterparts. Such a construct might elicit a more appropriate robust response and thus provide increased protection. This approach requires additional work to better understand the nature of needle polymerization. A method would need to be developed to manufacture recombinant needles with a defined, reproducible size distribution. In addition, interactions between tip proteins and needles need increased analyses to ensure correct association of the two.

Finally, any future vaccine will ultimately require trials in humans. Phase I trials would occur first to establish vaccine safety. If successful, those studies would lead to Phase II and III trials. As part of this process, testing in areas of the world where the diseases are endemic would provide valuable information on efficacy. In view of the necessary future experiments, the work presented here represents only the

first few steps on a journey towards a multivalent, efficacious vaccine against these serious infections.

6.3 References

1. Cornelis GR 2006. The type III secretion injectisome. Nat Rev Microbiol 4(11):811-825.
2. Hueck CJ 1998. Type III protein secretion systems in bacterial pathogens of animals and plants. Microbiol Mol Biol Rev 62(2):379-433.
3. Espina M, Olive AJ, Kenjale R, Moore DS, Ausar SF, Kaminski RW, Oaks EV, Middaugh CR, Picking WD, Picking WL 2006. IpaD Localizes to the Tip of the Type III Secretion System Needle of *Shigella flexneri*. Infect Immun 74(8):4391-4400.
4. Mueller CA, Broz P, Mueller SA, Ringler P, Erne-Brand F, Sorg I, Kuhn M, Engel A, Cornelis GR 2005. The V-Antigen of *Yersinia* Forms a Distinct Structure at the Tip of Injectisome Needles. Science (Washington, DC, United States) 310(5748):674-676.
5. Derewenda U, Mateja A, Devedjiev Y, Routzahn KM, Evdokimov AG, Derewenda ZS, Waugh DS 2004. The structure of *Yersinia pestis* V-antigen, an essential virulence factor and mediator of immunity against plague. Structure (Cambridge, MA, United States) 12(2):301-306.
6. Erskine PT, Knight MJ, Ruaux A, Mikolajek H, Sang NW, Withers J, Gill R, Wood SP, Wood M, Fox GC, Cooper JB 2006. High Resolution Structure of BipD: An Invasion Protein Associated with the Type III Secretion System of *Burkholderia Pseudomallei*. J Mol Biol 363(1):125-136.
7. Johnson S, Roversi P, Espina M, Olive A, Deane JE, Birket S, Field T, Picking WD, Blocker AJ, Galyov EE, Picking WL, Lea SM 2006. Self-chaperoning of the type III secretion system needle tip proteins IpaD and BipD. J Biol Chem.
8. Deane JE, Roversi P, Cordes FS, Johnson S, Kenjale R, Daniell S, Booy F, Picking WD, Picking WL, Blocker AJ, Lea SM 2006. Molecular model of a type III secretion system needle: Implications for host-cell sensing. Proc Natl Acad Sci USA 103(33):12529-12533.
9. Caroline G, Eric F, Bohn YS, Sylvie E, Attree I 2008. Oligomerization of PcrV and LcrV, protective antigens of *Pseudomonas aeruginosa* and *Yersinia pestis*. J Biol Chem 283(35):23940-23949.
10. Fan H, Kashi RS, Middaugh CR 2006. Conformational lability of two molecular chaperones Hsc70 and gp96: effects of pH and temperature. Arch Biochem Biophys 447(1):34-45.

11. Kueltzo LA, Ersoy B, Ralston JP, Middaugh CR 2003. Derivative absorbance spectroscopy and protein phase diagrams as tools for comprehensive protein characterization: A bGCSF case study. J Pharm Sci 92(9):1805-1820.
12. Bychkova VE, Dujsekina AE, Klenin SI, Tiktopulo EI, Uversky VN, Ptitsyn OB 1996. Molten globule-like state of cytochrome c under conditions simulating those near the membrane surface. Biochemistry 35(19):6058-6063.
13. Mach H, Ryan JA, Burke CJ, Volkin DB, Middaugh CR 1993. Partially structured self-associating states of acidic fibroblast growth factor. Biochemistry 32(30):7703-7711.
14. van der Goot FG, Gonzalez-Manas JM, Lakey JH, Pattus F 1991. A 'molten-globule' membrane-insertion intermediate of the pore-forming domain of colicin A. Nature 354(6352):408-410.
15. Broz P, Mueller CA, Muller SA, Philippsen A, Sorg I, Engel A, Cornelis GR 2007. Function and molecular architecture of the *Yersinia* injectisome tip complex. Mol Microbiol 65(5):1311-1320.
16. Veenendaal AK, Hodgkinson JL, Schwarzer L, Stabat D, Zenk SF, Blocker AJ 2007. The type III secretion system needle tip complex mediates host cell sensing and translocon insertion. Mol Microbiol 63(6):1719-1730.
17. Leary SE, Williamson ED, Griffin KF, Russell P, Eley SM, Titball RW 1995. Active immunization with recombinant V antigen from *Yersinia pestis* protects mice against plague. Infect Immun 63(8):2854-2858.
18. Sawa T, Yahr TL, Ohara M, Kurahashi K, Gropper MA, Wiener-Kronish JP, Frank DW 1999. Active and passive immunization with the *Pseudomonas* V antigen protects against type III intoxication and lung injury. Nat Med 5(4):392-398.
19. Druar C, Yu F, Barnes JL, Okinaka RT, Chantratita N, Beg S, Stratilo CW, Olive AJ, Soltes G, Russell ML, Limmathurotsakul D, Norton RE, Ni SX, Picking WD, Jackson PJ, Stewart DI, Tsvetnitsky V, Picking WL, Cherwonogrodzky JW, Ketheesan N, Peacock SJ, Wiersma EJ 2008. Evaluating *Burkholderia pseudomallei* Bip proteins as vaccines and Bip antibodies as detection agents. FEMS Immunol Med Microbiol 52(1):78-87.
20. Santos RL, Zhang S, Tsolis RM, Kingsley RA, Adams LG, Baumler AJ 2001. Animal models of *Salmonella* infections: enteritis versus typhoid fever. Microbes Infect 3(14-15):1335-1344.
21. Levine MM, Kotloff KL, Barry EM, Pasetti MF, Sztein MB 2007. Clinical trials of *Shigella* vaccines: two steps forward and one step back on a long, hard road. Nat Rev Microbiol 5(7):540-553.